อิทธิพลของวิธีกำจัดตัวกำหนดโครงสร้างต่อลักษณะสมบัติของนาโนคอมโพสิตของอนุภาคทอง/เมโซเซลลูลาร์โฟมซิลิกาเพื่อการตรึงเอนไซม์อะซิติลโคลีนเอสเทอเรส

นายนิธิ ธนานุกูล

วิทยานิพนธ์นี้เป็นส่วนหนึ่งของการศึกษาตามหลักสูตรปริญญาวิศวกรรมศาสตรมหาบัณฑิต
สาขาวิชาวิศวกรรมเคมี ภาควิชาวิศวกรรมเคมี
คณะวิศวกรรมศาสตร์ จุฬาลงกรณ์มหาวิทยาลัย
ปีการศึกษา 2558

EFFECT OF TEMPLATE REMOVAL METHODS ON GOLD NANOPARTICLES/MESOCELLULAR FOAM SILICA NANOCOMPOSITE CHARACTERISTICS FOR ACETYLCHOLINESTERASE IMMOBILIZATION

Mr. Nithi Thananukool

A Thesis Submitted in Partial Fulfillment of the Requirements
for the Degree of Master of Engineering Program in Chemical Engineering
Department of Chemical Engineering
Faculty of Engineering
Chulalongkorn University
Academic Year 2015

Thesis Title	EFFECT OF TEMPLATE REMOVAL METHODS ON GOLD NANOPARTICLES/MESOCELLULAR FOAM SILICA NANOCOMPOSITE CHARACTERISTICS FOR ACETYLCHOLINESTERASE IMMOBILIZATION
By	Mr. Nithi Thananukool
Field of Study	Chemical Engineering
Thesis Advisor	Associate Professor Seeroong Prichanont, Ph.D.
Thesis Co-Advisor	Chanchana Thanachayanont, Ph.D.

Accepted by the Faculty of Engineering, Chulalongkorn University in Partial Fulfillment of the Requirements for the Master's Degree

.....Dean of the Faculty of Engineering

(Associate Professor Supot Teachavorasinskun, Ph.D.)

THESIS COMMITTEE

.....Chairman

(Associate Professor Joongjai Panpranot, Ph.D.)

.....Thesis Advisor

(Associate Professor Seeroong Prichanont, Ph.D.)

.....Thesis Co-Advisor

(Chanchana Thanachayanont, Ph.D.)

.....Examiner

(Associate Professor Artiwan Shotipruk, Ph.D.)

.....External Examiner

(Lerdluck Kaewvimol, Ph.D.)

นิธิ ธนานุกูล : อิทธิพลของวิธีกำจัดตัวกำหนดโครงสร้างต่อลักษณะสมบัติของนาโนคอมโพสิตของอนุภาคทอง/เมโซเซลลูลาร์โฟมซิลิกาเพื่อการตรึงเอนไซม์อะซิติลโคลีนเอสเทอเรส (EFFECT OF TEMPLATE REMOVAL METHODS ON GOLD NANOPARTICLES/MESOCELLULAR FOAM SILICA NANOCOMPOSITE CHARACTERISTICS FOR ACETYLCHOLINESTERASE IMMOBILIZATION) อ.ที่ปรึกษาวิทยานิพนธ์หลัก: รศ. ดร. สีรุ้ง ปรีชานนท์, อ.ที่ปรึกษาวิทยานิพนธ์ร่วม: ดร. ชัญชณา ธนชยานนท์, 99 หน้า.

งานวิจัยนี้ศึกษาอิทธิพลของวิธีกำจัดตัวกำหนดโครงสร้างได้แก่ วิธีการเผาด้วยอุณหภูมิสูงและวิธีสกัดด้วยตัวทำละลาย ซึ่งมีผลต่อลักษณะสมบัติของเมโซเซลลูลาร์โฟมซิลิกา (เอ็มซีเอฟ) ที่ใช้เป็นวัสดุรองรับในการประยุกต์ใช้งานทางไบโอเซนเซอร์ของเอนไซม์อะซิติลโคลีนเอสเทอเรส (เอซีเอชอี) โดยในงานวิจัยนี้ได้แบ่งการศึกษาเป็นสามส่วน งานวิจัยส่วนแรกทำการศึกษาประสิทธิภาพของวิธีกำจัดตัวกำหนดโครงสร้างที่แตกต่างกันในการสังเคราะห์เมโซพอร์ซิลิกาชนิดเอ็มซีเอฟ พบว่าเมโซพอร์ซิลิกาชนิดเอ็มซีเอฟมีที่มีการกำจัดสารกำหนดโครงสร้างแบบเผา (เอ็มซีเอฟ-ซี) และสกัดด้วยตัวทำละลาย (เอ็มซีเอฟ-อี) มีรูพรุนขนาด 8.1 และ 6.7 นาโนเมตรและมีพื้นที่ผิวจำเพาะ 1,075 และ 1,221 ตารางเมตรต่อกรัมตามลำดับ จากนั้นทำการวิเคราะห์โดยเครื่องเอฟทีไออาร์ของวัสดุซิลิกาทั้งสอง พบว่าหมู่ฟังก์ชันมีความคล้ายคลึงกัน และยังสามารถกำจัดตัวกำหนดโครงสร้างออกได้ในทั้งสองกรณี แต่อย่างไรก็ตามเมื่อทำการวิเคราะห์วัสดุทั้งสองด้วยเครื่องเอสอีเอ็สและทีอีเอ็ม พบว่าวัสดุซิลิกาที่ผ่านการเผามีลักษณะการทรุดและหดตัวของอนุภาคซึ่งเกิดจากการเผาด้วยความร้อนสูง ในการศึกษาส่วนที่สองเป็นการศึกษาอิทธิพลของวิธีกำจัดตัวกำหนดโครงสร้างต่อการติดหมู่ฟังก์ชั่นเอพีทีเอส (3-อะมิโนโพรพิลไตรเอทอกซีไซเลน) และการสังเคราะห์อนุภาคนาโนทองบนพื้นผิวของวัสดุทั้งสอง จากผลการทดลองพบว่าสามารถสังเคราะห์ขนาดอนุภาคนาโนทองได้ในช่วง 2-3 นาโนเมตร และเมื่อใช้เวลาในการดูดซับสารตั้งต้นทองนานขึ้นพบว่าทั้ง เอ็มซีเอฟ-ซี/อนุภาคนาโนทอง และ เอ็มซีเอฟ-อี/อนุภาคนาโนทอง ให้ผลการกระจายตัวและขนาดของอนุภาคนาโนทองที่คล้ายคลึงกันจึงทำให้ปริมาณหมู่ซิลานอลบนพื้นผิวของวัสดุทั้งสองไม่ส่งผลอย่างมีนัยสำคัญต่อการเกิดอนุภาคนาโนทองที่ความเข้มข้นสารตั้งต้นทองนั้น จากนั้นทำการทดสอบการตอบสนองของกระแสไฟฟ้าต่ออะซิติลโคลีนคลอไรด์ด้วยวิธีโซคลิกโวลแทมเมตรีของวัสดุเอ็มซีเอฟ/อนุภาคนาโนทอง พบว่า เอ็มซีเอฟ-อี/อนุภาคนาโนทอง ให้ผลการตอบสนองทางกระแสไฟฟ้าดีกว่า เอ็มซีเอฟ-ซี/อนุภาคนาโนทอง และพบว่าปริมาณสารตั้งต้นทองที่ 0.5 มิลลิโมลาร์ มีความเหมาะสมสำหรับการใช้งานทางไบโอเซนเซอร์ อีกทั้งมีความสอดคล้องกับปริมาณการตรึงเอนไซม์เอซีเอชอี ในการศึกษาส่วนสุดท้ายเป็นการนำวัสดุที่เหมาะสมจากการศึกษาในส่วนก่อนหน้านี้คือ เอ็มซีเอฟ-อี และ เอ็มซีเอฟ-อี/อนุภาคนาโนทอง มาประยุกต์ใช้งานทางไบโอเซนเซอร์ของเอนไซม์เอซีเอชอีในการตรวจวัดสารฆ่าแมลงโดยนำเอนไซม์มาทำการตรึงรูปแล้วนำมาดัดแปลงกับอิเลคโทรดของไบโอเซนเซอร์ร่วมกับไคโตซานฟิล์ม จะได้อิเลคโทรด SPCE/MCF-e/AChE/Chitosan และ SPCE/MCF-e/AuNPs/AChE/Chitosan ในส่วนของ เอ็มซีเอฟ-อี สามารถวัดสารฆ่าแมลงประเภทออร์กาโนฟอตเฟต คือ คลอไพริฟอสได้ในช่วงความเข้มข้น 0.5 ถึง 200 พีพีบี และ 200 ถึง 2000 พีพีบี ซึ่งมีค่าความเข้มข้นต่ำสุดที่สามารถตรวจวัดได้คือ 0.894 พีพีบี และในส่วนของ เอ็มซีเอฟ-อี/อนุภาคนาโนทอง สามารถตรวจวัดได้ในช่วงความเข้มข้น 0.5 ถึง 200 พีพีบี และ 200 ถึง 2000 นาโนพีพีบี มีค่าความเข้มข้นต่ำสุดที่สามารถตรวจวัดได้คือ 0.701 พีพีบี จากนั้นทำการศึกษาความคงตัวในการตอบสนองของอิเลคโทรดที่ดัดแปลงขึ้น พบว่าเมื่อทำการเก็บรักษาไว้ที่อุณหภูมิ 4 องศาเซลเซียสเป็นเวลา 30 วัน พบว่าอิเลคโทรดที่ดัดแปลง SPCE/MCF-e/AChE/Chitosan และ SPCE/MCF-e/AuNPs/AChE/Chitosan สามารถเก็บรักษาสัญญาณในการตอบสนองได้ 74.25 และ 77.57 % ตามลำดับ เมื่อเทียบกับกระแสตอบสนองในวันแรก

ภาควิชา วิศวกรรมเคมี	ลายมือชื่อนิสิต .....
สาขาวิชา วิศวกรรมเคมี	ลายมือชื่อ อ.ที่ปรึกษาหลัก .....
ปีการศึกษา 2558	ลายมือชื่อ อ.ที่ปรึกษาร่วม .....

5670260221 : MAJOR CHEMICAL ENGINEERING
KEYWORDS: ACETYLCHOLINESTERASE / BIOSENSOR / ORGANOPHOSPHATE / GOLD NANOPARTICLE / MESOCELLULAR SILICA FOAM

NITHI THANANUKOOL: EFFECT OF TEMPLATE REMOVAL METHODS ON GOLD NANOPARTICLES/MESOCELLULAR FOAM SILICA NANOCOMPOSITE CHARACTERISTICS FOR ACETYLCHOLINESTERASE IMMOBILIZATION. ADVISOR: ASSOC. PROF. SEEROONG PRICHANONT, Ph.D., CO-ADVISOR: CHANCHANA THANACHAYANONT, Ph.D., 99 pp.

This research aimed at investigating the effect of template removal methods, calcination and solvent extraction, on characteristics of mesocellular foam silica (MCF) based materials and their applications in acetylcolinesterase (AChE) biosensors. In this study, the experiments were divided into 3 parts. Firstly, efficiency of different template removal methods were tested, and the synthesized MCF-based materials were characterized. Characteristics of calcined mesoporous foam silica (MCF-c) and solvent-extracted mesoporous foam silica (MCF-e) were revealed using nitrogen sorption technique. Both the MCF-c and MCF-e were categorized as a mesoporous materials with the total surface areas of 1075 and 1221 m^2/g, and the main pore sizes of 8.1 and 6.7 nm, respectively. The FTIR data showed that these two silicas contained similar surface functional groups, and the template was successfully removed in both cases. However, the SEM and TEM pictures exhibited obvious shrinkage of the MCF-c particles which was most likely due to the damage caused by the high temperature process of calcination. Secondly, effects of template removal methods on 3-aminopropyltriethoxysilane (APTS) and in-situ addition of gold nanoparticles (AuNPs) in the based MCF materials were studied. The synthesized were in the ranges of 2-3 nm depended on the based MCF materials. With long enough Au precursor adsorption time, both AuNPs/MCF-c and AuNPs/MCF-e contained roughly similar density of AuNPs suggesting that the difference in surface silanol concentrations in both materials did not significantly affected incorporation of AuNPs at this level of precursor concentration. Further tests of AuNPs/MCF based sensors revealed higher current responses to acetylthiocholine chloride (ATCl) in the case of MCF-e than MCF-c. Suitable Au precursor concentration was determined at 0.5 mM since the CV response and AChE loading were relatively high. Thirdly, MCF-e and AuNPs/MCF-e of the suitable fabrication method were then applied in AChE biosensors for pesticide detection. The obtained biosensor was denoted as SPCE/MCF-e/AChE/Chitosan and SPCE/MCF-e/AuNPs/AChE/Chitosan. For MCF-e, the inhibition of chlorpyrifos was in the linear ranges of 0.5 to 200 ppb and 200 to 2000 ppb with detection limit of 0.894 ppb. On the other hand, for Au/MCF-e provide the linear ranges of chlorpyrifos responses were from 0.5 to 200 ppb and 200 to 2000 ppb with detection limit of 0.701 ppb. The stability of biosensor stored on MCF-e and Au/MCF-e at $4^{\circ}C$ in dry condition was good since it could retain 74.25 and 77.57 % respectively of initial current response after 30 storage days.

Department:	Chemical Engineering	Student's Signature	.....
Field of Study:	Chemical Engineering	Advisor's Signature	.....
Academic Year:	2015	Co-Advisor's Signature	.....

ACKNOWLEDGEMENTS

In the preparation of this thesis, the author would firstly like to sincerely thanks and express his sincere gratitude and appreciation to his advisor, Associate Professor Seeroong Pricahnon, for her supervision, encouraging guidance, advice, discussion and helpful suggestions throughout the course of this Master Degree study. Also, he would like to give the very grateful to his co-advisor, Dr. Chanchana Thanachayanont, for suggestions.

In addition, the author would also be grateful to Associate Professor Joongjai Panpranot, as the chairman, Associate Professor Artiwan Shotipruk and Dr. Lerdluck Keawimol as the internal and external members of the thesis committee, respectively.

The author is grateful to National Metal and Materails Technology Center (MTEC) and their official for helps in equipment, location and suggestions. Especially, many thanks to Dr. Bralee Chayasombat for all helpful, advice and suggestions as well as characteristic technique.

Special thanks to Miss Angkana Phongphut and, PhD. And Master Degree students for suggestion, advice and information, and help.

Most of all, the author would like to express my highest gratitude to my parents, my family for affectionate support, blessing, inspiration, and love which guide me all the way throughout my life and study.

CONTENTS

Page

Page

Page

Page

Page

LIST OF FIGURES

LIST OF TABLES

Chapter 1
Introduction

Mesocellular foam silica (MCF) is a type of mesoporous materials (2-50 nm in diameter) that consists of windows and cells. The windows interconnect the spherical cells and form a continuous three-dimensional pore system. Since MCF is of high surface area (500-1000 m2/g), large pore volume (0.5-1.0 cm3/g) with a large number of active sites, MCF has been applied for enzyme immobilization. The immobilized enzymes were found to exhibit the ability to maintain its activity better than those of the free enzymes. Therefore, MCF has increasingly been used as carriers for of enzyme immobilization. [1-7]

Although MCF has been reported as an excellent support for enzyme immobilization in terms of its ability to retain enzyme storage stability and activity, it still has a major disadvantage of poor electrical conductivity which hinders applications in the field of biosensors. Thus, some adjustments are needed. To overcome this problem, metallic nanoparticles have been widely incorporated into MCF to enhance support conductivity [8-10]. Gold nanoparticles are high stable, have excellent electrical conductivity, good biocompatibility and considered to be strong material discovered [11]. To improve adsorption capacity of gold precursor on MCF surface, grafting of amine functional group(s) onto MCF by silanation method is necessary [12]. However, it was well known that the methods used for removal of template considerably affect the surface silanol groups of the prepared sorbents [13]. Some reports [14, 15] revealed that different template removal methods (extraction and the calcination methods) led to high quality large-pore samples with increased pore volume and pore size as well as enhancement regarding functional group loading on porous surface.

In this research, we present the synthesis and characterization of gold nanoparticles/mesocellular foam silica using different template removal methods, and applied as an acetylcholinesterase immobilization matrix for biosensor applications.

1.1 Objective

To investigate the influence of template removal methods on AuNPs/MCF characteristics and its application for acetylcholinesterase (AChE) immobilization.

1.2 Research scope

The research will be focused on comparisons of characteristics and potential applications as enzyme carriers between two types of MCF synthesized using different methods for template removal (solvent extraction and calcination).

1. The two types of as-prepared MCF will be grafted with excess amount of (3-Aminopropyl)triethoxysilane (ATPS)

Characterization techniques: BET, SEM, TEM. FTIR and TGA

2. The modified MCF from 1. will be adsorbed with varied amounts of gold precursor (0.1-10 mM) and ultrasonicate at 40 kHz for 120 min to incorporate AuNPs in the pores of MCF

3. The obtained AuNPs/MCF in 2. Will be tested for AChE immobilization and investigate enzyme loading, reaction, and stability.

    - The reaction of interest is enzyme inhibition from chlorpyrifos
    - An amperometric method will be used to follow enzyme activities

1.3 Expected benefits

1. To obtain the immobilized acetylcholinesterase on gold nanoparticles/mesocellular foam silica which high activity and stability

2. To obtain a good feature of acetylcholinesterase bioreceptors

Chapter 2

Theoretical backgrounds and literature reviews

2.1 Biosensor

Biosensor is an analytical and detectable device for determining the concentration of substrate or other parameters of biological interests by using principles of chemistry, biochemistry and electrochemistry. A biosensor has 3 main components which are a biological element, a transducer and a processing system. Mechanism of a biosensor is as the following **Figure 2.1** below;

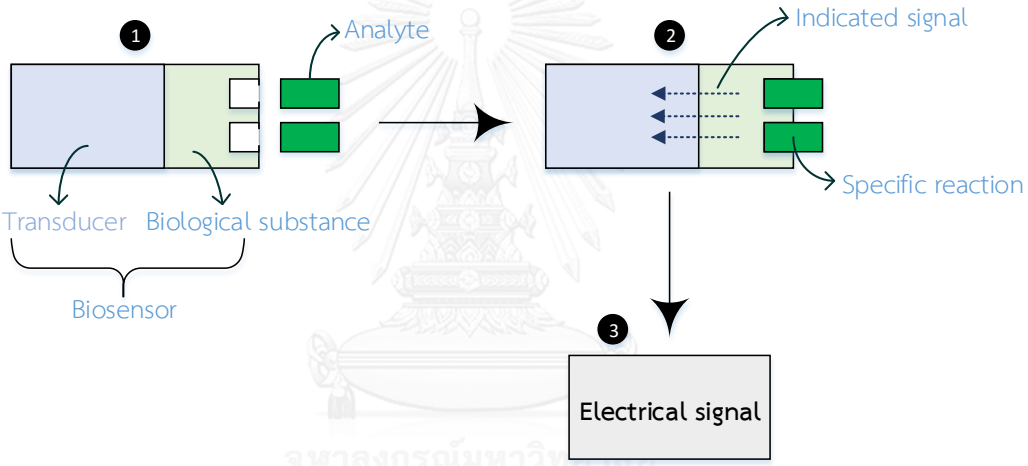

Figure 2.1 Principle of biosensor

The biological element such as enzyme, cells, antibodies and microorganisms is a component which is highly selective to a specific analyte. These biological components generate the signal when it reacts with the target analyte. The generated signal could be in the form of ion, electron, heat, gas, or mass change which is detectable by the transducer.

The transducer or detection device then converts the observable change of biological signal into measurable signal. The usual response utilized in analyses is electrical signal which magnitude would be proportional to the concentration of the substance or analyte specific to the biological element.

The electrical response then got converted to digital signal in the processing system and processed in microprocessors. Finally, the processed signal is then displayed on the output monitor, which can be used to calculate analyte concentration unit by the user.

Amperometric enzyme biosensors

Amperometric biosensors are one of the most popular types of biosensors, containing biological elements which commonly are enzymes specific to the target analyte. After the sample was processed by the enzyme, there would be electron transfer on the electrode surface. The transducer then converts these electron transfers to total electrical change generated by reaction between enzyme and sample. The electrical change can be used to indicate the amount of target solution analyte. This type of biosensor utilizes 3 electrodes in the same electrochemical cell which consists of a working electrode, a reference electrode, and a counter electrode. As the enzyme-generated product can be oxidized or reduced on the working electrode, the analysis technique is about applying voltage to the working electrode, affecting electron transfer reaction and the products which would bring about changes in electron transfer rate. If the change in transfer rate is detectable, it would then be converted to electrical current by the transducer, which would be relatable to the concentration of the sample.

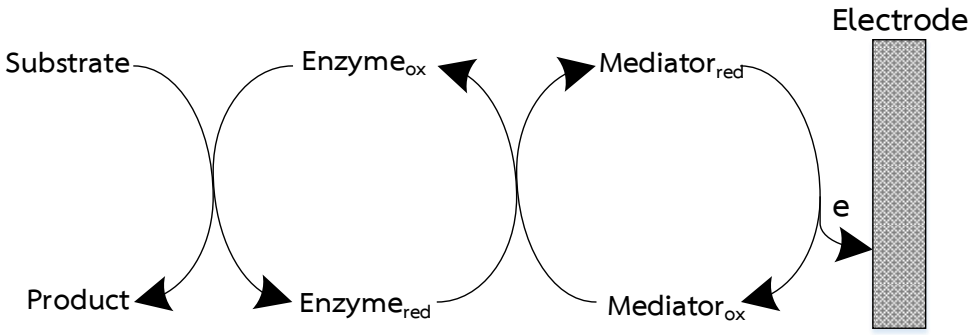

Figure 2.2 electron transmission procedure of oxidation-reduction both enzyme and electron approach to electrode surface [16]

As shown in **Figure 2.2**, electron transfer at the electrode surface is obtained from either oxidation or reduction reaction of enzyme in its oxidized state, which convert the substrate into product. This mechanism would reduce the enzyme, which in turn transfer its electrons to the mediator to return itself to equilibrium (oxidized) state. The reduced mediator, when applied the optimal voltage, would transfer its electron to the electrode and change back to the oxidized state. This chain of occurrences will result in electrical signals detectable by the transducer, which the amount of current corresponds to the concentration of target analyte.

2.2 Electrochemical method

2.2.1 Cyclic voltammetry (CV)

Cyclic voltammetry is an electrochemical analysis involving applications of revolving electrical potential between 2 voltage values on the working electrode, which would induce electron transfer reactions on the electrode surface, generating current. The current responses can then be detected by an electronic circuit, arranging the result into pattern called cyclic voltammetry as displayed in **Figure 2.3**.

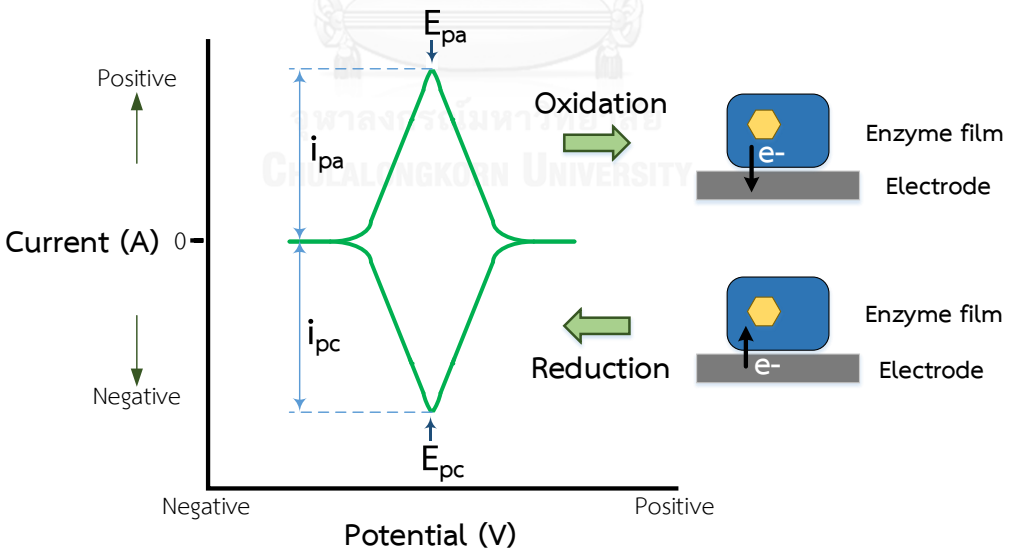

Figure 2.3 Character of detectable signal from cyclic voltammetry method [17]

Figure 2.3 shows that the anodic peak potential (E_{pa}), anodic peak current (i_{pa}) or oxidation current occurr because positive potential is applied. Anodic current occurs when the working electrode becomes an adequately strong oxidant. On the other

hand, when the scan direction is switched to the negative potential for the reverse scan, the electrode becomes a strong reductant, creating a cathodic peak (E_{pa}), cathodic peak current (i_{pc}), or a reduction current. This method has been applied in field of biosensor to investigate and find optimal potential that result in highest current possible, using experimental scan between anodic and cathodic potential values.

2.2.2 Amperometry

The Amperometry is an electrochemical analysis, operates at a constant potential to investigate the current variation in time. In biosensor applications, this method is used to differentiate the amount of current which occur from current changes between current of no sample addition, initial current (I_1), and after adding the sample to the new steady state, new equilibrium current (I_2). Differential current can be calculated as follows (Equation 2.1) [18] ;

$$\Delta I = I_1 - I_2 \qquad (2.1)$$

Where amount different of Current (ΔI) correspond to sample concentration which need to be detected. The mechanism of measurement can be described as **Figure 2.4**.

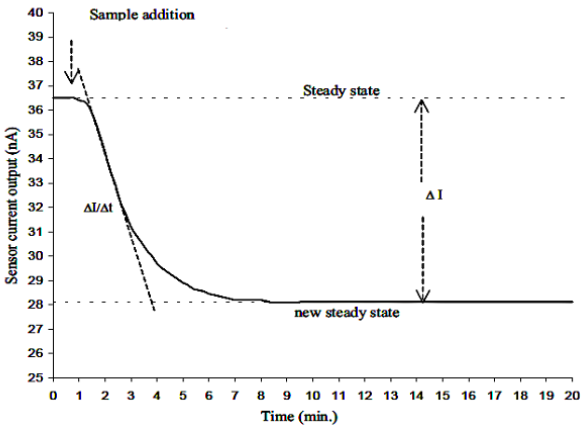

Figure 2.4 Character of detectable signal from amperometry method [18]

2.3 Pesticides

Insecticides are kind of pesticide which can be classified as further organophosphate, carbamate, cypermatrin, pyrethroid, and organochlorine.

Insecticides are widely used in agriculture despite environmental and human health hazard due to their effectiveness on insects. Even at low levels, pesticide residues can still be harmful to human being [19]. Research on detection and identification of pesticides that are contaminated in food can be detected via a biosensor. The most frequently used pesticide are organophosphate and carbamate groups, which their pesticide detection was based on the principle of acetylcholinesterases and cholinesterases inhibition.

2.3.1 Organophosphate

The organophosphorus (OP) compounds are one of the largest groups of insecticides in use today and the have largely replaced the organochlorine insecticides. It has short toxicity period as it degrade rapidly around 2 weeks to 6 months, depends on the climate and temperature. Accordingly, it was used for crops in short planting and harvesting [20]. However, they are generally the most toxic of all insecticides to insects and vertebrates (with some exceptions) by inhibiting cholinesterase. These are still being used in many areas of the world for the control of agricultural insect pests [21].

The OP compounds have two distinct features: firstly, they are acute toxicant of high level of activity, and, secondly, they are chemically unstable, or non-persistent, and are quite biodegradable by most organisms and in environment. These qualities make them useful as substitutes for persistent organochlorines for control of insect pests on agriculture and public health.

The toxicity of this insecticide, symptoms of poisoning in humans roughly follow general pattern of nerve poisoning, i.e., restlessness, hyper excitability, tremors (especially of the extremities), convulsions, paralysis, and death. The symptoms appear slowly and death may occur after several hours or up to 24 h. The ultimate cause of death is not certain but is regarded to be the results of cholinesterase inhibition by analogy with mammalian poisoning. In most insect species cholinesterase inhibition by OP compounds is not reversible [21].

2.3.2 Carbamate

This is the mostly used insecticides, and also an organophosphate. The toxicity and effects are similar to the previous group. However, its degradability is higher than OP compounds. Both OP and C can also inhibit acetylcholinesterase in the same mechanism but C is shortly activate than OP. This group apply to homoptera insects in soil. The insecticides in this group such as carbofuran, methomyl, methiocarb and carbalyl.

2.3.3 Illness from pesticides

The symptoms of poisoning in vertebrates, the toxicity of OP insecticides is due to their ability to inhabit the viral enzyme cholinesterase. Signs and symptoms of acute poisoning by OP insecticides are those of simulation of acetylcholine receptors in parasympathetic nervous system, such as sweating, salivation, urination, defecation, lachrymation, nausea, vomiting, abdominal cramps, constriction of pupil (miosis), slowing of the heart (bradycardia), and drop in blood pressure (hypotension) [21].

2.4 Acetylcholinesterase

Acetylcholinesterase (AChE, EC 3.1.1.7) is an enzyme, extracted from an electric eel. It is a serine esterase that belongs to the hydrolase category of enzymes. Its structural protein is of globular shape which has molecular size approximately 45 x 60 x 65 Å, molecular weight of 280 kDa, and isoelectric point of 5.5 [22]. AChE apply for inhibiton effects. When the analyte is not present in solution, the substrate acetylthiocholine is converted into thiocholine and acetic acid. Thiocholine is oxidized by the applied voltage. In the presence of an inhibitor, conversion of acetylthiocholine is decreased or even nullified [23]. The principle of an electrochemical biosensor base on AChE and oxidation of thiocholine is shown in Equation 2.2 and 2.3, indicating electrochemical reactions involved in response measurement. Moreover, the anodic oxidation current is inversely proportional to the concentration of pesticides in samples and the exposed time as well. The procedure of the preparation of AChE biosensor and pesticide detection is as shown in Equation 2.3 [24].

$$\text{Acetylthiocholine chloride} + H_2O \xrightarrow{\text{AChE}} \text{Thiocholine} + \text{Acitric acid} \quad (2.2)$$

$$2\text{Thiocholine}_{(red)} \xrightarrow[\text{Voltage}]{} \text{Thiocholine}_{(ox)} + 2H^+ + 2e^- \quad (2.3)$$

Furthermore, AChE is specific to organophosphate and carbamate which are a kind of pesticide mostly used in agriculture. These two pesticide groups can inhibit AChE in order to decrease catalytic hydrolysis, therefore, AChE is used investigating device for detection. This is called AChE biosensors.

2.5 Acetylcholinesterase inhibition

The principle of pesticide detection, AChE contained on the surface of the electrode reacts in the cell with acetylthiocholine chloride, a modified substrate, to give thiocholine. The analysis is done by measuring the current rising in the circuit by electrocatalytic oxidative dimerisation of thiocholine to dithiocholine. In common condition, the potential can be applied to reach the thiol oxidation. After the first measurements, the electrode is immersed for anytime in the sample solution containing OP or CA; this will inhibit a portion of the enzyme. When the incubation is carried out in samples, a long contact time between the electrode and sample can lead to the denaturation of the enzyme, while short contact time would result in decreased sensitivity. The second measurement is done by adding acetylthiocholine chloride to reaction cell at the same electrode which produces lower increase of electron current on the circuit and a lower response. The difference between both rising currents, before and after the inhibition, would be proportional to concentration of OP in the sample solution. A scheme of the theoretical curve is given in **Figure 2.5**. The inhibition is then calculatable by the following Equation 2.4 [25] :

$$\text{Inhibition}(\%) = \frac{\Delta I_1 - \Delta I_2}{\Delta I_1} \times 100 \quad (2.4)$$

Where ΔI1 is the difference between both steady state currents before and after the addition of the substrate acetylthiocholine chloride; ΔI2 is the same difference between both steady state currents after the incubation with the sample.

Consequently, inhibition percent is directly related to sample concentration of pesticide. It can identify concentration of sample solution, therefore, the concentration increase, inhibition percent is also increased, respectively.

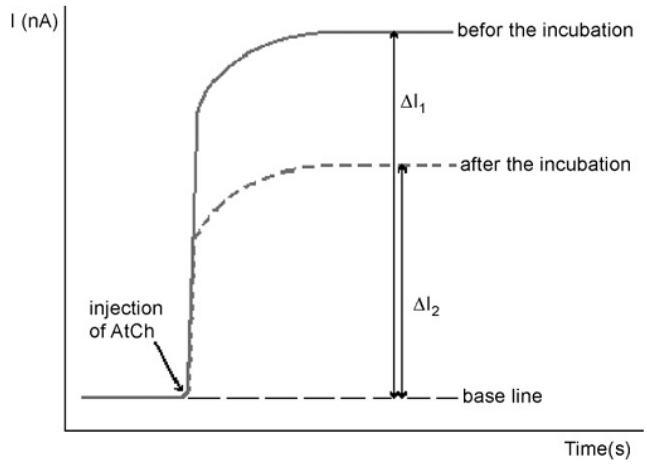

Figure 2. 5 Relation of current response and time of biosensor; before incubation and after incubation. [25]

2.6 Mesocellular Foam Silica

Mesoporous silica is an inorganic material with high porosity (Pore size of up to 100 Å), large surface area of 1,000 m^2/g, large pore volume of 1 m^3/g and orderly structure [26]. Different types of mesoporous silica such as MCM-41, SBA-15 and HMS have been widely studied and used as catalyst supports for various incorporations [27, 28]. The International Union of Pure and Applied Chemistry (IUPAC) classified the porous materials by using the internal pore width (diameter) as a criteria. Therefore, porous materials can be divided into 3 types; micropore (diameter < 2 nm), mesopore (diameter 2-50 nm), and macroporous (diameter > 50 nm). Consequently, mesoporous materials are classified as nanoporous materials owing to their diameters are in the range of nanosize (1-100 nm) [6].

Regarding functionality of mesoporous materials as host matrices for various enzyme immobilizations, the primary advantage of the immobilization process is its preservation of enzyme behavior in regard to its native form. It is worth referring that

immobilization of enzyme result in significant changes of its properties including catalytic activity, optimum pH conditions, thermal and storage stability. In general, the activity of enzyme decreases, but its stability would also increases after the immobilization process. The reusability of immobilized enzyme is also a very important parameter to determining its potential applications. This aspect is defined as operational enzyme stability after multiple reuses as catalyst and subsequent recover and reuse [29]. The most useful porous silica materials in regard of biosensor applications is the mesoporous-type, consisting of 3D pore structure of large cells interconnected by narrow windows. This model had presented enhanced performance as a support for immobilization of macromolecules and which have diameter in range of 2-50 nm due to suited size correspond to enzyme size in range of 2-20 nm [30, 31].

Silica encapsulation presents remarkable stability to the encapsulated enzyme with regard to both operational stability (reverse during catalysis) and inherent catalytic stability (resistance to denaturation). Butyryl-cholinesterase (BuChE), for instance, shows superior thermal stability when encapsulated in silica nanospheres. The immobilized enzyme displayed enhanced resistance to denaturation at upper temperature conditions that led to rapid denaturation of the native enzyme. The enzyme Immobilization in biosilica demonstrated especially versatile and suited systems for screening drug potency and for development of organophosphate detection system [32-34].

The synthetic mesoporous silica are used in various applications. It has different structures and pore sizes such as FSM-16, MCM-41, MCM-48, SBA-15 and MCF [28, 35]. The difference of them are pore structure and pore size. Chi et al. [36] synthesized MCM-41, MCM-48 and SBA-15, pore size was obtained 2.9, 2.3, and 5.5 nm, respectively. Wilawan et al. [37] synthesized MCM-41, SBA-15 and MCF, obtained pore size of 3.2, 5.4 and 14.6 nm. The schematic diagrams representing pore structure of various mesoporous silica are MCM-41 has a hexagonal structure and dimentional cylindrical pore, next, SBA-15 is similar to MCM-41 but it has larger pore size than MCM-41 about 6-15 nm. And the last one is MCF, which has cubic shape and the largest pore size at all. When compare to pore size of each materials, it can be summarized as MCF>SBA-15>MCF-41 respectively, as shown below in **Figure 2.6**.

The difference of materials pore size are also used in enzyme immobilization, as it affect the stability of enzymes. Insertion of horseradish peroxidase (HRP) into porous materials such as MCM-41, SBA-15 and MCF, which have pore size of 3.2, 5.4 and 14.6 nm, showed that the immobilized enzyme can be stored up to 6 weeks at 4°C and room temperature. MCF can kept the highest activity of 90%, while MCM-41 and SBA-15 were just at 60% [37], which correspond to a study by Orita et al. [38] regarding cholesteryl ester hydrolase (EC 3.1.1.13) immobilization in mesoporous materials such as MCM-41, SBA-15 and MCF, which have pore sizes of 2.7, 9.5 and 22.5 respectively. **Figure 2.7** shows that MCF gave high activity, effectively retain enzyme stability, and has less effect to activity of enzyme when compare other materials. Immobilized enzyme appeared to have decreased enzyme activities when compared to non-immobilized enzymes. However, it is better in long-term as mesoporous materials can protect the enzyme from its surrounding environment, which could rapidly degrade unprotected enzymes.

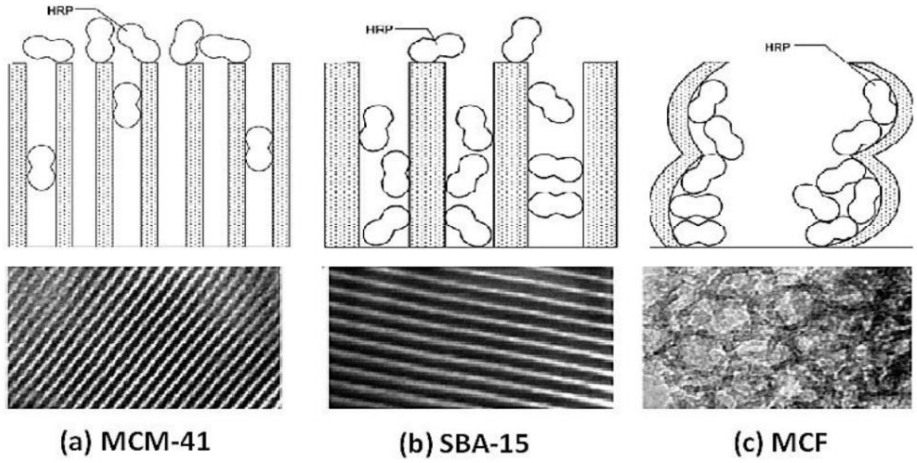

Figure 2.6 Schematic diagram of porous structure and TEM images n (a) MCM-41, (B) SBA-15 and (c) MCF. [37]

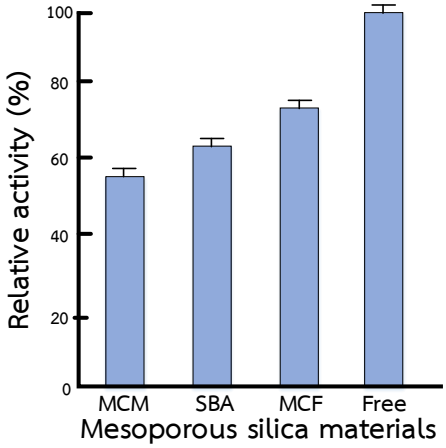

Figure 2.7 Relative activity of various mesoporous silica materials compare with free enzyme [38]

2.6.1 The synthesis of mesoporous silica

The synthetic method including 3 main procedures are micelle chemistry, sol-gel process and drying and calcination. The chemical precursors are used to synthesis including (1) Inorganic materials are major structure and silica source for instance sodium silicate and tetraethyl orthosilicate, (2) Structure-directing agents act as template in order to specify pore structure of mesoporous silica for example cetyltrimethyl ammonium bromine (CTAB), sodium dodecyl sulfonate (SDS) and pluronic P123 and finally (3) solvent such as ethanol and water.

In the synthetic procedure, firstly, the micelle chemistry; structure-directing agent (e.g. pluronic P123) is dissolve in the solvent (e.g. water or ethanol) which is polar molecule. The structure-directing agent will attach each other as group and arrange around non-polar molecule orderly, then occurs as various structural shape such as spheres, oval and rod depend on amount of structure-directing agent in the solvent. Next, the inorganic material which source of silica (e.g. tetraethyl orthosilicate) is added in homogenous solution containing structure-directing agent and solvent. This silica source will attach with structure-directing agent, it is called sol-gel process which initiate from hydrolysis occurs the solid particle called sol). These solid particles aggregate as network and became the gel, via condensation polymerization. Finally, the gel is dried about 100°C and next calcined at temperature approximately 500°C under oxygen or air atmosphere in order to eliminate contaminant such as water,

unstable cation and anion as well as structure-directing agent which is the organic agent. Subsequently, the inorganic porous stricture or mesoporous silica is obtained after high heating process [39].

For instruction of synthesis has described above. They illustrate the different selection in inorganic materials, solution, condition and the others for the specific type of synthetic mesoporous silica as shown in **Table 2.1**.

Table 2.1 Physical characteristics of mesoporous silica materials.

Type	Structure-directing agent	Source of silica	Catalyst	Surface area (m2/g)	Pore size (nm)	Pore volume (cm3/g)	Ref.
MCM-41	CTAB	TEOS	NaOH	888	3.20	0.84	[37]
	CTAB	SiO2	H2SO4	1194	2.65	0.98	[40]
	CTAB+P123	TMOS+TEOS	NH3	1174	2.70	1.10	[38]
	CTACl+EAc	TEOS	Na2SiO3	1045	3.76	0.91	[41]
	CTAB+	SiO2	TMAOH	1490	3.32	0.99	[42]
SBA-15	P123	TEOS	HCl	798	5.40	1.06	[37]
	P123	TEOS	HCl	801	6.42	1.12	[40]
	CTAB+P123	TMOS+TEOS	NH3	656	9.50	1.30	[38]
	P123	TEOS	HCl	518	10.8	1.10	[43]
	P123	TEOS	HCl	894	8.50	1.06	[44]
MCF	P123+TMB	TEOS	HCl	618	14.60	1.60	[37]
	P123+TMB	TEOS	HCl	537	26.0	1.02	[45]
	P123+TMB	TEOS	HCl	840	15.30	1.16	[40]
	CTAB+P123+TMB	TMOS+TEOS	NH3	618	22.50	2.30	[38]
	P123+TMB	TEOS	HCl	700	21.5	1.95	[46]

Note CTBA: Cetyltrimethyl ammonium bromine

P123: Poly(ethylene glycol)-B-poly(propylene G)

TMB: 1,3,5-trimethylbenzene

TEOS: (Tetraethyl orthosilicate)

TMOS: Tetramethoxysilane

2.6.2 Effect of characteristics of mesoporous foam silica

2.6.2.1 Structure-directing agents

In this factor focused on swelling agents and surfactant which affected to characteristics and particle of mesoporous foam silica such as pore volume, pore diameter, surface area as well as cell and window diameters [4, 47-50] . Oda et al. [49] synthesized mesoporous foam silica by the conventional method. In a typical procedure, the dissolution of 1,3,5-trimethylbenzene (TMB) variation. They had found that the increasing the ratio of TMB/P123 led to the case of the change on pore size and surface area distributions. As shown in **Table 2.2**, shows the values for S_{BET} and V_p is considered to have a uniform structure in order to find the optimum template for the synthesis.

Table 2.2 Mesostructural characteristics of MCF-Silica [49]

Silica	TMB/P123 (w/w)	$2R_p$(ads) nm	$2R_p$(des) nm	S_{BET} M^2/g	V_P M^3/g
S1	0.5	16	9.8	619	3.3
S2	1.0	24	9.8	477	2.3
S3	1.5	24	10	769	3.0
S4	2.5	30	14	569	2.3

In Jamalluddin et al. [48] study, had investigated variation in the amount of TMB. They had found the TMB ratio with surfactant had significantly influenced the physical appearance of the mesostructured silica materials as can be seen in **Figure 2.8 (a)–(d)**, confirmed that an appropriate ratio of TMB/P123 could play a significant role in transforming the desired shape of mesoporous silica. Furthermore, based on the TEM images as shown in **Figure 2.9**, indicated that the addition of TMB at any amount into the synthesis solution caused a dramatic change in the mesophase with the development of mesostructures.

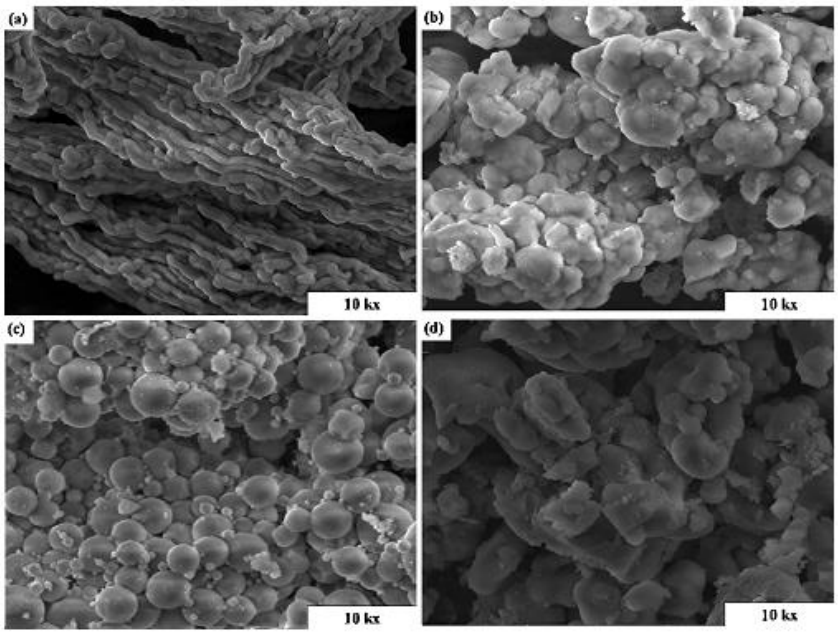

Figure 2.8 SEM images of MCF materials prepared with different TMB dosage (a) S0, (b) S1, (c) S2 and (d) S3. [48]

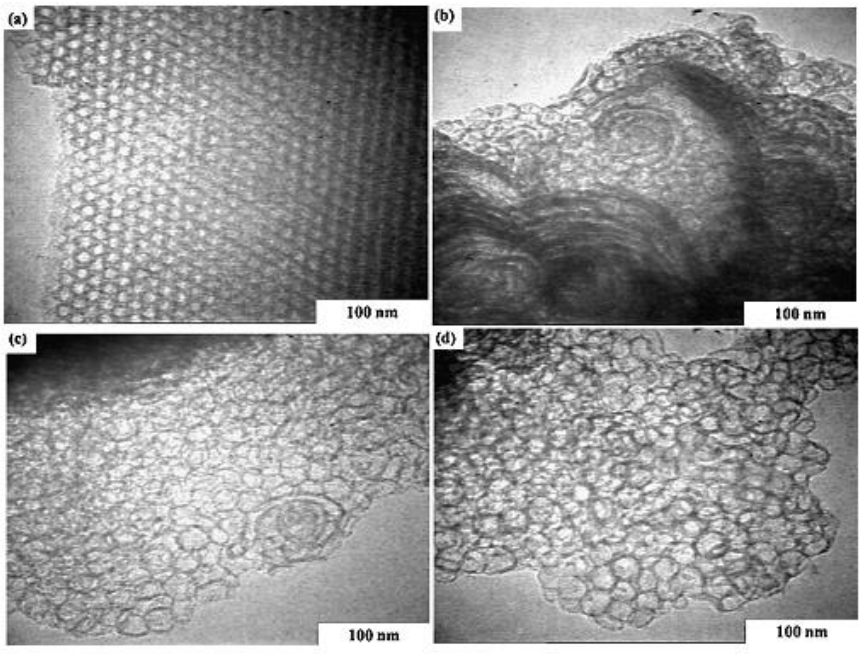

Figure 2.9 TEM images of MCF support prepared with different TMB dosage (a) S0, (b) S1, (c) S2 and (d) S3. [48]

2.6.2.2 Thermal processes

This effect has studied regarding effect of thermal procedures (e.g. hydrothermal aging, calcination and steam treatment) lead to the changes of characteristics of mesoporous foam silica. Li et al. [51] had studied hydrothermal stability of mesostructured cellular silica foams, found that the used temperature and time of hydrothermal aging had affected to the mesostructural silica, can be seen this **Figure 2.10**.

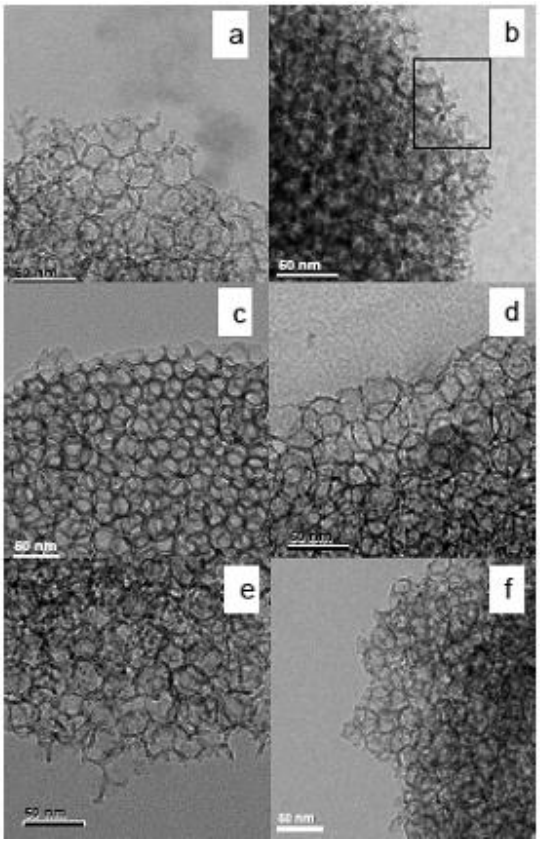

Figure 2.10 TEM images of MCF-1 aging70°C (a), MCF-2 aging100°C (b), MCF-3 aging130°C (c), MCF-4 presenceKCl (d), MCF-5 aging100°C cal700°C (e) and MCF-6 aging100°C cal900°C (f). [51]

Moreover, from Mokaya [52] et al. study, had investigated regarding the hydrothermal aging of MCM-41 and found that variation of aging time had affected to MCM-41 shape as shown in **Figure 2.11**, led to the change of shapes due to the increasing aging time had affected to increase the crystallization times in aging process. Han et al. [53] studied effect of calcination process on porous silca in calcination

process. As **Table 2.3**, they found that the high temperature influence to surface area, pore size as well as pore volume of mesocellular foam silica.

Table 2.3 Characteristic of different porous silica materials [53]

	Pore siza (nm)	Window size (nm)	S_{BET} m^2/g	Pore volume (cm^3/g)
MCF calcine at 550°C	21.0	10.5	701	1.65
MCF calcine at 900°C	13.5	9.5	590	1.30

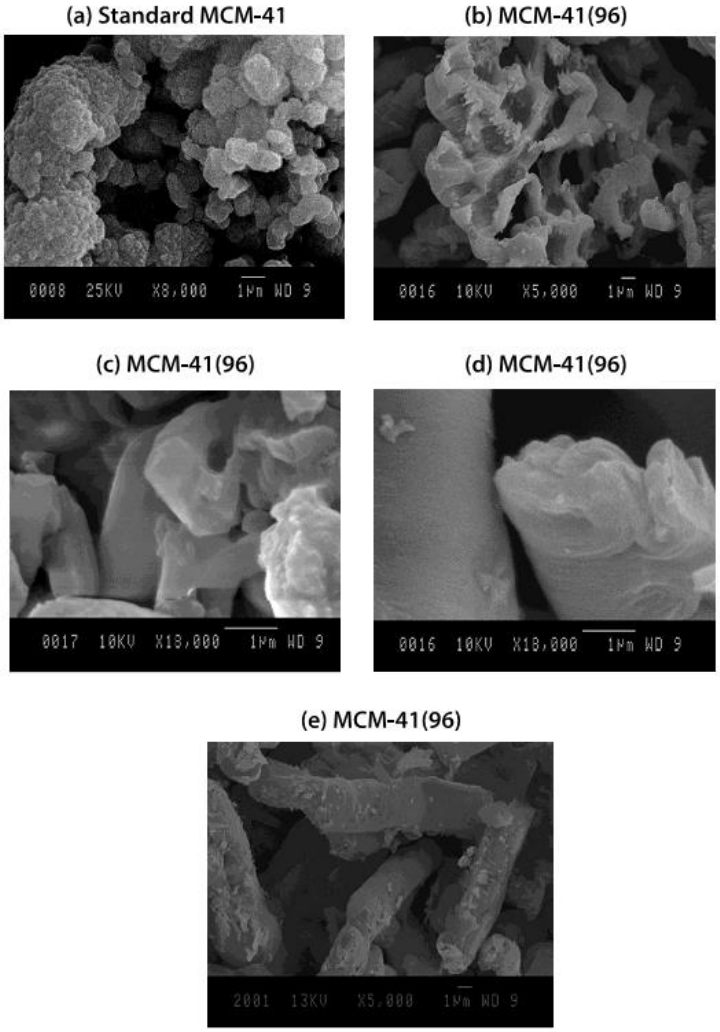

Figure 2.11 Representative SEM micrographs of (a) standard MCM-41 and (b-c) MCM-41 at aging time of 48, 96, 120 and 144 s respectively. [52]

2.6.2.3 Methods for template removal

This topic has investigated template removal by calcination or ethanol extraction that affected to characteristics of mesocellular foam silica. Yao et al. [54] had researched regarding calcination and ethanol extraction, were proved to be able to remove the template P123 from as-synthesized MCF to prepare mesoporous MCFs as the supports of amine-grafted composite sorbents as shown in **Figure 2.12**. It was found that removal template methods has affected to graft the amine group on MCF surface. Moreover, the textural properties have significantly changed of porous surface after grafting with amines follow in **table 2.4**.

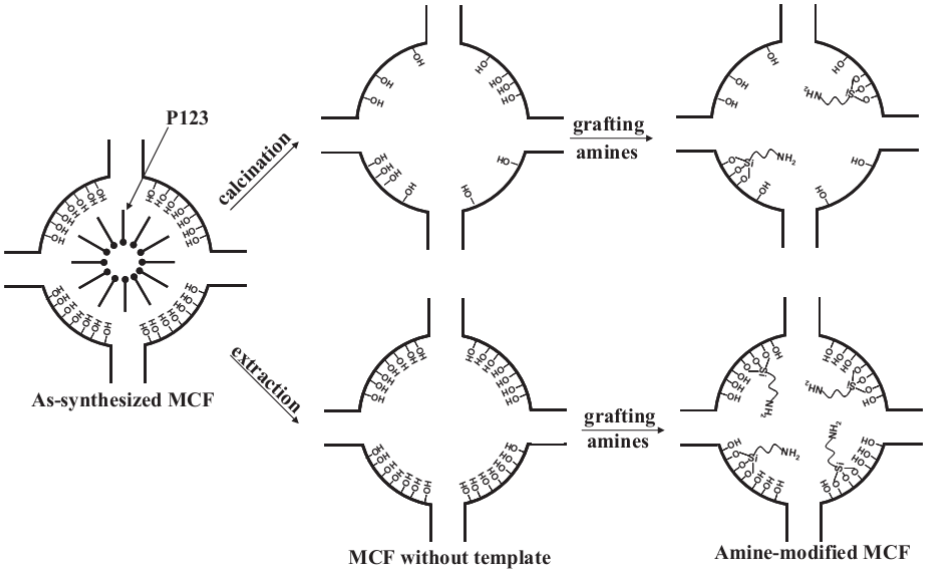

Figure 2.12 Schematic representation of the removal of template from as-synthesized MCF and the amine functionalization on MCF surface. [54]

2.6.2.4 Additives

This topic regading the important additive in order to improve the regular cell shape of mesocellular foam silica. From many report found that inorganic mineralizing agent as ammonium fluoride, was the dominant agent for enlarge pore size and improve irregular shape problem of mesocellular foam silica [47, 53, 55-57]. The synthesis is similar to conventional method, except that ratio of template/surfactant as 1 and ammonium fluoride was added to solution prior to aging. Ping et al. [56] has investigated the synthesis of MCF support, had a high surface area

of 720 m^2/g, and a very large mesopore volume of 3.0 cm^3/g. The pore size analysis of the MCF shown large mesopore cell diameter of 39 nm with interconnecting windows of approximately 17 nm, providing lower internal diffusion resistance than other typical porous supports. This synthetic method resulting SEM and TEM images as shown in **Figure 2.13**.

Table 2.4 Textural properties for MCF materials before and after grafting amines.

Sample	S_{BET} (m^2/g)	Pore volume (m^3/g)	Cell diameter (nm)	Window diameter (nm)	Amine content (mmol/g)
MCF-c	650	1.84	21.4	11.1	-
APS-MCF-c	441	1.44	21.4	11.1	1.72
APMS-MCF-c	371	1.36	21.5	11.1	2.73
MCF-e	573	1.85	21.4	13.4	-
APS-MCF-e	381	1.34	21.4	11.1	2.47
APMS-MCF-e	338	1.26	21.4	11.1	3.23

Note c: Calcination process

E: Ethanol extraction process

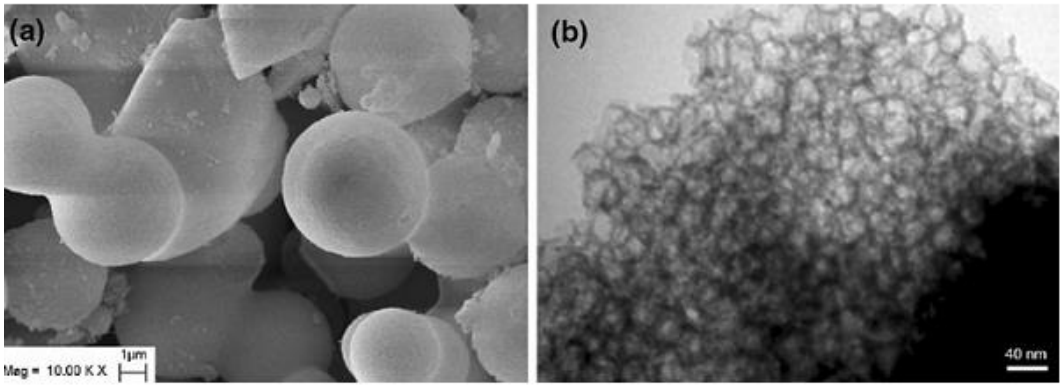

Figure 2. 13 (a) SEM and (b) TEM images of MCF support, showing a small particle size and foam-like pore structure [56]

2.7 Enzyme immobilization method

Enzyme immobilization is introduced by adhere the enzyme on another phase with any reaction such as chemical binding or non-chemical binding in order to improve limitations of free enzyme for instance unstable, impurity sensitive and denaturation from extreme condition (e.g. pH, temperature and solution concentration). In various immobilizations which can found improving to increase the stability of enzyme whether aspects of operating stability or storage stability directly regarding to heat from system. But nonetheless, the immobilization has mainly had any weakness that is decrease of activity effect or catalytic performance of enzyme as well as it probably occur from the loss of enzyme catalytic or mass transfer performance which in both of problems have affected to limitation of reaction rate.

Enzyme immobilization can perform numerous method, it is separated 2 main methods that are immobilization (e.g. binding to carrier and cross-linking) by binding and immobilization by physical retention (e.g. matrix entrapment and membrane) as shown in **Figure 2.14**.

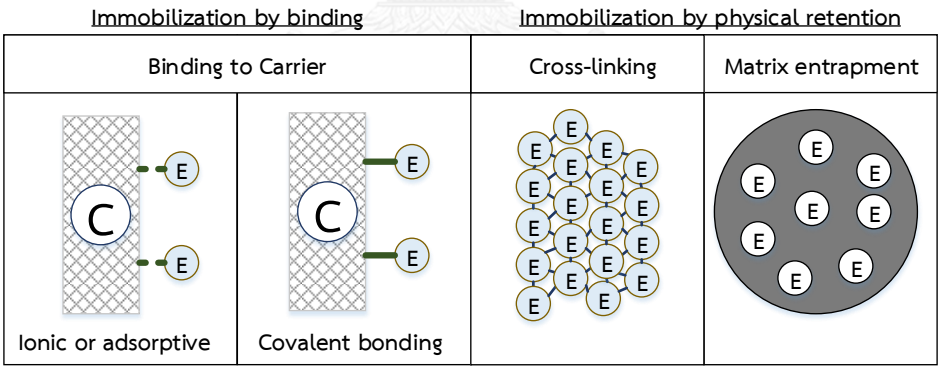

Figure 2.14 Classification of enzyme immobilization methods; E: Enzyme and C : Carrier [58]

2.7.1 Immobilization by binding

2.7.1.1 Physical adsorption method

The physical adsorption method for the immobilization of enzyme is based on the physical adsorption of enzyme protein on the surface of water-insoluble carriers or materials. This method often causes little or no conformational change of

the enzyme protein, or destruction of its active center. Accordingly, if a suitable carrier or material for the target enzyme is found, this method may be both simple and effective. However, this method has the dis advantage that the adsorbed enzyme may leak from the carrier during utilization, because the binding force between the enzyme protein and carrier is weak. As carriers for this method, inorganic materials such as activated carbon, porous glass, acid clay, bleaching clay, kaolinite, alumina, silica gel, bentonite, hydroxylapatite and calcium phosphate gel, as well as natural polymers such as starch and gluten, have been employed.

2.7.1.2 Ionic binding method

The ionic binding method is based on the ionic binding of enzyme protein to water-insoluble carrier containing ion-exchange residues. In some cases, not only ionic binding but also physical adsorption may take part in the binding. Consequently, in section, cases in which ionic binding appears to play a more important role than physical adsorption are described. As carriers for binding, polysaccharide and synthetic polymers having ion-exchange residues are used. The binding of enzyme to be carrier is easily carried out, and condition are mild in comparison with those necessary for the covalent binding method. Therefore, the ionic binding method causes little or no changes of confirmation and active site of the enzyme protein, and yields immobilized enzymes having high carriers are less strong than in covalent binding, leakage of enzyme from the carrier may occur in substrate solutions of high ionic strength or upon variation of pH.

2.7.1.3 Covalent binding method

The covalent binding method is based on the binding of enzyme to carriers by covalent bonds. Among the various carrier-binding methods, most study have utilized this method. The functional group that take apart in covalent binding of enzyme to carrier are as follow amino, carboxyl, sulfhydryl and phenolic group. The selection of conditions for immobilization by covalent binding is more difficult than in cases of physical adsorption and ionic binding. The reaction conditions required for covalent binding are relatively complicated and not particularly mild. There, in some

cases, covalent binding alters the conformational stricture and active center of enzyme, resulting in major loss of activity and/or changes of substrate specificity. However, the binding force between enzyme and carrier is strong and leakage of the enzyme does not occur even in presence of substrate or salt solution of high ionic strength.

2.7.1.4 Cross-linking method

This immobilization method is based on the formation of chemical bonds, as in covalent binding method, but water-insoluble carriers are not used in this method. The immobilization of enzymes is performed by the formation of intermolecular cross-linking between the enzyme molecules by means of bi- or multifunctional reagents. As cross-linking reagents, glutaraldehyde, isocyanate derivatives, bisdiazobenzidine, *N,N'*-polymethylene bisiodoacetoamide and *N,N'*-ethylene bismaleimide have been employed. The cross-linking reactions are carried out under relatively serve conditions, as in the case of covalent binding methods. Thus, in some cases, the confirmation of active center of the enzyme may be affected by the reaction, leading to significant loss of activity.

2.7.2 Physical retention

This is entrapping method is based on confirming enzymes in the lattice of polymer matrix or enclosing enzymes in semipermeable membranes, and can be classified into the lattice and microcapsule types. This method differs from the covalent binding and cross-linking methods in that the enzyme itself does not bind to the gel matrix or membrane. Thus, this method may have wide applicability. However, if a chemical polymerization reaction is employed for entrapping, relatively serve condition are required and loss of enzyme activity occurs in some cases. Therefore, it is necessary to selection the most suitable conditions for the immobilization of various enzymes.

Generally, the selection of immobilization method must consider from suitable work. Moreover, the other factors concluding cost, retention time and catalytic performance of enzyme immobilization, have been investigated. For this work, we

choose ionic binding method for enzyme immobilization due to the main point of work to improve the effective and extend the storage time of biosensor. This method selection resulting that this ionic binding cannot occur the loss of enzyme activity, simple preparation and low lost. It is considerable when compare with other methods as shown in **Table 2.5**.

Table 2.5 Preparation and characteristics of immobilized enzymes [59].

Characteristic	Carrier binding method			Cross linking method	Entrapping Method
	Physical adsorption	Ionic binding	Covalent binding		
Preparation	easy	Easy	difficult	difficult	difficult
Enzyme activity	low	High	high	moderate	high
Substrate specificity	unchangeable	unchangeable	changeable	changeable	unchangeable
Binding force	weak	moderate	strong	strong	strong
Regeneration	possible	possible	impossible	impossible	impossible
General applicability	low	moderate	moderate	low	high
Cost of Immobili-zation	low	Low	high	moderate	low

2.8 Enzyme immobilization on mesoporous silica materials

A suitable carrier is of critical importance for the activity of immobilized enzyme [6]. The chemical and physical properties such as surface area, functional group, surface charge pore size, morphology and stability of carriers must be considered for effective enzyme immobilization.

In this decade, mesoporous silicas which possess the pore diameters in the range of 2-50 nm have strong potential for applications as carriers for biomolecules. This is because they are of ordered and uniform size, adjustable pore size, large surface area, chemical and mechanical stability, and resistance to microbial attack [6, 60, 61].

The chemical properties demonstrate surface properties such as the functional groups and surface charge of carriers. The different carrier materials possess the different function groups and charge on their surface. The interaction of the enzyme and carrier depended strongly on the nature of the functional groups that attached to the surface [62]. The interactions may result in the activity, leaching, and stability of immobilized enzyme. The interactions between enzyme and surface of mesoporous silica by adsorption as described in paragraph following.

2.8.1 Hydrogen bond

Hydrogen bond is the attractive force between one electronegative atom and a hydrogen covalently bonded to another electronegative atom. It results from a dipoledipole force with a hydrogen atom bonded to nitrogen, oxygen or fluorine (thus the name "hydrogen bond". In the case of enzyme immobilization, because of the functional group properties on silica surface, the silanol groups are suitable for the physical adsorption of enzyme molecules by hydrogen bonding. As shown in **Figure 2.15**, the hydrogen bond is occurred by the hydrogen atom of amino groups or carboxylic groups of enzyme bind with the hydrogen atom of silanol groups. Nevertheless, the hydrogen bond is weak interaction, resulting in the immobilized enzyme is easy to leach. In addition, Chong and Zhao et al. [63] found that hydrogen bonding brought about the penicillin acylase slowly adsorbed into the mesoporous silica [63].

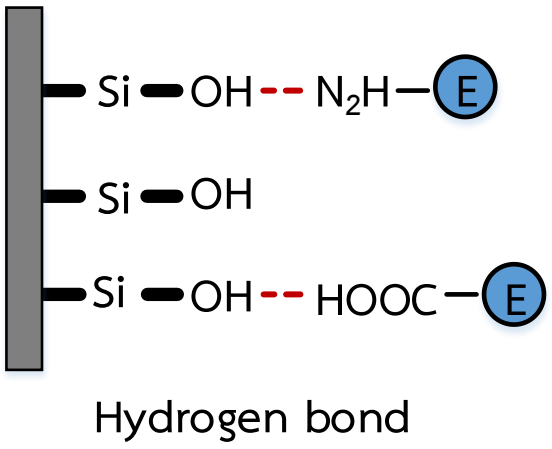

Figure 2.15 Hydrogen bond between enzyme and silica surface [63]

2.8.2 Hydrophobic interaction

The hydrophobic interaction is the interaction between organic molecules. The hydrophobic and hydrophilic properties of carrier surface have more affect to the adsorption of some proteins on mesoporous silicas than electrostatic interaction [64, 65]. The hydrophobic properties of silica surface can be enhanced by functionalization with organosilanes. The hydroxyl groups of silica surface are co-condensation with organosilanes as will be more explained later in section 2.9. The hydrophobic interaction between enzyme and silica surface is shown in **Figure 2.16** This surface modification can enhance the interaction between enzyme and silica surface and also increase the electrostatic charge of enzyme and silica surface [63].

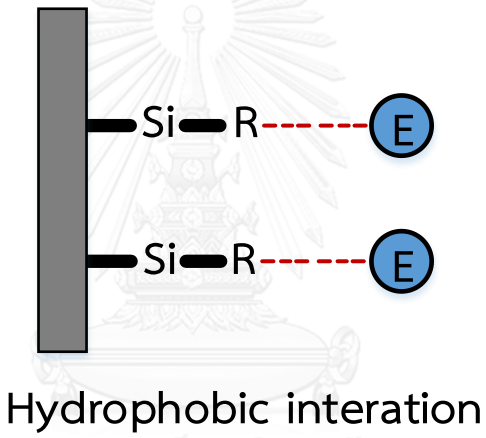

Figure 2.16 Hydrophobic interactions between enzyme and silica surface [63]

2.8.3 Electrostatic interaction

Electrostatic interaction is the charge action of enzyme and silica surface (**Figure 2.17**). It depends on many factors including; (1) charge properties of enzyme and carrier considered from their isoelectric point (pI), (silica surface has pI approximately 2) (2) surface functionalization of silica with chemical [66] (3) template type e.g. cat-ionic surfactant provided more negative charges of silanol group on the silica surface. Appropriately, enzyme absorbed more on silica carrier surface prepared from cat-ionic surfactant than nonionic surfactant [67].

Focus on pH of enzyme solution (containing phosphate buffer) during immobilization, net charge difference between enzyme and carrier is obtain, this will

influence their electrostatic interaction. Furthermore, this interaction depends on pI of enzyme and carrier. Loading and adsorption rate of enzyme on mesoporous silica materials was faster when pH value of enzyme solution was lower than its pI [63]. For instance, at pH value of 3.4 highest activity of immobilized Chloroperoxidase (CPO) absorbed on mesocellular foam silica (MCF) was observed [68]. As this pH, enzyme had a negative net charge while MCF had a positive charge. Resulting in an electrostatic interaction was obtained. However, reduced enzyme activity was observed at lower pH value, due to strong binding of enzyme and MCF which caused inactive of enzyme. Chloroperoxidase was unabsorbed on mesocellular foam silica when enzyme solution with pH 5 was used because both enzyme and mesocellular foam silica had negative charges.

In addition, ionic strength is one factor that influences to adsorption of enzyme. It was found that the adsorption of enzyme and protein when exhibited a high amount of ion in buffer solution was reduced [60, 64].

Chouyyok et al. [37] immobilized the horseradish peroxidase (HRP) on 3 types of mesoporous silica including MCM-41, SBA-45 and MCF. The pI of mesoporous silica has around 2 and horseradish peroxidase around 8.9 and using enzyme solution with pH 8. They found that horseradish peroxidase could be absorbed on mesoporous silica when enzyme solution with pH 8 was used because the enzyme exhibited as positive charge due to enzyme had the pI value is higher than pH of enzyme solution. Furthermore, the MCF also had negative charges based on the pI value that is lower than pH of enzyme solution as well.

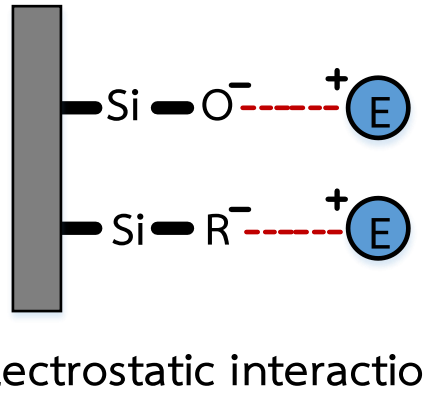

Figure 2.17 Electrostatic interaction between enzyme and silica surface [64]

2.9 Gold nanoparticles (AuNPs)

The investigation of acetylcholinesterase/mesocellular foam silica for pesticide detection. The mesocellular foam silica act as the support for enzyme immobilization in terms of the ability to retain enzyme storage and catalytic activity. Nonetheless, the major drawback of mesocellular foam silica for biosensor application is poor conductivity. The overcome this problem, metal nanoparticles have been attached on the support surface for the enhancement of electron transfer. Gold nanoparticles (AuNPs) are most stable metal nanoparticles, of goods electron conductivity, and high biocompatibility as well as gold nanoparticles could improve in term of poor electron transfer and assist for detection of acetylcholinesterase biosensor.

2.9.1 Gold nanoparticle properties

First, the gold core is essentially inert, non-toxic, and biocompatible, making it an ideal starting point for carrier construction. Secondly, gold nanoparticles with a wide range of core sizes (1–150 nm) can be fabricated easily with controlled dispersity. Gold nanoparticles can be readily fabricated with sizes commensurate with biomolecules such as enzymes and DNA, facilitating their integration into biological systems. Furthermore, the high surface area-to-volume ratio of nanoparticles (NPs) provides dense loading of functionalities incorporating targeting. For example, approximately 100 ligands are covalently conjugated to gold nanoparticles. Finally, the highly tunable and multivalent surface structures of gold nanoparticles offer the diversity to incorporate multiple biomacromolecules by covalent or non-covalent conjugation on the surface of a nanoparticle [69].

From consider regarding the gold nanoparticle advantages with enhance the performance in biosensor applications in terms of conductive property, acts as the excellent mediator. For Ahiriwal et al. [70] studied the direct electrochemistry of horseradish peroxidase (HRP) coupled to gold nanoparticles using electrochemical techniques. Gold nanoparticles capped with glutathione and lipoic acid was covalently linked to HRP. The immobilized HRP/AuNPs displayed good electrocatalytic response with good sensitivity and without any electron mediator. The covalent linking of HRP and gold nanoparticles did not affect the activity of the enzyme significantly. They

prepared the covalent coupling process using (1-ethyl-3-(3-dimethyl aminopropyl) carbodiimide hydrochloride (EDC) generally involves two steps, one is activation of the carboxylic acid group and next step involves the amide bond formation between the activated carboxylic groups of one species with amino group of the other as shown in **Figure 2.18**, they found that the property of pH dependent precipitation of AuNP was utilized for the crosslinking of HRP and AuNP, at acidic pH the free carboxylic group is activated by EDC.

Bioconjugated gold nanoparticles are synthesized from the negative charge on the gold nanoparticles, (arising from [AuICl2] on the surface of the particle) having an affinity for proteins that are positively charged at neutral or physiological pH. Some proteins, namely; enzymes, antibodies and DNA, can adsorb strongly to colloidal gold to form stable conjugates with the enzymes retaining its biological property. The adsorption of enzymes to gold particles is non-covalent process based on three separate but dependent phenomena such as ionic interaction between the negatively charged nanoparticle and the positively charged sites on the enzyme; hydrophobic attraction between the enzyme and the metal surface; and co-ordinate binding between the metal and the conducting electrons of nitrogen and sulphur atoms of the protein as shown in **Figure 2.19**.

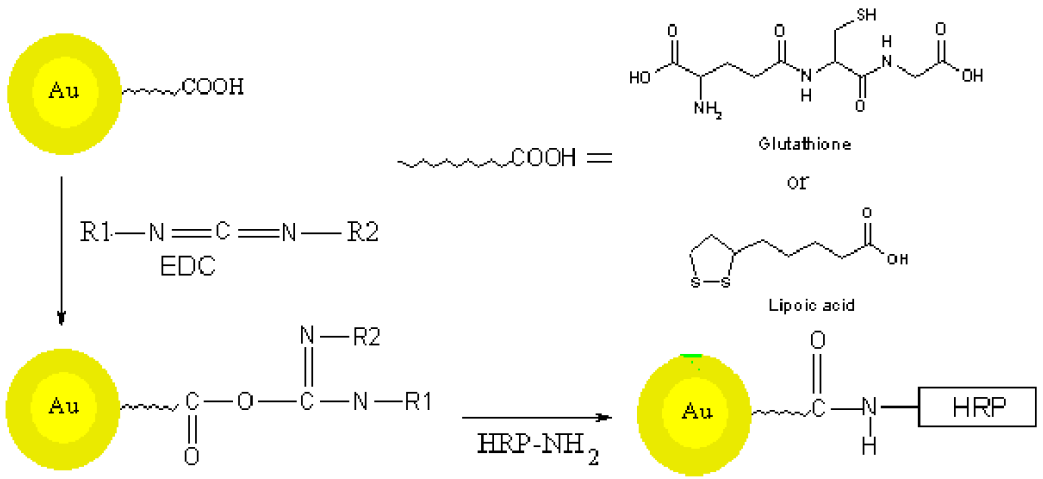

Figure 2.18 Schematic representation of the covalent coupling of HRP to capped AuNP [70].

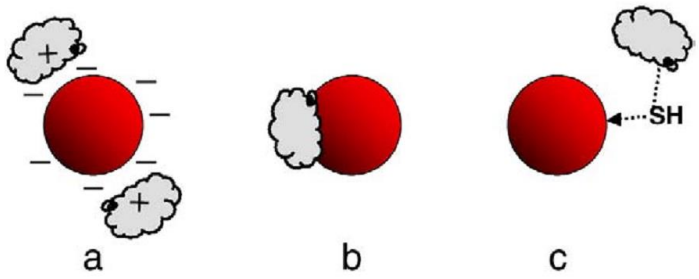

Figure 2.19 Schematic diagram of enzyme adsorption onto gold nanoparticles conjugation; (a) ionic interaction, (b) hydrophobic attraction and (c) dative binding. [71]

2.9.2 Synthesis of gold nanoparticles

The synthesis of gold nanoparticles could produce by reducing the gold ions (Au^{3+}) into the gold atoms (Au^{0}) [72]. The gold ions are prepared by chloroauric acid ($HAuCl_4$) as the precursor, and the reducing agent probably is reducing agent or free radical. For this topics presented the synthesis method of gold nanoparticles, separate to two methods including chemical reduction method and ultrasonic irradiation.

2.9.2.1 Chemical reduction method

Chemical reduction method is one of the methods for synthesize the gold nanoparticles, the reduction reaction occurs by reducing agent in order to reduce gold ions (Au^{3+}) into the gold atoms (Au^{0}). In mostly used reducing agent as strong acid such as sodium borohydride ($NaBH_4$) and trisodium critrate ($Na_3C_6H_5O_7$). The particle size of gold atom depend on ratio of gold ions/reducing agent in synthetic solution which the gold ions are most obtained from chloroauric acid ($HAuCl_4$). Petersen at el [73] synthesized gold atom by using the reducing agent as trisodium critrate ($Na_3C_6H_5O_7$) which the reaction mechanism can see at reaction 2.5, 2.6 and 2.7 respectively below;

$$Na_3C_6H_5O_7 \xrightarrow{H_2O} C_6H_5O_7^{3-} + 3Na^{3+} \quad (2.5)$$

$$3C_6H_5O_7^{3-} + 2Au^{3+} \rightarrow 2Au + 3C_5H_4O_5^{2-} + 3CO_2 \quad (2.6)$$

$$3C_5H_4O_5^{2-} + 16Au^{3+} \rightarrow 16Au + 15CO_2 \quad (2.7)$$

This synthesis of gold nanoparticles is simple method. On the other side, it has any disadvantage which the synthesis obtained strong acid residue form

reducing agent. For Petersen at el [73], they reported the effect of strong acid in gold synthesis, it could generate the anions on gold particle surface as sown in **Figure 2.20**.

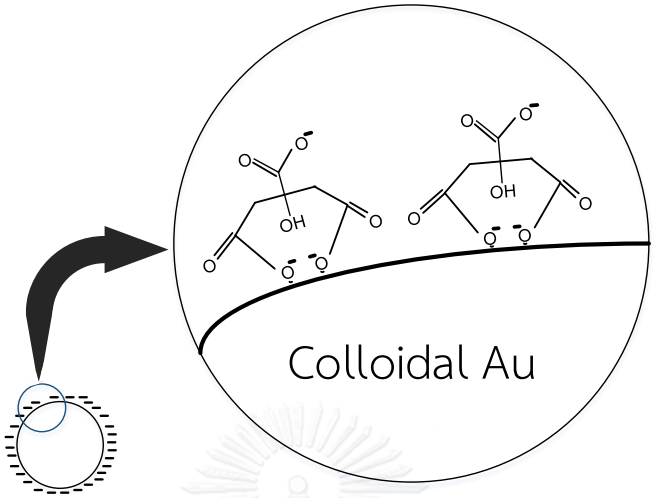

Figure 2.20 The effect of synthesis by using strong acid as reducing agent. [73]

2.9.2.2 Ultrasonic irradiation

This synthesis employs the free radicals to reduce gold ions into gold atom. The reaction mechanism is shown below;

$$M^{n+} + \text{reducing radicals} \longrightarrow M^0 \quad (2.8)$$

$$n(M^0) \longrightarrow M_n^0 \quad (2.9)$$

For the reduction of gold ion (Au^{3+}) to generate into gold atom (Au^0), can operate by apply the frequency in chloroauric acid ($HAuCl_4$) solution. This applied frequency is able to produce bubbles in the solution, and next the bubble dispersion will spontaneously produce thermal decomposition of water (H_2O) in order to generate hydrogen radicals (H•) and hydroxyl radicals (OH•) which as the reducing radicals react with the gold ions rapidly. The reaction mechanism is shown below;

$$H_2O \longrightarrow H\bullet + OH\bullet \quad (2.10)$$

$$Au^{3+} + \text{reducing rediacals} \longrightarrow Au^0 \quad (2.11)$$

$$n(Au^0) \longrightarrow Au_n \quad (2.12)$$

Both of these methods are able to reduce the gold ions in order to synthesize gold nanoparticles/mesoporous silica nanocomposites. By the time, when

consider regarding the effect of acid residue on gold nanoparticles in chemical reduction method, found that the ultrasonic irradiation method is quite interesting due to it has no the effect of residue for reducing agent, and this method is controllable the distribution of gold particles on mesoporous silica, it depend on applied frequency, duration time and concentration of chloroauric acid [ref].

2.9.3 The synthesis of gold/mesoporous silica nanocomposites

According to the application of mesoporous silica in biosensor, it promotes the stability of enzyme in order to preserve the performance of device. However, it has any disadvantage in term of electron transfer property, therefore, it is crucial to improve the problem because the electrochemical methods need to mainly employ the performance of electron transfer. Consequently, the gold nanoparticles (AuNPs) is needed to employ as co-synthetic material caused gold nanoparticles can provide the satisfying properties in term of the conductivity which further promote electron transfer, in addition, it can improve the performance of acetylcholinesterase biosensor as well.

Chen et al. [74] synthesized gold nanomaterial in mesoporous silica (SiO_2) by using ultrasonic irradiation and the precursor was used in synthesis as chloroauric acid, in order to obtain the nanocomposites of gold nanoparticles and mesoporous silica (AuNPs/MPS). Initially, mesoporous silica was immersed in chloroauric acid ($HAuCl_4$) solution in stirring system around 24 hours for employing the gold attach on mesoporous surface. Subsequently, the ultrasonic irradiation was used for reduce gold ions (Au^{3+}) from gold chloride ($AuCl_4^-$) into gold atoms (Au^0) which adhere on mesoporous silica surface. The expected reactions can be shown in reaction 2.13, 2.14, 2.15 and 2.16 where H• and •OH radicals originated due to vibration decomposition of H_2O with intense frequency as shown in reaction 2.13. Reaction 2.14 indicates the formation of strong reducing radicals $(CH_3)_2C$•OH via hydrogen abstraction from the isopropanol by H• and •OH hydroxyl radicals. Multivalent $AuCl_4^-$ ions in the pores were reduced rapidly by multistep radical reactions and subsequently the Au atoms aggregated, as shown in reactions 2.15 and 2.16 [74].

$$H_2O \xrightarrow{\text{Ultrasonic irradiation}} H\bullet + \bullet OH \quad (2.13)$$

$$H\bullet(\bullet OH) + (CH_3)_2CHOH \rightarrow (CH_3)_2C\bullet OH + H_2(H_2O) \quad (2.14)$$

$$3(CH_3)_2C\bullet OH + AuCl_4^- \rightarrow Au + 3(CH_3)_2CO + 4Cl^- + 3H^+ \quad (2.15)$$

$$nAu^0 \rightarrow (Au^0)_n. \quad (2.16)$$

Resulting from synthesis of gold nanoparticles in mesoporous silica from chen et al. [74] experiment by ultrasonic irradiation for 120 minutes, found that the observation of the as-prepared Au/SiO2 mesoporous composite is shown in **Figure 2.21a**. It indicated that nearly spherical-shaped Au particles are dispersed uniformly in amor-phous silica. The histogram of the particle sizes (**Figure 2.21b**) exhibits a narrow size distribution with a mean particle diameter of 5.2 nm.

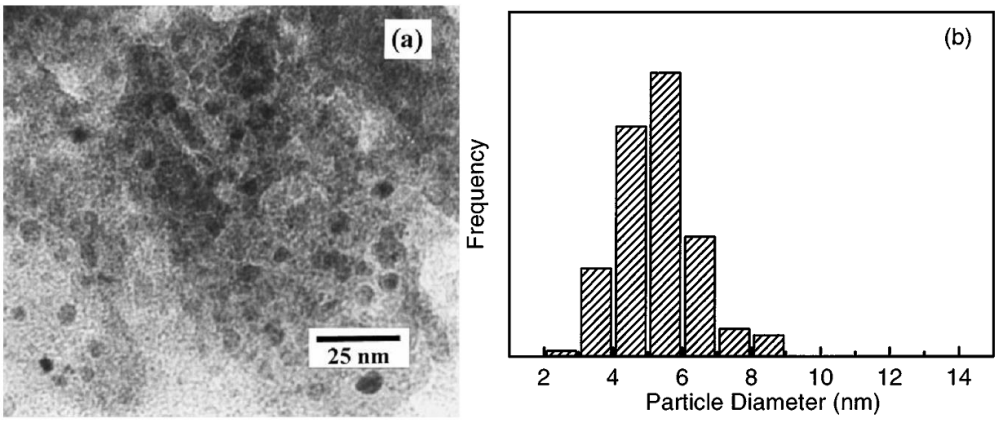

Figure 2.21 (a) The morphology micrograph of the as-prepared Au/SiO2 Mesoporous composite. (b) Size distribution histogram of the gold particles within the pores of the mesoporous silica. [74]

For the synthesis of gold nanoparticle/mesoporous silica (AuNPs/MPS). Firstly, the mesoporous silica was immersed in chloroauric acid solution in order to adsorb the gold ions on mesoporous silica surface before chemical reduction process for converting gold ions into gold atom adhere the surface. The most problem was encountered during adsorption process that is the mesoporous silica perform to slight adsorb the gold ions and spend the long duration time for adsorb gold ions for 3 weeks (from Chen et al. work [74]), since the physical property of mesoporous silica including

silanol group (Si-OH) cover on the surface which exhibits the negative charge, it is hard to attach with the gold ion which exhibits the negative charge as well. To overcome this problem, it must improve and develop the adsorption process of gold ions on mesoporous silica surface by using functional ligand, it can improve silica surface bring about the suited functional group for adsorb the gold ions and promote the positive charge on the porous surface, is able to better attach with the negatively charged gold ions. The charged surface of mesoporous silica can determine by zeta potential, from **Table 2.6** show the functionalization of MSPs for determine percent gold loading.

Gutiérrez et al. [10] modified the silica surface with organic functional groups (commonly named grafting) prior to the gold loading, has been a surface-engineering strategy to promote the interaction between the frequently used $HAuCl_4^-$ gold precursor and the mesoporous silica support, which lead to avoid the mobility and aggregation of the AuNPs on the silica surfaces. After functionalization, the MSP adsorb easily the $AuCl_4^-$ ions, by the formation of a monolayer of positively charged groups on the pore surface. Upon calcination or chemical reduction with NaBH4, the metallic gold precursor evolves in highly dispersed metal gold nanoparticles (AuNPs). The general procedure to synthesize gold catalysts following this approach, summarized in **Figure 2.22**, consists normally of two general steps: (i) the funtionalize of the stabilizing ligands into the inner surfaces of the mesoporous silica material; and (ii) the gold loading. The first step consists in the reaction of a suitable organic functional group (usually organosilanes containing amine or thiol groups) with the mesoporous silica support using an appropriate solvent (normally toluene or ethanol) in a refluxing system under nitrogen. The resulting solids are subsequently recovered by filtration, washed with the solvent and dried. In the second step, the functionalized MSP are dispersed in a yellow solution of the gold precursor (commonly $HAuCl_4^-$) under vigorous stirring. Then, the solution turns colorless, while the solids become yellow, indicating that the ion-exchange between the gold precursor solution and the functionalized MSM support has been attained. After filtration, the gold catalysts are washed with abundant deionized water to remove the residual chloride ions, dried and subsequently calcined to remove the functional ligands, and to reduce the

oxidized Au^{3+} species to metallic Au^{0} gold particles strongly attached to the support. The gold nanoparticle/mesoporous silica nanocomposites prepared under this approach, can also be reduced in H_2 or chemically using $NaBH_4$ solution.

Table 2.6 Comparison of various functional ligands in functionalization of mesoporous including MAM-41, SBA-15 and MCF in order to increase percent of gold loading.

Support	Functional ligand	Au Precursor	Au loading (%wt)	Au size (nm)	Ref.
MCM-41	-	$HAuCl_4$	0.13-1.21	-	[75]
	-	$HAuCl_4$	1.3	20	[76]
	MPS	$HAuCl_4$	3.2-2.5	3.2±0.5	[77]
	APS	$HAuCl_4$	3.1-3.2	3.4±0.5	[77]
	APS	$HAuCl_4$	5.0	3.9±0.7	[78]
	APS	$HAuCl_4$	4.0	5.1	[36]
SBA-15	-	$HAuCl_4$	1.0	3.0-8.0	[79]
	-	$HAuCl_4$	0.77	-	[75]
	MPS	$HAuCl_4$	3.0	2.7-6.4	[80]
	MPTS	$HAuCl_4$	4.53	6.5	[81]
	APS	$HAuCl_4$	4.0	5.8	[36]
	APTS	$HAuCl_4$	6.0	3.0-5.0	[82]
MCF	$C_{10}H_{23}ClSi$	$HAuCl_4$	15.0	4.0	[83]

Note APS: 3-Aminopropyltrimethoxysilane

APTS: 3-Aminopropyltriethoxysilane

MPS: 3-Mercaptopropyltrimethoxysilane

MPTS: 3-Mercaptopropyltriethoxysilane

$C_{10}H_{23}ClSi$: Chlorodimethyloctylsilane

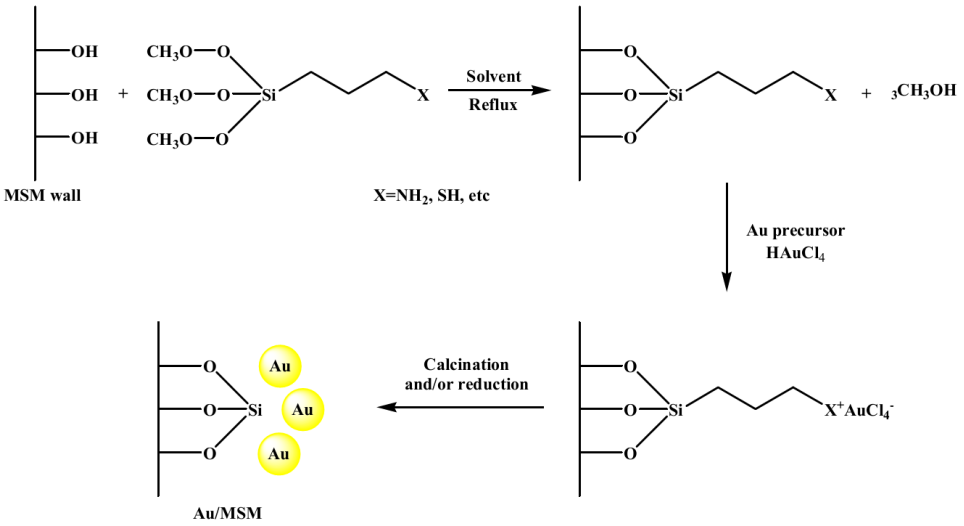

Figure 2.22 General procedure to synthesize AuNPs-MPS nanocomposites initiate from functionalization, next adsorption of gold chloride ions ($AuCl^-$) and reduction [10].

Ashayer et al. [8] synthesized gold nanoparticles on nanosilica particle by using ultrasonic method, and compare 2 functional ligands such as 3-aminopropyltrimethoxysilane (APTMS) and polydiallyldimethyl ammonium chloride (PDADMAC) for functionalization on silica surface. These functional ligands provide the different electric surface property, can determine from the zeta potential measurements. They found that zeta potential measurements also showed a higher value for PDAD-MAC whereas APTMS showed a lower value (**Figure 2.23**).

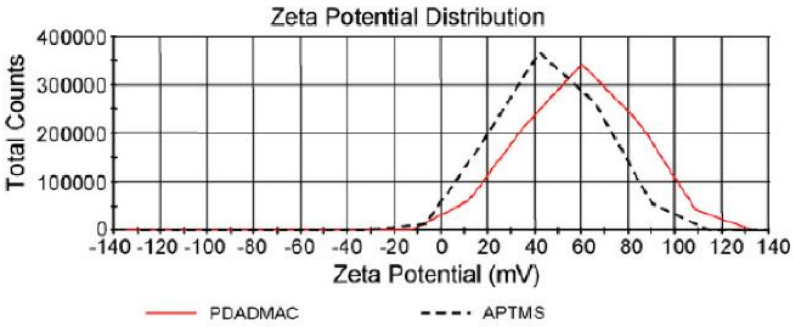

Figure 2.23 The comparison of potential values between APTMS and PDADMAC (Functional ligands). [8]

Therefore, higher level of adsorption of negatively charged gold on the surface of silica could be due to the higher level of positively charged group of PDADMAC on the surface of silica in comparison with APTMS. It can be seen that when using the

optimum amount of linkers, the PDADMAC/silica particles (**Figure 2.24a**) gives more coverage than APTMS/silica particles (**Figure 2.24b**). The coverage for the PDADMAC/silica nanoparticles in the nucleation stage was found to be approximately 40% whereas the APTMS/silicananoparticles give coverage of approximately 25%.

Subsequently, the synthesis obtained gold nanoparticles/mesoporous silica composites, it is employed on electrode surface for biosensor application. The chitosan is one of biopolymers which act as the connector between gold nanoparticles/mesoporous silica composites and immobilized enzyme. It is be able to strong attach on electrode surface and prevent the enzyme leaching. The properties of chitosan are reviewed in the next topic

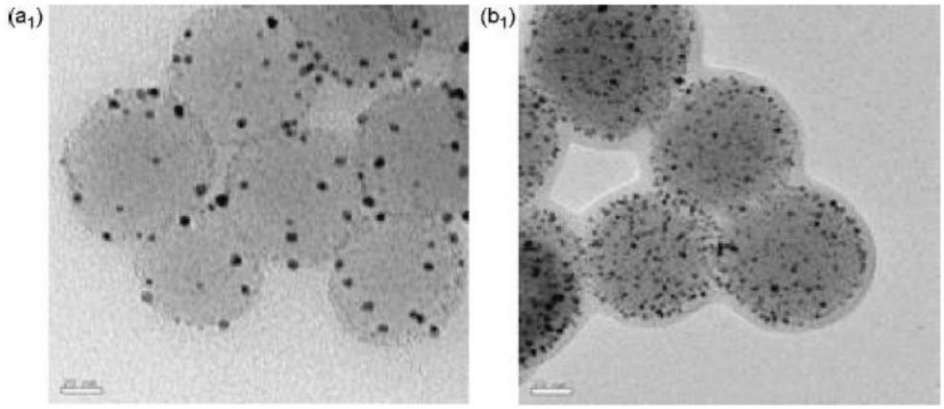

Figure 2.24 TEM micrographs of attachment of gold nanoparticles to silica particles and nanoshell formation at optimum quantity, i.e. using (a_1) APTMS and (b_1) PDADMAC with scale bar of 20nm. [8]

2.10 Chitosan

The Chitosan is one of biopolymers, its type is polycationic polymer which containing the units of D-glucosamine. The structural of chitosan was shown in **Figure 2.25**. Chitosan is natural extract, commonly it was mainly obtained from crustacean group such as shrimp and crab or insect group. The good properties of chitosan are degradable material, non-toxicity and biocompatibility. In biosensor application, it was used in binding between immobilized material and electrode surface. Moreover, Chitosan included amine group which can adhere alkyl group of enzyme [84]. And the

chitosan particles showed improved immobilization capacity for enzyme and good biocompatibility for preserving the activity of immobilized enzyme [85].

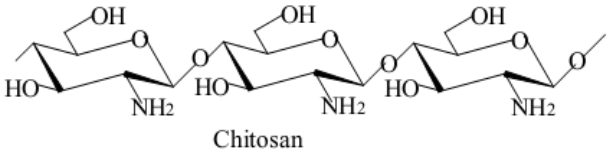

Figure 2.25 Structure of chitosan. [86]

Ngnamak et al. [46] investigated biosensor application for pesticide detection of malathion and used chitosan as binding materials for covering enzyme immobilization on mesoporous silica on electrode surface. In modified matrix containing prussian blue layer is mediater which promotes electron transfer and cover on The first layer screen-printed carbon electrode (SPCE) and next layer, chitosan used for binding with mesoporous silica , immobilized acetylcholinesterase (AChE). The Selection of Chitosan in biosensor found that it can perfectly bind and cover with other materials, simplified synthesis or ease to use, good biocompatibility with enzyme and low cost, unless, it have any disadvantages such as poor conductivity, nevertheless, this advantage can improve by modifying and cooperating with other materials; e.g. gold silver conducting-polymer or even prussian blue which was used cooperate with chitosan in this work.

2.11 Performance factors and Effect of parameters of electrochemistry

2.11.1 Performance factors

The performance factors are effective test of biosensor in order to testify the capability and ability in the operation of this detection device. The elementary properties of the detection device can explain to;

2.11.1.1 Linear range

The Linear range, it means performance of detection device in substance analysis which affect to the analysis from device. It has linear relation which correspond to concentration of sample concentration on identified range of concentration. The range of linear can be determined from plotting the relation

between the signal (vertical axis) and the concentration of analyte (horizontal axis) by using linear equation. In the part of range, mean that range of concentration of analyte since maximum until minimum concentration which device is detectable, provide values of accuracy and precision in exact and acceptable points.

2.11.1.2 Limit of detection (LOD)

Limit of detection is the lowest concentration which can be measured. It can be found by a plot of the relation between signal identifier (e.g. % inhibition) and analyte concentration which measurable value absolutely has acceptable to accuracy and precision. Generally, LOD is amount of substance which generate the signal around 10 times of noise.

2.11.1.3 Sensitivity

Sensitivity is performance factor, detect relation of response and concentration change in order to observe response ability of detection device. The value of sensitivity can be calculated by the slope of calibration plot between R = f(c) or S = dR/dc and C; where R is detectable signal response related to concentration of desired sample (C), it obtain to linear plot (R = kc). The slope can explain performance of sensitivity, thus, if the high value of slope, it can confirm to high sensitivity for detection device.

2.11.1.4 Selectivity

The selectivity is performance on analyte detection in contaminant sample. This is study in order to investigate effect of the other substance that probably affect to disturb detection, however, this detection device is able to exactly detect the concentration of desired sample in acceptable range, indicated that the device has a good specific to desired sample.

2.11.1.5 Reproducibility

The ability of a test the biosensors to be accurately reproduced, reproducibility is not similar repeatability. The result is insignificant if error of the experiment cannot be determined. Repetition of numbers of experiment must be

performed followed by standard deviation in order to compare the result from new experiment to the standard value.

2.11.1.6 Response time

Response time is the amount of time required for the system to access equilibrium or steady state. This response time can be varied for each biosensor. However, the typical value is around 5-10 minutes depend on experimental system.

2.11.1.7 Storage stability

This is the experiment for storing a part of biological component in device at any time and test residue activity. In commonly, immobilized biological component that is stored as the time passed, it will be denaturation and affect to decrease effective of detectable device as well as more deviation from initial value of experiment. Therefore, this procedure is used in determine life time that device able to detect in range of acceptable value.

2.11.2 Effect of parameter of electrochemistry

Sun et al. (2010) [87] has studied AChE/Chitosan/PB/GCE biosensor for pesticide detection in dichlovos type, consist of 2 layers, first layer for enhance electron transfer by prussian blue (PB) layer which was electrodeposited on the surface of glassy carbon electrode (GCE), another layer has been design for loading a large amount of enzyme and prolong the enzyme storage life by chitosan layer that used for immobilizing acetylcholinesterase through glutaraldehyde cross-linking. The modified electrode was used in detection by immerse to solution containing phosphate buffer and acetylthiocholine chloride, subsequently, apply any voltage in order to occurs the current from electron transfer which generate from hydrolysis of enzyme and acetylthiocholine chloride substrate on electrode surface. The factors have affected to response are pH and acetylthiocholine chloride. According to **Figure 2.26**, this review studied pH adjusting has affected to current response, in range of pH 5 to 8.5 and they found that the optimum condition of pH is 8 because this value gave the highest current. Moreover, they has investigate substrate factor between 5 to 30 mg/ml

acetylthiocholine chloride, found that substrate of 15 mg/ml brought about the highest current response. Thus, these two values are suite for detection.

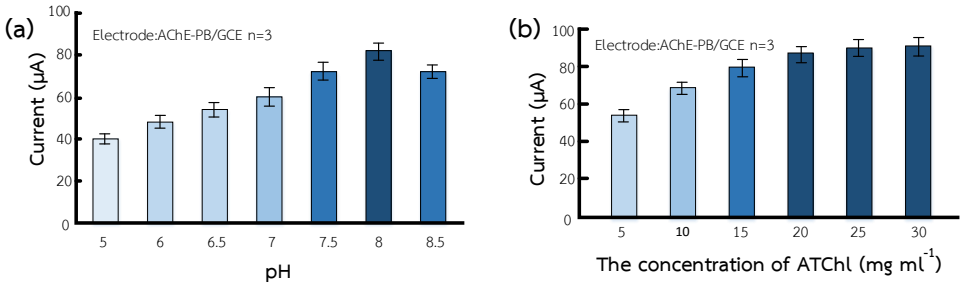

Figure 2.26 The investigation of optimum parameters; (a) pH of solution system and (b) concentration of acetylthiocholine chloride substrate. [87]

From **Figure 2.27**, after investigation of optimum pH and acetylthiocholine chloride concentration for use pesticide detection by adding dichlovos in detection system. This pesticide can inhibit catalytic hydrolysis of enzyme to decrease electron transfer at electrode surface. The current will decrease relate to added pesticide concentration.

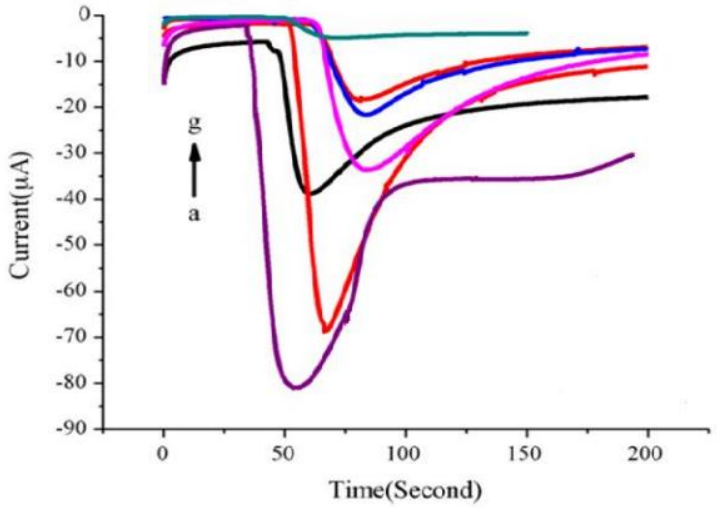

Figure 2.27 The response of AChE/Chitosan/PB/GCE biosensor containing 0.1 M pH 8 Of phosphate buffer and 15 mg/ml of acetylthiocholine chloride after adding dicholvos at (a) 0, (b) 10, (c) 30, (d) 100, (e) 300, (f) 500 and (g) 1000 ng/l. [87]

Moreover, another factor has affected and regarded is incubation time, it respond to the pesticide since start point to adding pesticide until reach to steady state by using the same standard for concentration of sample detection. Therefore,

incubation time might be found in order to the suited time which cover on whole pesticide concentrations. Sun et al. (2010) [87] has investigated on incubation time at 10 min as shown in **Figure 2.28** due to the pesticide was added to system, approach to equilibrium or steady state at the suitable time.

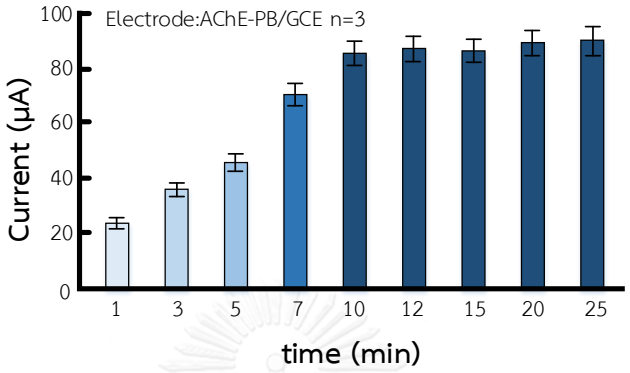

Figure 2.28 The optimum incubation time

Basically, the significant parameters of biosensor that affect to detection are linear range, limit of detection, storage stability. In Sun et al. [87] has found that linear range for detectable to dichlovos of 10 ng/L to 10 μg/L, detection limit of 2.5 ng/L and study of storage stability, they found that the modified electrode was immerse in solution of system which containing pH 8 of 0.1 M phosphate buffer and 15 mg/ml acetylthiocholine chloride solution, indicated that it has kept storage for 20 days and activity residue of enzyme of 95.1% when compare with the fresh electrode.

Chapter 3
Materials and methods

3.1 Reagents

Pluronic P123 was obtained from BASF corporation, USA. Hydrochloric acid (37% HCl) was available from RCI Labscan. 1,3,5-trimethylbenzene (TMB), tetraethoxysilane (TEOS, 98%), tydrogen tetrachloroaurate ($HAuCl_4 \bullet 3H_2O$), sodium borohydride ($NaBH_4$),acetylthiocholine chloride (ATC) and acetylcholinesterase (AChE, EC 3.1.1.7, Type VI-S, 844 U mg^{-1} from electric eels) were purchased from Sigma-Aldrich. 3-aminopropyl triethoxysilane (APTES) was obtained from Fluka. Toluene (97% C_7H_8), dichloromethane (97% CH_2Cl_2), acetic acid (CH_3COOH) was purchased from QReC Chamical. Sodium hydrogen phosphate (Na_2HPO_4), sodium dihydrogen phosphate (NaH_2PO_4), and sodium hydroxide (NaOH) were obtained from Ajax Finechem. Chitosan (deacetylation degree 95%, MW 550 kDa) was available from Seafresh chitosan Co., Ltd., Thailand. Deionized water were prepared from Thermo Scientific Barnstead EASYpure deionization unit. All chemicals were of analytical reagent grade and used without further purification. And all the aqueous solutions were prepared with deionized water.

3.2 Apparatus

Electrochemical measurement of cyclic volammetry and amperometry were performed with an Autolab potentionstat (Metrohm, model PGSTAT101) with Nova software version 1.5. The electrochemical cell consisted of a three-electrode system (containing a screen-printed carbon (SPE) working electrode, a platinum wire counter electrode, and a silver/silver chloride (Ag/AgCl) reference electrode).

3.3 Synthesis of mesocellular foam silica

Initially, 2 g Pluronic P123 was dissolved in 75 mL of HCl aqueous solution (1.6 M) and homogenously mixed using while mixing magnetic stirrer. After that, an amount of 3.4 ml TMB was added to the prepared homogenous solution, the resulting

solution was heated to 40°C with virgorous stirring. After 2 h of stirring, adding 9.2 ml TEOS, a silica source, and the solution was continually stirred at 40°C for 5 min. Next, the mixture was aged in Teflon bottle at 40°C for 20 h in the oven under static condition. It was the aged at 100°C for 20 h. The obtained dried particles were filtered by Whatman No. 5 paper and washed with ethanol and deionized water until the water pH (approximately twice washings) [47]. The synthesized silica particles were dried at ambient temperature for 24 h, the as-synthesized MCF obtained was denoted as MCF-a. Two different methods, calcinations at high temperature and solvent extraction to remove the residue template. For calcination method, the MCF-a was placed in a crucible and heated at 550°C for 6 h under an air flow. The MCF obtained was designated as MCF-c. When ethanol extraction approach was used, 1.5 g MCF was first packaged with a filter paper and refluxed with the mixture of 100 mL ethanol and 1 mL concentrated hydrochloric acid in a round bottomed flask at 90°C for 24 h by using Soxhlet extractor. The MCF obtained with the extraction was denoted as MCF-e. The obtained MCF after template removal was kept at desiccator and ready for use [54].

3.4 Functionalization of mesocellular foam silica with APTES

Preparation of functionalized MCF was initiated by 1.5 ml APTES in 20 mL anhydrous ethanol in a Teflon bottle. The mixture was stirred at room temperature for 5 min to obtain a well-dispersed aminosilane solution. Then, 1.2 g of MCF-c or MCF-e was dispersed in the mixture at room temperature for 30 min. And then the mixture was refluxed at 85°C for 24 h in oven. Next, the functionalized particles were filtrated by Whatman No.5 paper and washed once with ethanol solution. And the last one, functionalized materials were dried at 80°C for 12 h [45, 54].

3.5 Synthesis of AuNPs/APTS/MCF

3.5.1 Adsorption of gold ion on MCF/APTES

A gold precursor was varied in range of 0.1 to 1 mM, was prepared by adding 50 mL aqueous solution of gold precursor ($HAuCl_4$) to 1 g of MCF. The mixture was continuously stirred for any time 1 to 6 h. After filtered with Whatman No.5, the original

yellow $HAuCl_4$ aqueous solution turned colorless, whereas the white mesoporous silica powder attained a yellowish hue.

3.5.2 Reduction of gold ion into gold nanoparticle within MCF

Reduction of Au(III) was performed by adding 1 mL of a 0.1 M $NaBH_4$ aqueous solution to 50 mg of the $AuCl_4^-$ adsorbed MCF and stirred for 10 min. The product was recovered by filtered, washed with a large amount of distilled water and air dried. The red wine solid Au/MCF was obtained [88, 89].

3.6 Immobilization of Acetylcholinesterase on MCF/APTES/AuNPs

The immobilization of AChE within MCF/APTES/AuNPs was initiate by dissolving 0.001 g AChE in 2 mL PBS 0.1 M pH 6 under mild stirring at 4°C. Then, MCF/APTES/AuNPs was added to homogenous the prepared AChE solution with mild continuous stirring at 4°C for 2 hr [2]. The particles was then filtered and washed with 0.1 M PBS (pH 6) to remove unattached enzyme. Finally, MCF/APTS/AuNPs/AChE was obtained and kept at 4°C for further uses [45].

3.7 Characterization of MCF, MCF/APTES/ and MCF/APTES/AuNPs/AChE

Determination of surface area, pore size, and pore volume of nanomaterials were carried out by nitrogen adsorption and desorption according to Brunauer-Emmett-Teller (BET) method. The Functional groups on nanomaterial surfaces were identified by Fourier Transform Infra-Red (FT-IR) by using the powder technique via FT-IR model 1760x. Transmission electron microscope (TEM) was applied for nanostructure investigation. The type and structure of gold nanoparticles on MCF were considered using by X-Ray Diffraction (XRD). And, surface charges of materials were measured in the form by Zeta potential using Zetasizer Nano, 1 mg of supports were dispersed in 5 ml of buffer solutions of pH 6.

3.8 Preparation of chitosan solution

The chitosan solution (0.5 %w/v) was prepared by dissolving 0.1 g of chitosan flakes in 20 mL of acetic acid solution (1% v/v). The viscous chitosan solution was

stirred by magnetic stirrer overnight at room temperature. Finally, the prepared chitosan solution was adjusted to pH 6.0 with 0.1 M NaOH.

3.9 Electrode Modification

First, 0.05 g MCF/APTES/AuNPs/AChE was added to 1 mL of 0.1 M PBS (pH 6) and stirred at 4°C. 3 µL of solution was dropped on the surface SPCE and dried at room temperature for 20 min. Next, 3 µL chitosan solution was dropped on the modified SPCE and dried in a desiccator for 20 min. Finally, the modified electrode (SPCE/MCF/APTES/AuNPs/AChE/Chitosan) was achieved and kept at 4°C. All electrodes were freshly prepared for all experimental.

3.10 Pesticide determination

First, the modified electrode was placed into phosphate buffer solution pH 9.0 at constant applied potential of 10.5 V. After the steady state current was reached , 15 mM of acetylthiocholine was injected then the steady state current response was recorded as ΔI_1 ,later the modified electrode was transferred to phosphate buffer pH 9.0 containing specified amounts of malathion between 1-2000 ng/ml. After 20-30 mins of incubation, the modified electrode was placed again in phosphate buffer solution pH 9.0 and then 15 mM of acetylthiocholine was injected the steady state current was record as ΔI_2.

Chapter 4
Results and discussion

The results and discussion in this thesis is divided into 3 main parts. Firstly, the physical and textural properties among as-synthesized mesoporous foam silica (MCF-a), calcined mesoporous foam silica (MCF-c), and solvent-extracted mesoporous foam silica (MCF-e) as well as APTS grafted MCF-c and MCF-e are illustrated. Effects of template removal method and surface modification will be interpreted by TEM and SEM micrographs, BET-method, TGA, FT-IR, XRD, and NMR. Secondly, the syntheses of AuNPs/MCF nanocomposites will be investigated by TEM, SEM, XRD, electrochemical responses, BET-method and zeta potential. Finally, different MCF-based carriers will be exploited for enzyme immobilization and biosensor applications.

4.1 Effects of template removal method on MCF

4.1.1 Characterization of the Materials

To investigate the success of the surfactant removal, thermogravimetric analysis was used. The corresponding results shown in **Figure 4.1** compare the silica materials obtained after calcination and solvent extraction with the as-synthesized silica. The total mass losses of 56%, 28% and 10% were determined for MCF-a, MCF-e and MCF-c, respectively. The TGA curves can be divided into two main parts. At low temperatures (below 100°C), desorption of physisorbed species, for example water and/or alcohol, took place [90]. In the region of 37 to 100°C approximately, weight losses of 10% and 16% were detected for the calcined and solvent-extracted silica, respectively, indicating that a significant amount of water/alcohol resulting from the calcination and solvent-extraction procedures remained adsorbed on the MCF-c and MCF-e. At higher temperatures above 140°C, decomposition of the template P123 occurred [90], the release of chemisorbed species and the progressing of the condensation of the silica network are to be considered. In case of the as-synthesized silica, a significant mass loss of 56% is detected after 150°C which is mainly related to the presence of template within the material. The solvent-extracted silica was

characterized by a weight loss of only 10% which was observed at temperatures above 350°C, showing that silanol content from the solvent extraction method gradually begins to decompose [91]. For the calcined silica, no further mass loss was observed at these temperatures due to the other species were decomposed by calcination process at high temperature before TGA analysis. Thus, the TGA results indicate that a significant removal of template was carried out by ethanol solvent when compared with as-synthesized silica.

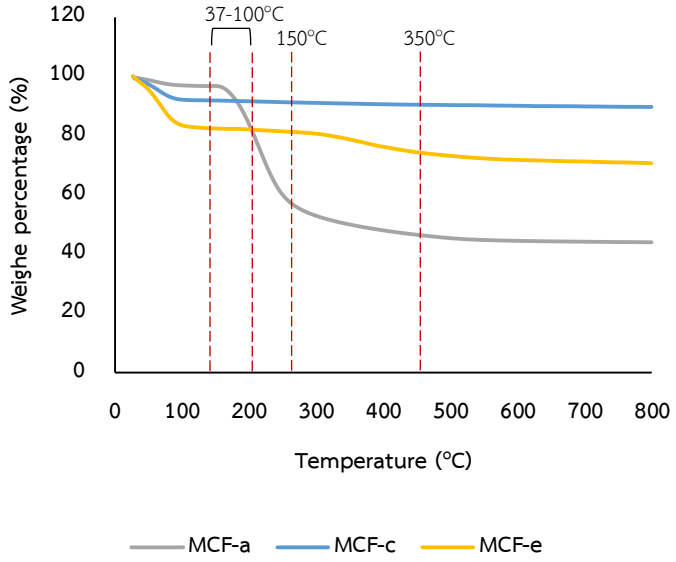

Figure 4.1 TGA curves for the as-synthesized silica (MCF-a), solvent-extracted (MCF-e) and calcined (MCF-c) silica [N_2 atmosphere, heating rate: 10 °C/min].

The template or surfactant content of the MCFs can be identified using FT-IR (**Figure 4.2**). The absorption bands at 2926, 2855, 1465 and 1378 cm^{-1} ascribed the stretching vibrations of methyl groups [92] in hexadecylamine (Pluronic P123) while that observed at 810 and 956 cm^{-1} ascribe respectively the stretching vibration of the silicon monoxide (Si-O) and silanol (Si-OH) groups in silicon molecule (SiO_2) [93] indicates two distinct differences between MCF-c and MCF-e spectra are clearly noted, and consequently, the MCF-e sample shows a distinct peak at 956 cm^{-1} which attributes to the presence of a significant number of surface silanol groups were more abundant than other silica samples [90, 94, 95]. The FT-IR spectrum of the MCF-a clearly shows the presence of the template molecules while that of the calcined sample shows no peaks related to the surfactant in regions of 2926-2855 and 1465-

1378 cm^{-1}. The spectrum of MCF-e also hardly displays no peaks related to the hexadecylamine, showing that the extraction procedure using ethanol was effective for removing the template [96].

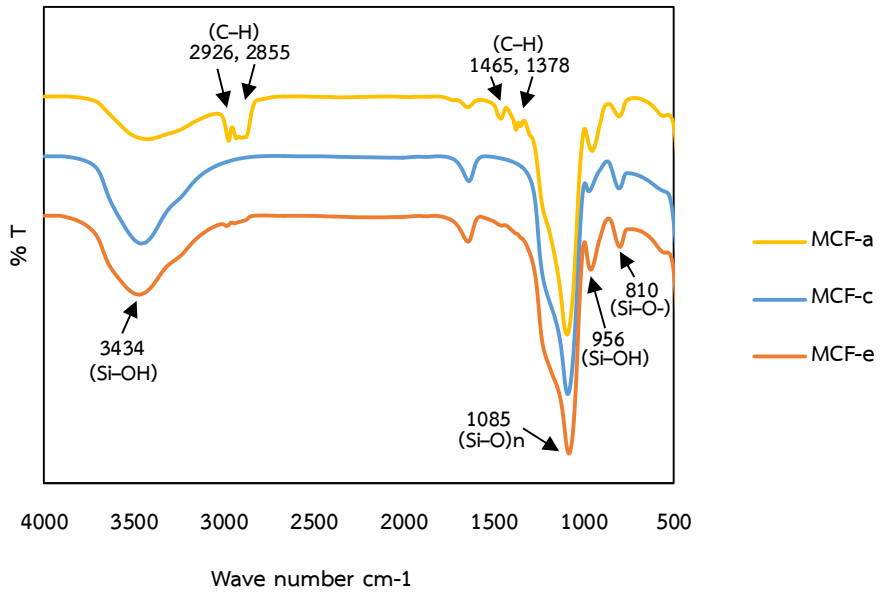

Figure 4.2 FTIR spectrum of silica materials: MFC-a, MCF-c and MCF-e.

This is, however, for all MCFs, Si–O (1085 cm^{-1}) and Si–OH (3434 cm^{-1}) stretching vibrations of surface could be observed the siloxane and silanol groups respectively, and whereas Si–OH (956 cm^{-1}) of the silanol groups were able to present as well [97, 98] which the peak at 956 cm^{-1} are not clearly observed in the MCF-c sample. Thus, the IR-spectra for both MCFs show that the MCF-c sample contained less surface silanol groups whereas in the solvent extracted sample, which indicates that the extraction at low temperature would be helpful for preserving silanol groups. Since aminosilanes in APTS is grafted on the surface of MCFs by the reaction of aminosilanes with the surface OH, it is expected that the higher OH surface concentration on MCF-e surface will be in favor of grafting more aminosilane.

The characteristics of X-ray powder diffraction patterns reported in the literature for mesoporous silica varies widely [99, 100]. XRD patterns (**Figure 4.3**) of MCFs synthesized in this investigation do not exhibit three well resolved intense reflections as in the case of hexagonal mesoporous silica. MCF-a demonstrates similar diffraction pattern to that of MCF-e at low reflection angles. In contrast, the broad

peaks of 2θ angle at 0.8 and 1.1 are observed for the case of MCF-c. These data indicate that the removal of the template by solvent extraction better preserves the structural order and pore structure of the original materials [92]. Moreover, the diffraction peak of MCF-c shown at 2θ = 0.8 indicates a cubic space group [101] whereas the peak of other samples are not resolved at this angle suggesting different mesoporous structures [90, 102].

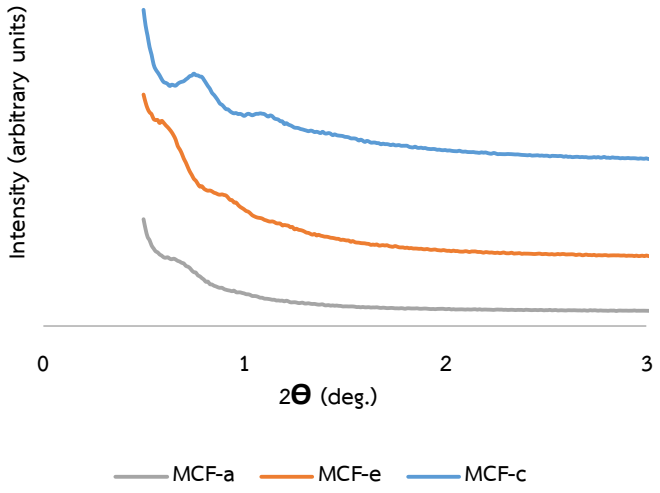

Figure 4.3 Powder XRD patterns of mesoporous silicas: MFC-a, MCF-c and MCF-e.

TEM micrographs of different MCF-based materials as shown in **Figure 4.4** confirm the spherical cells and frame structure of MCF-a, MCF-c and MCF-e in this research. These images corresponded to Chouyyok et al. [102] and V. Meynen et al. [103] who reported the TEM images of MCF-c, as a 3D sponge-like and foam mesostructure with specific character of pores. Nevertheless, the MCF-c in this research does not show well-defined cell and frame structure compares with those of MCF-e and MCF-a. Moreover, the synthesized MCF in some researches were of large, irregular particles [46] which are not suitable for biosensor applications. In this research, spherical MCF-c and MCF-e particles with narrow size distribution with the main diameter of 2 and 3 μm were obtained (**Figure 4.5 and 4.6**). As indicated in **Figure 4.5c**, MCF-e exhibits particle morphology similar to that of MCF-a (**Figure 4.5a**), whereas

the SEM image of MCF-c (**Figure 4.5b**) shows significant shrinkage of the structure compared to that of MCF-e which the template was removed by solvent extraction.

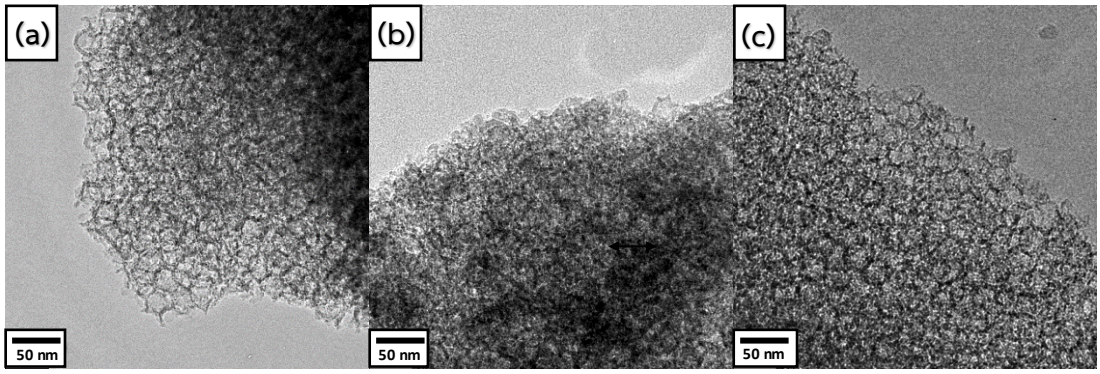

Figure 4.4 TEM images of mesoporous foam silica: (a) MFC-a, (b) MCF-c and (d) MCF-e

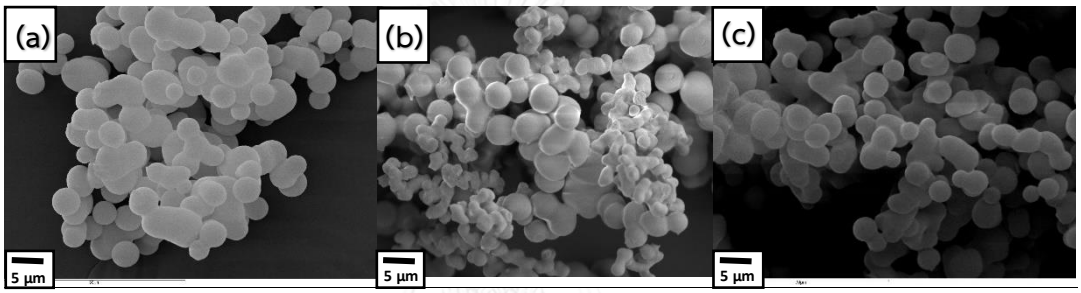

Figure 4.5 SEM images of mesoporous foam silica; (a) MFC-a, (b) MCF-c and (c) MCF-e.

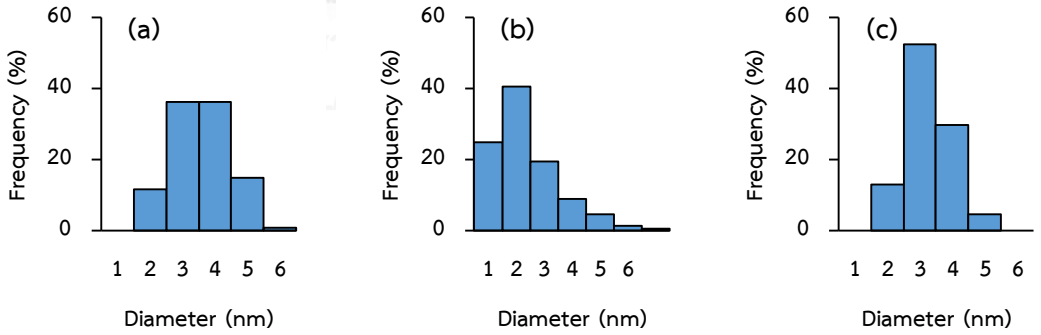

Figure 4.6 Particle size distribution of mesoporous silica foams: (a) MFC-a, (b) MCF-c and (c) MCF-e.

In **Figure 4.7**, the nitrogen sorption isotherms are presented and the results are summarized in **Table 4.1**. All the MCFs are characterized as a type IV isotherm with large hysteresis loops which indicate that all the three MCF materials were mesoporous [104]. As summarized in **Table 4.1**, the MCF-a displayed the lowest surface area (125

m^2g^{-1}) and total pore volume (0.75 cm^3g^{-1}). On the other hand, MCF-e and MCF-c possessed much higher surface areas (1221 and 1075 m^2g^{-1}) and total pore volumes (3.32 and 3.19cm^3g^{-1}) which the increase of surface textural characteristics were provided subsequent to the template removal process. In case of similar desorption BJH average pore sizes were calculated for a three silica materials, 7.4, 8.1 and 6.7 nm for the as-synthesized, calcined and extracted silica, respectively. However, the differences of all the three MCFs regarding the surface area and pore volume can be attributed, firstly indicate from MCF-a sample, it was reported that the formation of the lower surface textural properties in silica materials prepared with triblock copolymers is mainly due to the permeation of the PEO blocks in the silica walls before template removal. Therefore, two different template removal method shows distinct pore and surface characteristics [105]. The calcined sample was treated at much higher temperatures, which is related to a stronger shrinkage and densification of the silica material and which also leads to the surface area and pore volume are less than solvent-extracted sample after template removal procedure [106]. Furthermore, the lower value of pore size for the extracted silica may be also created during the extraction process. Indeed, it is well known that water/ethanol molecules can hydrolyze and break siloxane bridges (Si–O–Si) [107], which could lead to the creation of microporous channels and silica beads within the silica framework.

From **Table 4.1**, by comparing this work with others, the results show that synthesized MCFs in this work, exhibit high surface areas and pore volumes, in contrast to the pore sizes, This might be due to synthesis conditions such as temperature, time and silica source/surfactant ratio. However, The results of mesostructure from the pore sizes and TEM images (as shown in **Figure 4.4**) of MCF can indicate that is able to be used for immobilization of enzyme such as acetylcholinesterase with approximate size of 4.5 x 6.0 x 6.5 nm [108].

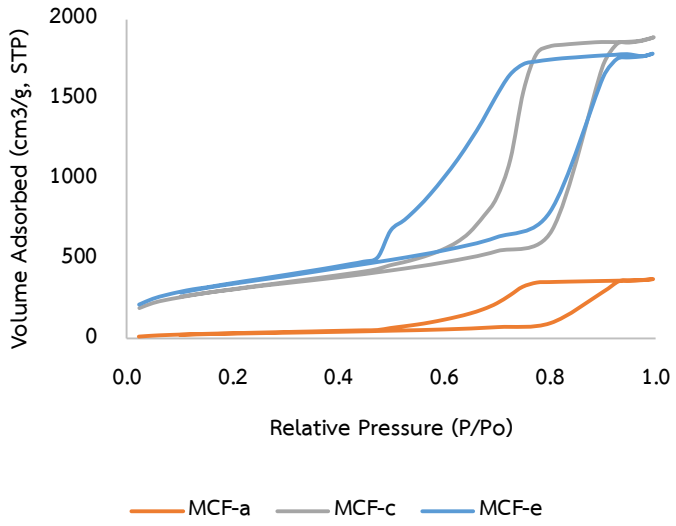

Figure 4.7 Nitrogen Adsorption-Desorption isotherm of mesoporous silica foams.

Table 4.1 Pore characteristics of silica materials.

Material	P123:TMB:TEOS	Surface area (m^2/g)	Pore volume (cm^3/g)	Pore diameter (nm)*	Ref.
MCF-a	2 : 1.35 : 8.40	125	0.75	7.4	This work
MCF-c	2 : 1.35 : 8.40	1075	3.19	8.1	This work
MCF-e	2 : 1.35 : 8.40	1221	3.32	6.7	This work
MCF-c	2 : 3.00 : 4.40	650	1.84	11.1	[54]
MCF-c	2 : 1.00 : 4.25	537	1.02	26.0	[45]
MCF-c	2 : 1.00 : 4.25	700	1.95	21.5	[46]
MCF-c	2 : 1.00 : 4.25	618	1.60	14.8	[102]
MCF-e	2 : 3.00 : 4.40	573	1.85	13.4	[54]

*Pore diameter of each materials were obtained from BJH desorption.

4.1.2 APTS grafted MCFs

Thermal decomposition method was used to estimate the amount of grafted APTS on MCF surfaces [13, 109-111]. **Figure 4.8** shows the weight losses of grafted-MCF-e and grafted-MCF-c with temperature. According to the results from Thongthai et al. (2011) [112], the weight loss from ambient temperature to 100°C was attributed to the removal of water and/or alcohol associated with incomplete hydrolysis of the alkoxysilane. While the weight lost at temperatures above 200°C were due to the decomposition of grafted amine on MCF surface [110]. Information on weight losses of the samples were used to estimate APTS content of the samples. The amine contents of APTS-MCF-c and APTS-MCF-e were thus calculated to be 0.41 mol/g and 0.69 mol/g, respectively. Therefore, APTS-MCF-e contained approximately 68.29% higher APTS than MCF-c. The higher amount of APTS grafted on APS-MCF-e was most likely due to the more available active hydroxyl groups with the aminosilane covalently bonded on its surface as already demonstrated in section 4.1.1. This hypothesis can be proved by the previous IR results in **Figure 4.2** that more silanol groups can be preserved on solvent-extracted silica materials than on calcined silica materials [13]. Hence, it can be concluded that the higher content of silanol as an APTS carrier could lead to higher APTS loading.

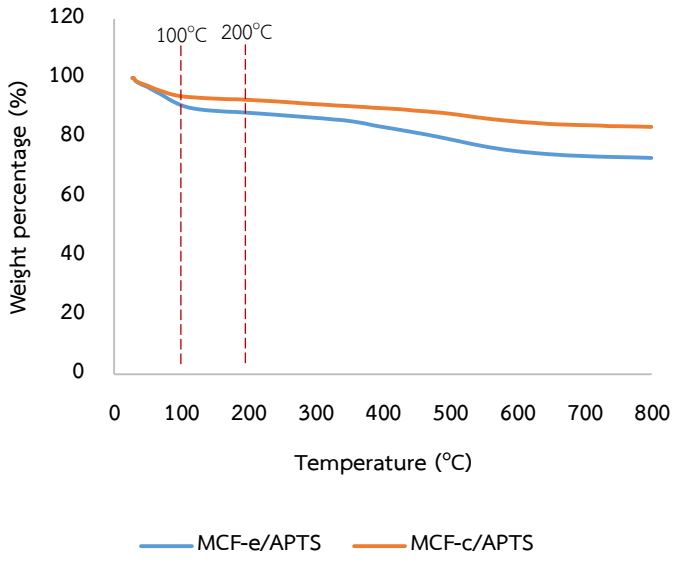

Figure 4.8 TGA curves for the amine-grafted MCFs.

Figure 4.9 shows the nitrogen adsorption-desorption isotherms of MCFs prior to and after grafting of APTS. The N_2 adsorption-desorption isotherms of grafted MCF-c and MCF-e exhibit the typical adsorption curves of a type IV material, which strongly support the proposed MCF pore structure [5]. **Table 4.2** gives the textural properties of MCF supports and the prepared composite sorbents. The surface area of grafted MCF-e is 392 m^2/g, slightly lower than that of MCF-c (464 cm^2/g). The total pore volumes of the grafted MCF-c and MCF-e are 1.61 cm^3/g and 1.39 cm^3/g, respectively. Nitrogen adsorption-desorption results confirm that both template-removal methods are effective to obtain supports with well-developed porous structures due to those of both materials are able to graft amine on the surface. Nevertheless, the surface chemistries are different due to the fact that the materials prepared using ethanol extraction at low temperature contains more silanol groups than the calcined one at higher temperature. APTS grafting leads to significant loss in BET surface area and decrease in the pore volume compared to unmodified MCFs. In addition grafted MCF-e displayed the more reduction of surface area and pore volume when compare to grafted MCF-c, thus conclusion could be made here that solvent-extracted silica provided higher amine grating corresponded to higher weight loss in TGA. A explanation for the decrease in surface area is the loss in mesoporosity of the samples as the grafted species could sterically hinder the access to the micropores of the MCFs [113], and thus block pore entrance through the formation of amine groups on the external and internal surface of sorbents.

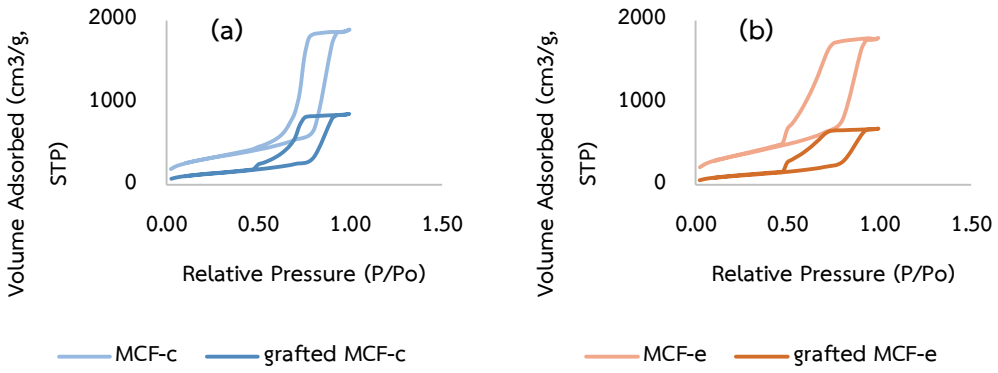

Figure 4.9 Nitrogen Adsorption-Desorption isotherm (a) MCF-c, (b) MCF-e and MCF supports after aminosilane-grafted.

Table 4.2 Textural properties for MCF materials before and after amine grafting.

Material	Surface area (m^2/g)	Pore volume (cm^3/g)	Pore diameter (nm)
MCF-c	1075	3.19	8.1
MCF-c/A	464	1.61	3.9
MCF-e	1221	3.32	6.7
MCF-e/A	392	1.39	3.9

4.2 Synthesis of AuNPs/MCF nanocomposite

4.2.1 Synthesis of AuNPs

Synthesis of AuNPs was achieved after consecutive steps of gold ion adsorption and chemical reduction in an aqueous solution of sodium borohydride ($NaBH_4$). The mechanism of the reduction of gold ions into gold atoms by chemical reduction method is expressed in reaction 4.1.

$$HAuCl_4 + 4NaBH_4 + 12H_2O \rightarrow Au + 4B(OH)_3 + 4NaCl + 28H^+ \quad (4.1)$$

Formation mechanism

Mechanism of AuNPs formation on silica surface is discussed in this section. After addition of silica particles to the gold precursor solution, adsorption of gold ions was accomplished by coordination of $AuCl_4^-$ with amine nitrogen [9]. Next, the attached gold ions were reduced to gold atom (Au^0) by $NaBH_4$ which was applied as a reducing agent. Further reduction resulted in the growth of Au^0 nuclei to AuNPs. Clusters of AuNPs were formed on the silica surface if further reduction was allowed.

As shown in **Figure 4.11(1a and 1b)**, the sizes of AuNPs are compared between the two MCFs of different template removal methods, the main particle diameter of AuNPs of Au/MCF-c and Au/MCF-e were respectively determined at 3 and 2 nm as show in **Fig 4.12 (1a and 1b)**. It was found that the template removal method significantly affected the size of synthesized gold nanoparticles. This result was most likely due to the shrinkage of structure of MCF-c which carried out at the high

temperature and thus gold ions were hard to diffuse through the silica pore. In addition, for the case of MCF-c, lesser amount of the silanol group (as discussion in section 4.1) could generate larger AuNPs at the same gold precursor concentration due to the lesser amounts of nuclei produced.

Adsorption time

In the synthesis of AuNPs on MCF-based supports, adsorption of $AuCl_4^-$ on the silica surface is the preceding step before Au ion reduction. Longer adsorption time resulted in more homogenous distribution of the adsorbed ions towards the core of the MCF-based particles (as shown in **Figure 4.10**). Therefore, reduction of the adsorbed gold precursor will cause lesser particle sizes with more homogenous dispersion on the porous surface of the particles.

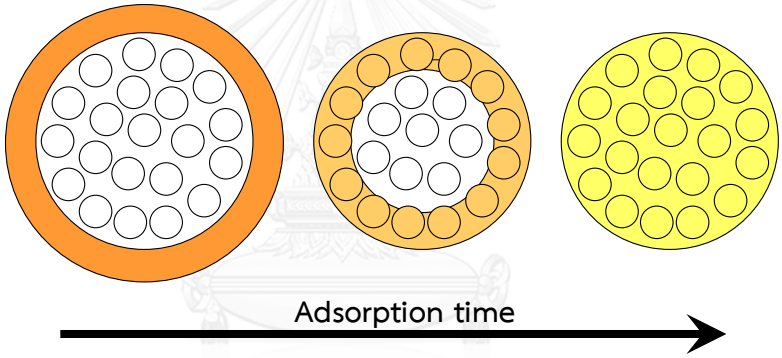

Figure 4.10 schematic diagram demonstrating propagation front of the gold ion diffusion towards the inner core of the support. The darker orange color represents higher concentration of gold ions.

Effects of $AuCl_4^-$ ion adsorption time on the synthesis of Au/MCF nanocomposite were studied at a fixed gold precursor concentration ($HAuCl_4$) of 10 mM, and the chemical reduction time of 10 min. **Figure 4.11 and 4.12**, shows that higher distribution and regular size of AuNPs are observed with adsorption time. Allowable time at 1 h resulted in densely adsorption of gold ions thus larger AuNPs are observed on the outer surface of MCF-based particles. In cases that adsorption time was extended beyond 3 hours, it was found that AuNPs were more homogeneously distributed.

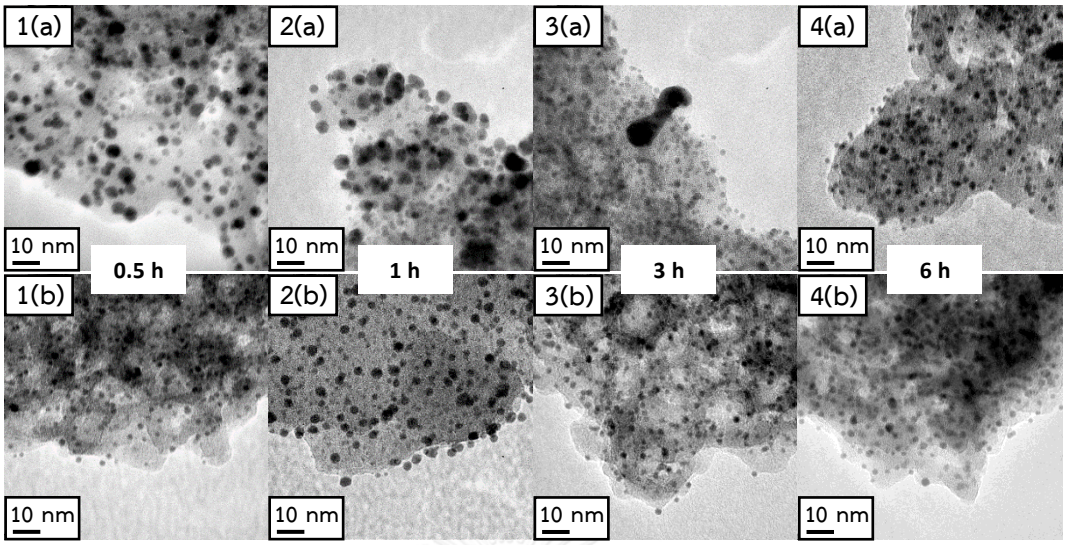

Figure 4.11 TEM micrographs of gold nanoparticles on (a) Au/MCF-c and (b) Au/MCF-e, prepared from 10 mM of gold precursor with 0.5, 1, 3 and 6 h adsorption time at room temperature.

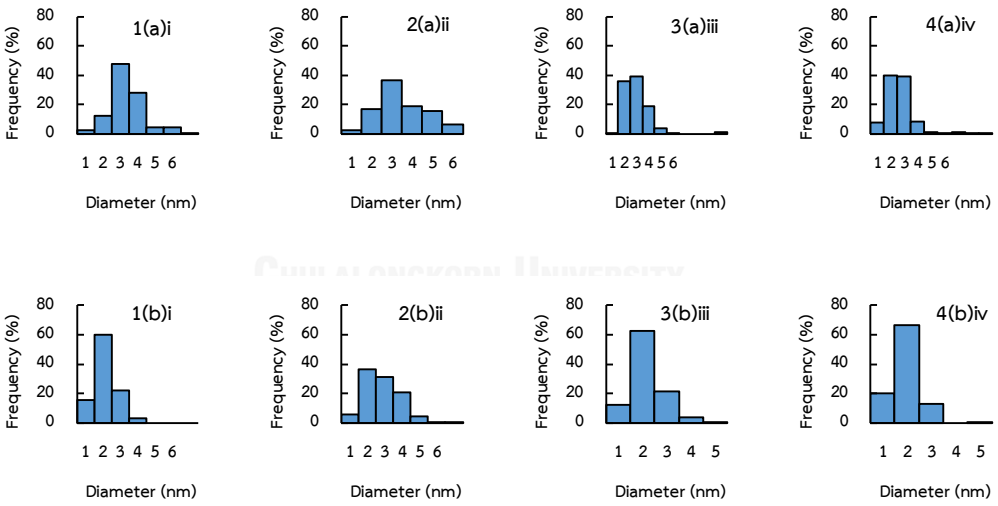

Figure 4.12 Gold nanoparticle size distribution of mesoporous foam silica: (a) Au/MFC-c and (b) Au/MCF-e. The synthesis condition was proceeded by using 10 mM of gold precursor and gold ion adsorption of 0.5(i), 1(ii), 3(iii), and 6(iv) h at room temperature.

Preliminary test of electrochemical response using modified electrodes on electrochemical response of the oxidation of thiocholine.

Electrochemical characterization was provided to investigate various modified electrodes, as shown in **Figure 4.13**. Acetylthiocholine was provided as a reactant which was hydrolyzed to thiocholine and acetic acid by AChE. The electroactive product, thiocholine, was then oxidized at the electrode surface producing the oxidizing current.

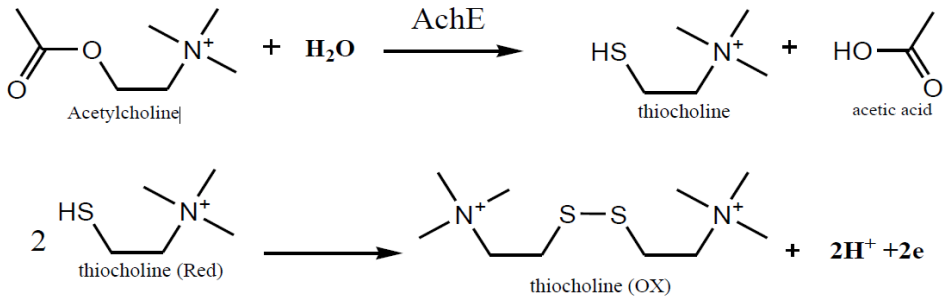

Figure 4.13 The biosensor reactions on the oxidation of thiocholine for determining current response [114].

The modified electrodes tested were obtained using MCF-e and MCF-c synthesized under the same precursor adsorption time of 3 hr with varied $HAuCl_4$ of 1, 5 and 10 mM. The resulted CVs in **Figure 4.14** show reduction in current responses with $HAuCl_4$ concentration. Moreover, expected oxidation peak of thiocholine at +0.8V is not clearly observed. We postulated that this was due to the hindrance effects of AuNPs to ATCl diffusion in the MCF-based pores, thus advantageous electron conductivity caused by higher amounts of AuNPs was not noticed. Therefore, lower $HAuCl_4$ concentration range was further investigated in order to lessen the substrate mass transfer effect.

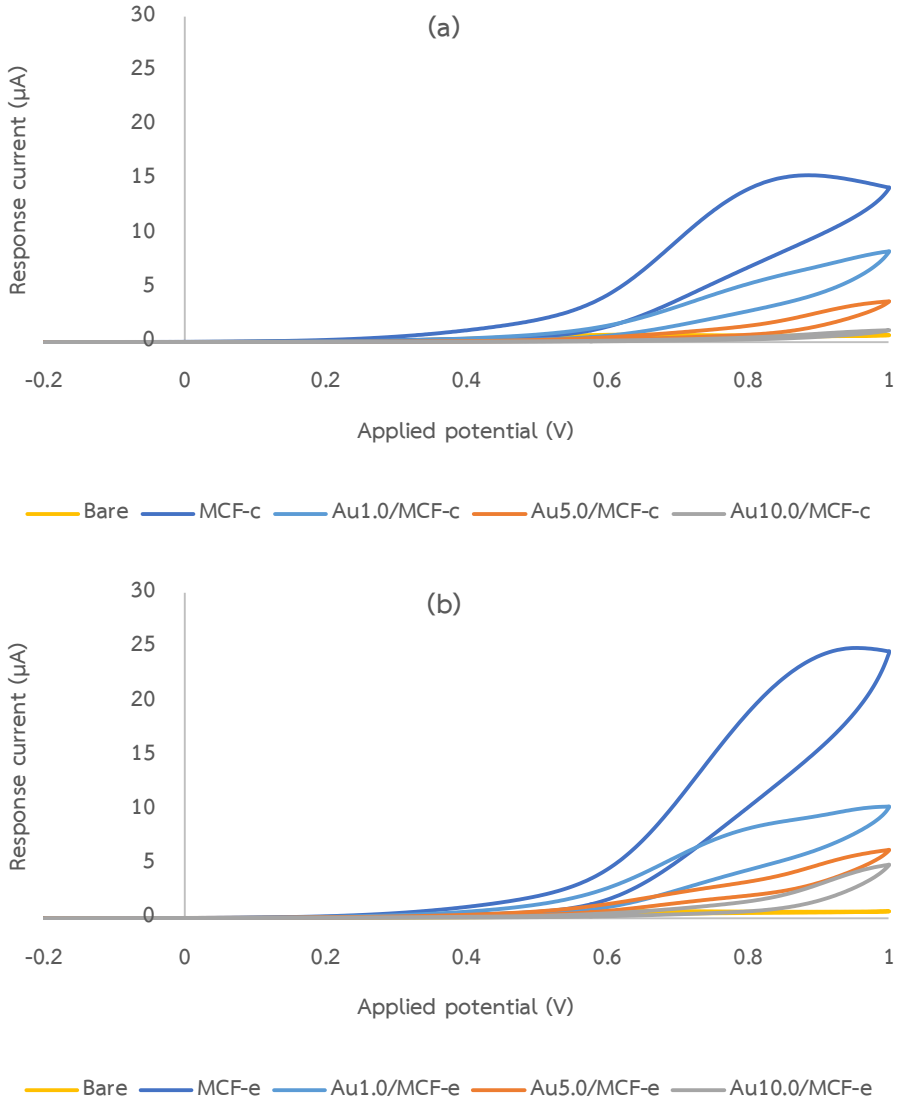

Figure 4.14 Cyclic voltammograms of AChE-AuNPs/MCF modified electrodes in phosphate buffer pH 9.0 containing 15 mM of acetylthiocholine chloride. Potential range -0.2 to 1.0 V at 10 mV/s; (a) calcined and (b) solvent extracted MCFs and All electrodes containing AChE.

4.2.2 Effect of Au precursor concentrations

In order to investigate influences of gold precursor concentration on the AuNPs/MCF nanocomposite, gold ion adsorption time was fixed at 3 h, while the gold precursor concentrations were varied from 0.1 to 1 mM. **Figure 4.15** illustrates that the higher gold precursor concentration resulted in an increase number of gold nuclei during the early stage of nucleation, which led to increasing numbers of gold nanoparticles [115]. However, different template removal method did not seem to affect the characteristics of AuNPs/MCF at this low $HAuCl_4$ concentration. This was because the silanol groups were in abundance, it could attach more amines even in the case of MCF-c which some of the silanol groups were likely decomposed during the calcination.

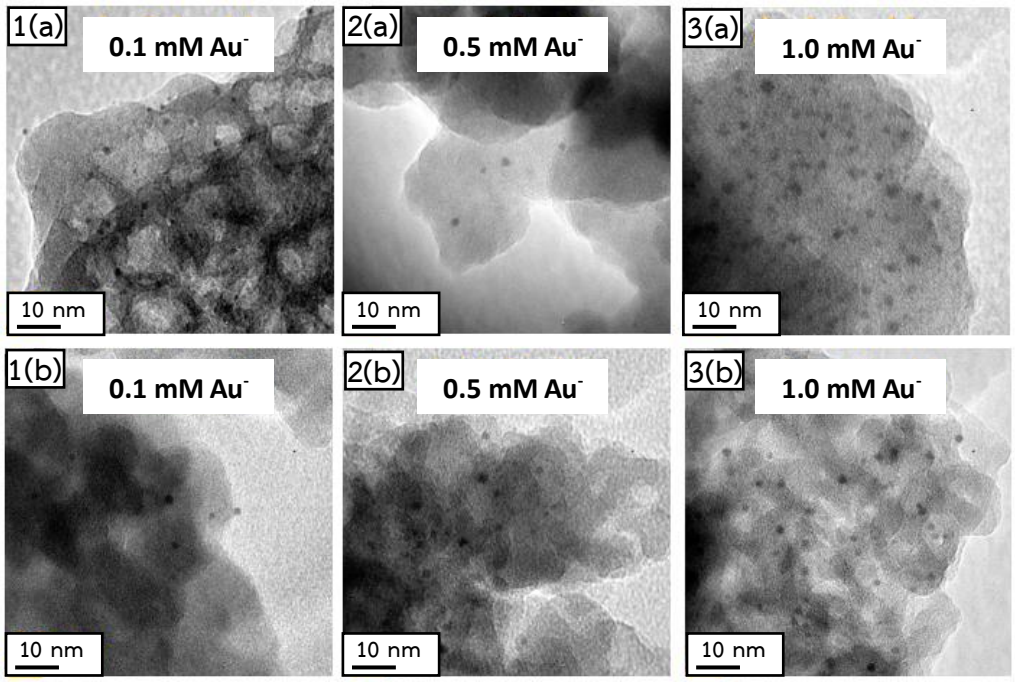

Figure 4.15 TEM micrographs of gold nanoparticles on MCFs, prepared from 0.1, 0.5 and 1 mM of gold precursors, 3 h of adsorption; (a) MCF-c and (b) MCF-e.

The modified electrodes investigated in this section were then electrochemically analyzed using cyclic voltammetric technique in a 15 mM acetylthiocholine chloride in 0.1 M PBS (pH 9.0). The potential was scanned in the range -0.2 and 1.0 V at the rate 10 mV/s. **Figure 4.16** shows the cyclic voltammograms of MCF-c and MCF-e based electrodes with different attached amounts of AuNPs. A well-defined CV were obviously obtained with increased peak currents after electrodes modification. The peak current resulted from nanocomposite modified electrodes (ii-iv) significantly show increased peak currents compared to the bare (unmodified) electrode (i), as shown in **Figure 4.16**, we can conclude that nanocomposites (included MCFs or modified-MCFs) act as mediator to provide the higher electron transfer. Therefore, the nanocomposites proved to help enhancing electrode efficiency.

To study the influences of gold precursor concentrations on electrode behavior of silica material by two different template removal methods, the CVs of modified electrodes with various loading of AuNPs on MCF-c and MCF-e are shown in **Figure 4.16**. Obviously, the CV profile of **Figure 4.16 a(iv) and b(iv)** show the highest current response compared to other gold precursor concentrations, which indicated the mass transfer limitation of substances. **Figure 4.9** and **Table 4.2** (from section 4.1) confirmed that limitation of substrate mass transfer was caused by the smaller surface area and pore volume of grafted MCFs, corresponded to the obtained lower response current when increasing the gold precursor concentration. Comparing between AuNPs/MCF-c and AuNPs/MCF-e, the peak potentials were sharper and higher in the latter case. The shrinked MCF-c structure likely caused higher mass transfer resistance, therefore, lower current responses were achieved.

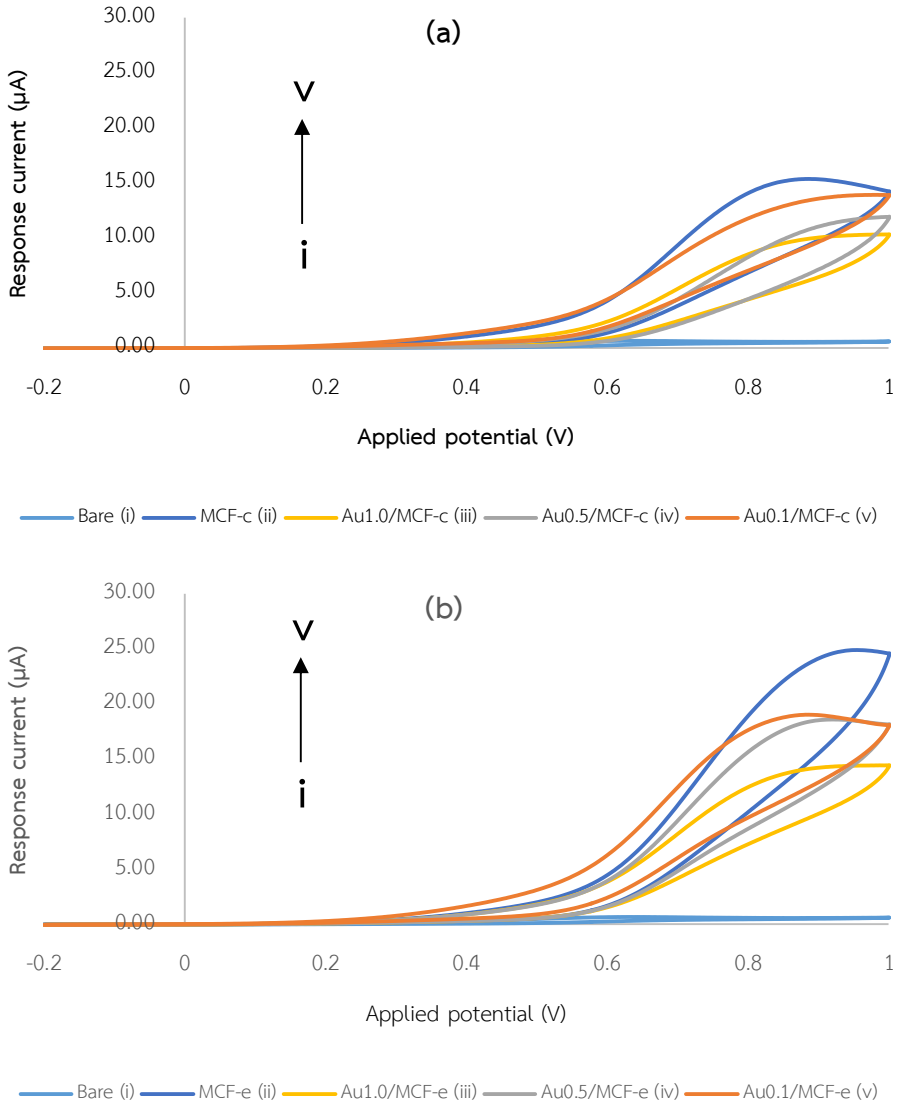

Figure 4.16 Cyclic voltammograms of AChE-AuNPs/MCF modified electrodes in phosphate buffer pH 9.0 containing 15 mM of acetylthiocholine chloride. Potential range -0.2 to 1.0 V at 10 mV/s; (a) calcined and (b) solvent extracted MCFs and All electrodes containing AChE.

4.3 The Immobilization of AChE on AuNPs/MCF nanocomposite

4.3.1 Effect of enzyme loading and activity on AuNPs/MCF nanocomposites

AChE immobilization capacities of MCFs with different template removal methods and gold loading, are shown in **Figure 4.17**, MCF-c and MCF-e provided relatively similar enzyme loadings of 53.76 and 55.70% respectively, while the enzyme loading decreased dramatically after surface modification with APTS. This was certainly caused by the pore blockage due to densely incorporated APTS molecules. BET results also confirmed considerable reduction in surface area, pore volume, and pore diameters after APTS grafting (see **Table 4.2**). Moreover, AChE loadings were discovered to increase with AuNPs concentration. With the Au precursor concentration of 1 mM, the enzyme loadings were even higher than MCF-c and MCF-e before APTS grafting. We postulated that AuNPS with high enzyme adsorption capacity tremendously enhanced amounts of immobilized enzymes [116-118]. Therefore, these data indicated that AChE could diffuse through the pore and was immobilized in pore of MCF-c and MCF-e.

In terms of enzyme activity, it could be determined by Ellman's method which DTNB was used to react with thiocholine to produce the yellow acid. The rate of color production between thiocholine and DTNB was measured from the absorbance at the wavelength of 410 nm. **Figure 4.18** demonstrates enzyme loadings as well as immobilized AChE activities as percentages of the initial enzyme amounts in the solution prior to immobilization process. All the enzyme carriers under investigation were MCF-e based. The results clearly evidenced that the immobilized AChE was not denatured, correspond to electrochemical tests by CV which show the oxidation peak of thiocholine product from the enzyme hydrolysis in section 4.2.2. This was because the immobilized amounts of AChE measured by the UV and Ellman's methods were closely resembled. However, in the previous discussion (section 4.2.2), we identified the mass transfer limitation in modified materials. In order to select the suitable enzyme carrierss, CV was used to test electrochemical responses of the oxidation of

thiocholine to observe the optimal potential and current responses which will be discussed as follows.

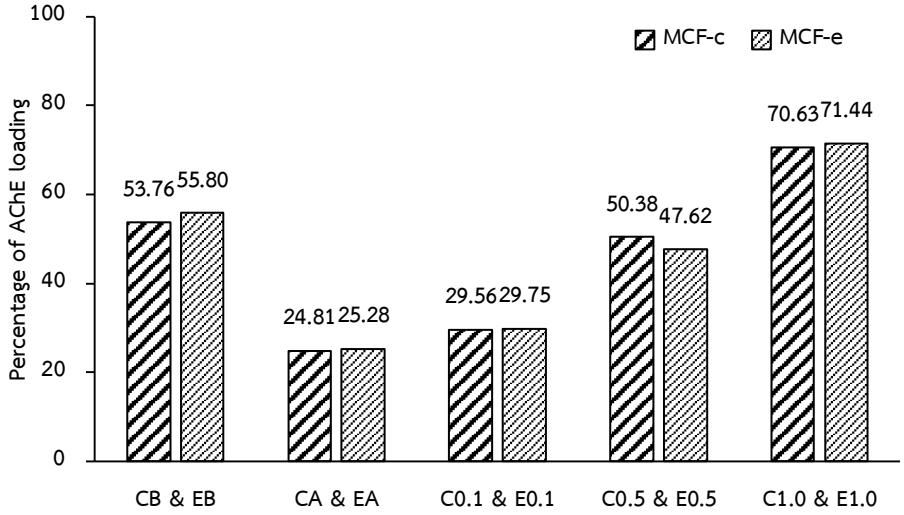

Figure 4.17 Effects of MCF support and AuNPs concentration on AChE immobilization; MCF-c and MCF-e without surface modification and present of gold nanoparticles, % AChE loadings compared to initial enzyme amounts.

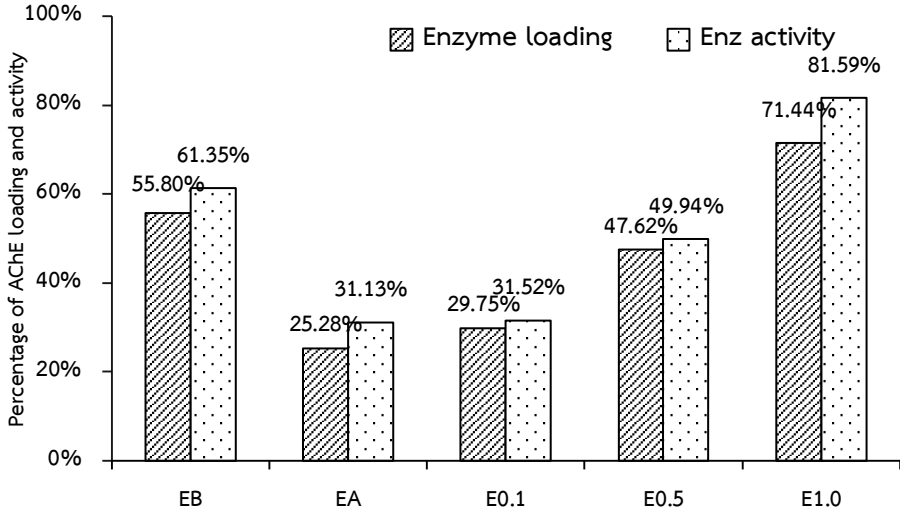

Figure 4.18 Effects of support structure and surface properties on AChE immobilization; MCF-e with surface modification and present of gold nanoparticles, % AChE loading compared to initial enzyme and % AChE specific activity compared to free enzyme.

Note **CB** : MCF-c, **EB** : MCF-e, **CA** : APTS/MCF-c and **EA** : APTS/MCF-e
C0.1-1.0 and **E0.1-1.0** : MCF-c and MCF-e with Au loading of 0.1-1.0 mM respectively

The influences of substrate concentration on the modified electrodes (SPE/MCF/AuNPs/AChE/chitosan) were studied to ensure that the enzyme was supplied with sufficient substrate concentration. This is similar to Zamfir et al., (2011) [119] who reported that the suitable amount of substrate concentration should be firstly determined. From **Figure 4.19** the suitable substrate concentration was determined at 40 mM acetylthiocholine for both MCF-e and MCF-c. However, MCF-c resulted in lower peak current than that of MCF-e.

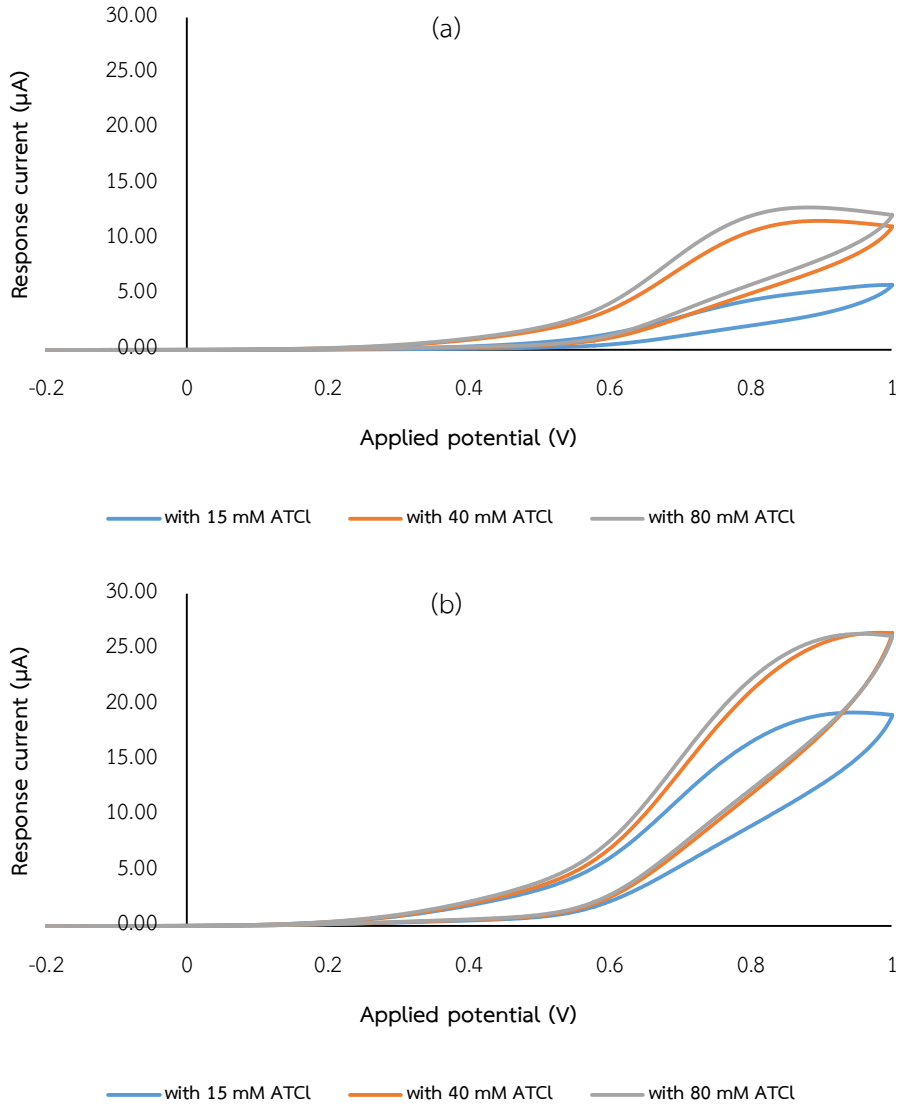

Figure 4.19 Effect of acetylthiocholine concentration on (a) SPE/MCF-c/AChE/Chitosan and (b) SPE/MCF-e/AChE/Chitosan on the peak current of CV scan in 0.1 M PBS (pH9.0) with the scan rate of 100 mV/s vs Ag/AgCl.

Alternate electrode modifications resulted in marked differences in electrochemical behaviors via cyclic voltammogram, as shown in **Figure 4.20**. Surely, AuNPs/MCF-e (i-iii) caused significant enhancement of the current response which the peak current was obtained, this is because of AuNPs acted as a mediator which enhanced electron transfer, on the other hand, effect of higher gold precursor concentrations still show the lower response current peak due to mass transfer limitation of sub substances. In case of the chitosan film that covered on outer layer, in this study, played two roles; one as an enzyme covering film to pretend the enzyme and composite material leak out while the other might be an obstacle to substrate mass-transfer from the bulk solution. However, influence of the covering of chitosan film resulted in lowering current responses as reported from Ion et al., (2010) [120] who investigated that modified electrode covered with the chitosan film showed no detectable signal. This was probably due to the electron barrier character of the chitosan film. In the presence of both MCF and AuNPs/MCF in SPE/MCF/AChE/Chitosan or AuNPs-MCF/AChE/Chitosan electrode (i-iv) demonstrates a dominant role of enzyme catalysis and shows the highest current peak in case of MCF-e. In addition Au0.1/MCF-e (ii) exhibits the peak current similar to that of Au0.5/MCF-e (iii). The current response was found to be the highest in the case of MCF-e which was probably due to the more homogeneous distribution of AChE and larger pore size (From **Table 4.1**). Addition of AuNPs to MCF-e resulted in lower current responses which was, again, likely due to blockage of substrate mass transfer by incorporated AuNPs.

Considering that MCF-e contained higher surface area and pore volume than MCF-c, higher substrate concentration and higher enzyme distribution should be achieved thus higher current responses than that of MCF-c due to obtained structure was provided in different template removal methods. However, in case of gold loading, AuNPs caused lower current responses due to the limitation of mass transfer which was evidenced by the decreased pore volume, pore diameter, and surface area of the silica supports as previously discussed. For this reason, the un-modified silica supports still exhibited better current responses in aspect mass transfer substances. Nevertheless, the gold nanoparticles could enhance electron transfer and their biocompatibity retain good enzyme activity and increase enzyme loading, Au0.1/MCF-

e exhibited the best results amongst various AuNPs/MCF-e carriers in terms of current response despite the least enzyme loading. The results emphasize, once again, eminent effect of mass transfer limitation. For this reason, Au0.5/MCF-e was selected for further experiments because it provided the optimum current response comparing to the other AuNPs/MCF-e supports.

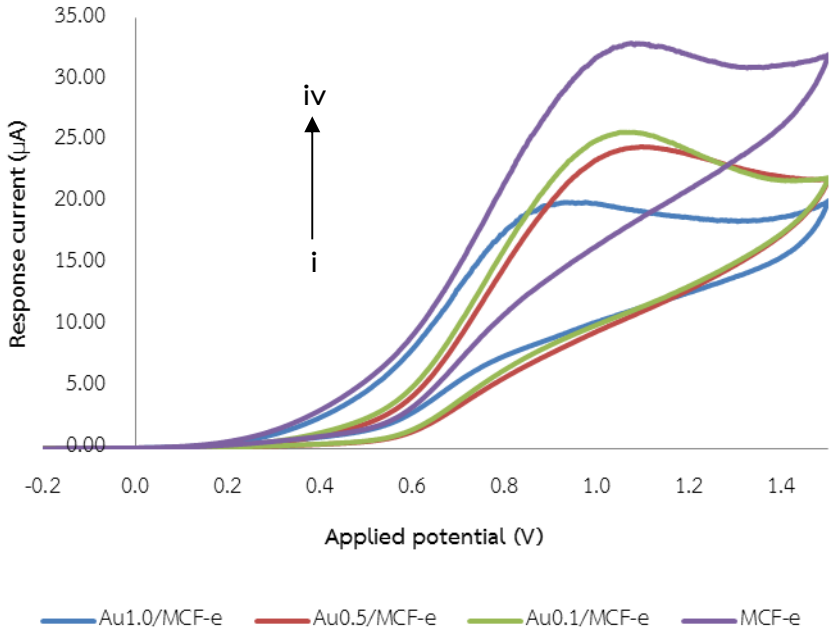

Figure 4.20 Cyclic voltammograms of the screen-printed modified electrode in phosphate buffer pH 9.0 containing 15 mM of acetylthiocholinechloride. Scaning potential between -0.2 and 1.4 V and scan rate 10 mV/s; i (SPE/MCF-e/Au1.0/AChE/Chitosan), ii (SPE/MCF-e/Au0.5/AChE/Chitosan), iii (SPE/MCF-e/Au0.1/AChE/Chitosan), iv (SPE/MCF-e/AChE/Chitosan). All of modified electrodes under enzyme immobilization process with AChE solution 0.25 mg/ml.

4.3.2 Biosensor Application for pesticide detection

Incubation time

In order to utilize the desired biosensor for pesticide detection, the pesticide incubation time was investigated. The optimum time for incubation of modified electrodes in pesticide solutions showed inhibitory effect of pesticide to enzyme activity. The enzyme catalytic process can be illustrated in **Figure 4.21**. After incubation

with pesticide, the enzyme activity is lowered due to irreversible inhibition by the pesticide which is phosphorelated to the serine hydroxyl group at the enzyme active sites [121]. Therefore, lower current responses are detected.

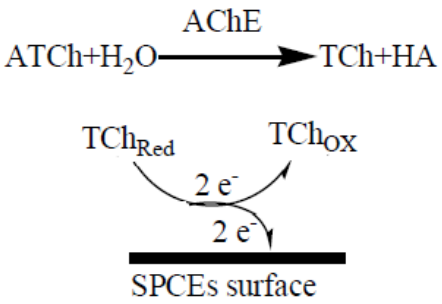

Figure 4.21 Catalysis mechanism of AChE and acetylcholine chloride *[122]*.

Figure 4.22, shows effect of pesticide incubation time on AChE inhibition. It is noticed that inhibition level of 100% is not achieved when using MCF-e or 0.5Au/MCF-e as enzyme supports which was suggested by Du et al., (2010) [123] who indicated that the binding sites between pesticides and enzymes could reach saturation and equilibrium of inhibition. However, the %I was not reached full 100% inhibition correspond to the results in **Figure 4.22** due to sufficient time of MCF-e and Au0.5/MCF-e to obtain the highest inhibitory effect and saturation by pesticide was 20 and 30 min, respectively. Lower required incubation times than this work were revealed at 8 mins by Caetano et al., (2008) [124], and 10 mins by Sun et al., (2010) [87]. The inhibition time in this work was highly influenced by mass transfer limitation. In addition, the inhibition time of Au0.5/MCF-e was longer than that of MCF-e. Incorporation of AuNPs to MCF-e slowed the mass transfer rate of the pesticide, thus longer incubation time was required until the saturation inhibition level was reached. However, the incubation percentage was similarly determined at approximately 65% for both MCF-e and Au0.5/MCF-e which pointed out that AuNPs did not interfere with the phosphorelation of the serine hydroxyl group at the enzyme active sites.

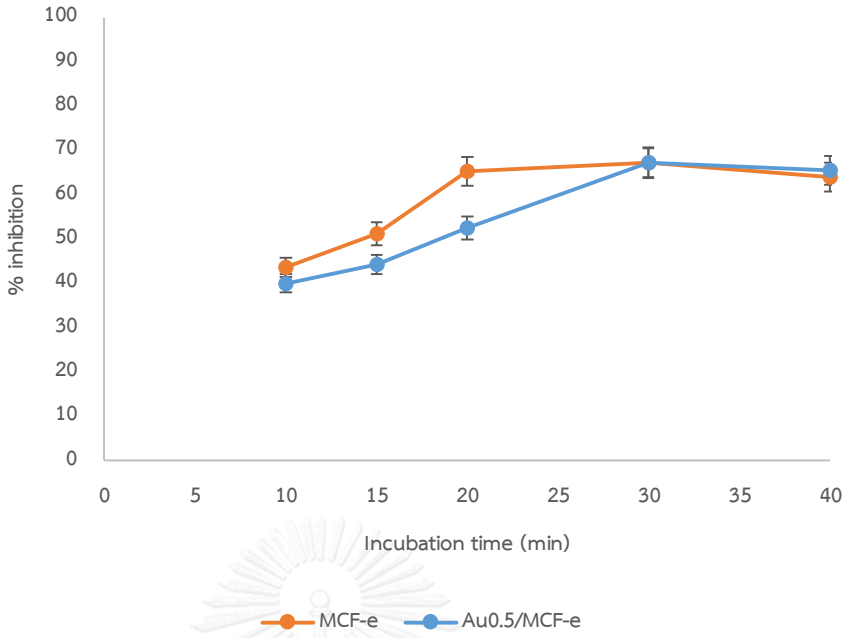

Figure 4.22 Percentage of inhibition (%I) as a function of incubation time for the MCF-e and 0.5Au/MCF-e based biosensors at +105 mV vs Ag/AgCl in 0.1 M PBS pH 9.0 with 2000 ng/ml of malathion and 40 mM of acetylthiocholine as substrate at 25±2°C.

Calibration curve

In this part, the fabricated biosensors were tested for their performance using the pesticide, chlorpyrifos, as a model analyte. The optimum conditions for incubation time as reported in the former section were utilized in this section. The experiments were tested by amperometric method as mentioned in chapter 3. After incubation with chlorpyrifos, the oxidation current was decreased due to the AChE inhibition. The degree of inhibition as %I depends on the inhibitor concentrations [125] and is displayed in Equation 2.4.

In this work, the fabricated biosensors were tested using chlorpyrifos as a model organophosphate pesticide. The inhibition of chlorpyrifos on AChE was monitored by measuring the oxidation current of thiocholine. In presence of chlorpyrifos, the deactivation mechanism was based on the formation of a permanent covalent bond due to the phosphorylation between AChE and pesticide [126]. Similarly Dan et al., (2010) [123] reported that organophosphate bound with the serine peptide which located at AChE's active site and led to phosphorelation between AChE-pesticide.

Considering AChE-pesticide inhibition system, the irreversible inhibition occurred. **Fig. 4.23** shows two linear ranges of the calibration curves. The linearity was evaluated by linear regression analysis. In this experiment, incubation times of MCF-e and Au0.5/MCF-e were at 20 and 30 min, respectively, in standard solution of chlorpyrifos of known concentrations (0.5-2000 ng/ml) and 40 mM acetylthiocholine solution in phosphate buffer pH9.0 was used as the substrate. The detection limits, estimated base on signal to 3S.D./Sensitivity, were determined and shown in **Table 4.3**.

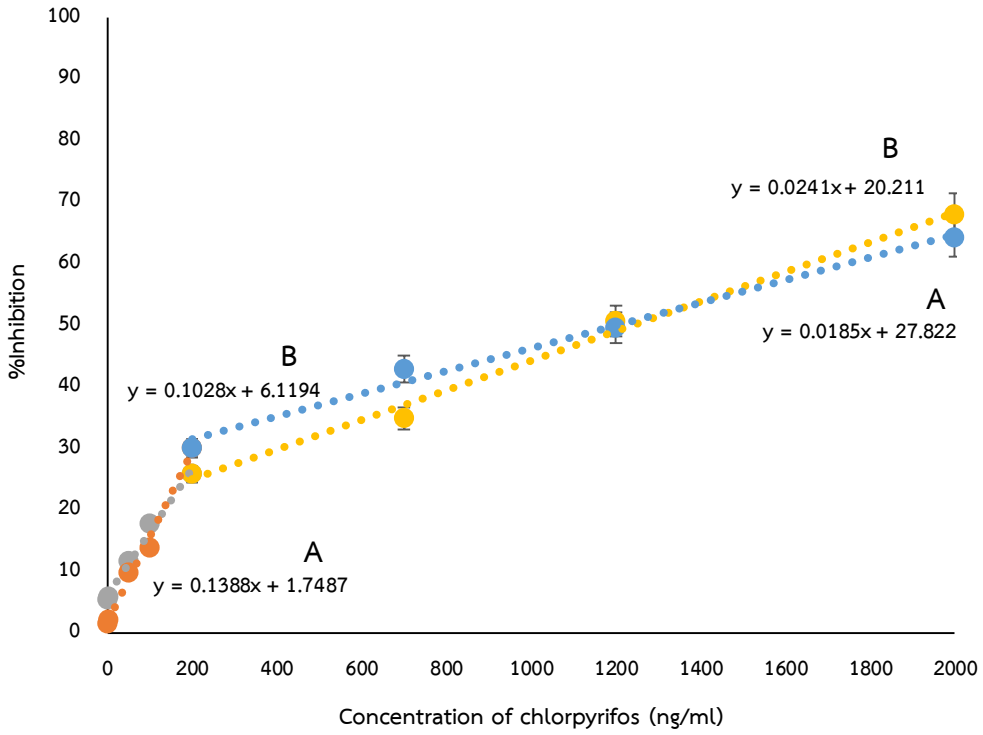

Figure 4.23 Calibration curve of modified (A) Au0.5/MCF-e and (B) MCF-e electrode for chlorpyrifos detection at concentration range 0.5-2000 ng/ml.

Table 4.3 Detection of chlorpyrifos with the SPE/nanocomposite/AChE/chitosan

Concentration ranges	Linear equation	
	MCF-e	Au0.5/MCF-e
0.5-200 ppb	y = 0.1028x + 6.1194	y = 0.1388x + 1.7487
200-2000 ppb	y = 0.0241x + 20.211	y = 0.0185x + 27.822
Detection limit	0.894 ppb	0.701 ppb

Au0.5/MCF-e-electrode showed slight lower detection limit compared to MCF-e-electrode. This could be resulted from the textural characteristic such as surface area, pore size and pore volume. Firstly, the electrode surface might be covered by MCF without gold nanoparticles which acted as a hindrance to substances of enzyme reaction, as same as Elena et al., (2009) [127] indicated that silica materials could reduce diffusion limitations inherent due to their nano-sized structure. Secondly, in presence of gold nanoparticles, AChE immobilized onto Au0.5/MCF-e which a smaller porous characteristic, but can promote the direct electron transfer hopping contact between metal particles and electrode surface unlike MCF-e because of sensing response need to be raised to the electron transfer where gold nanoparticles are achieved. However, in order to solve this problem of mass diffusion, we could take longer time of incubation both of nanocomposites.

Storage stability

Figure 4.24, the modified electrodes were stored in dried form at 4 °C and 34 °C when not in use. The storage stability of the biosensor was investigated by measuring the current responses with 40 mM of acetylthiocholine every 1, 20, 30 and 60 storage days. The residual activities of the biosensors decreased to 46.95, 74.25 and 77.57% respectively after storing for 30 days for free enzyme, MCF-e and Au0.5/MCF-e at 4 °C. And at 34°C after 30 days of storage, the residual activity of free enzyme, MCF-e and Au0.5/MCF-e were about 21.37, 47.87 and 56.20%. And finally when take a long time for 60 days, for free enzyme, MCF-e and Au0.5/MCF-e at 4 °C found the response percentage decreased to 24.41, 32.33 and 34.26% respectively. And 34°C after 60 days found 11.79, 9.08 and 13.77% respectively. So, we can conclude that the modified electrode have comparable and enhancing stability. In case, when duration

of longer storage was extended to 60 days, the response current had substantially deceased in storage of all electrodes, may cause the enzyme was denatured by temperature, acidity and microbial contamination.

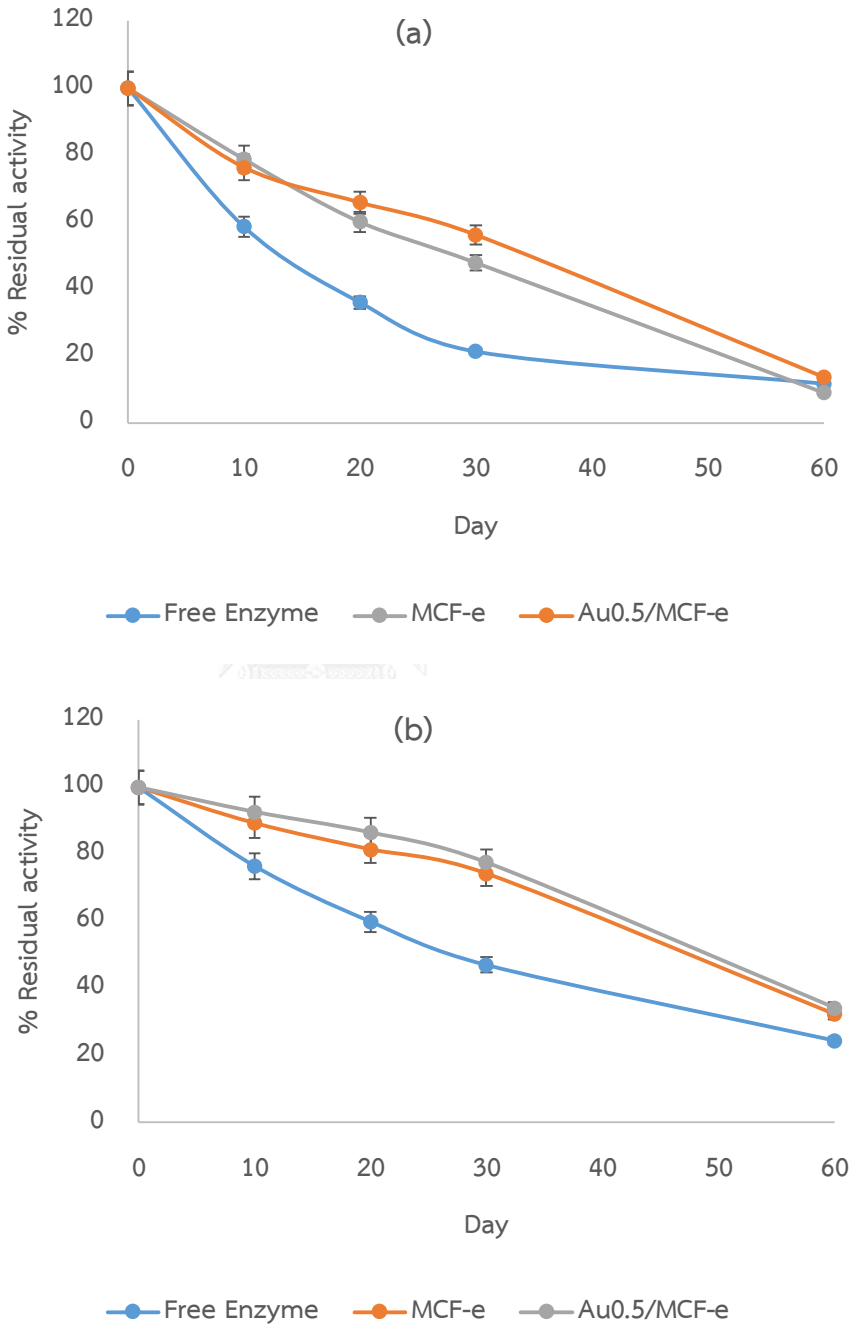

Figure 4.24 Influence of storage time at (a) 34°C and (b) 4°C on the residual activities of AChE immobilized in MCF-e and Au0.5/MCF-e modified electrodes tested in 40 mM of acetylthiocholine

Reproducibility

The reproducibility of 10 modified electrodes was evaluated under the optimum experimental conditions. The relative standard deviation (RSD) of the biosensor current responses to 40 mM acetylthiocholine in 0.1M PBS (pH 9.0) was achieved at 1.05V. The results show reproducibility of 5.66 and 5.07% RSD (n=10) for MCF-e and Au0.5/MCF-e, respectively, which exhibited good reproducibility.

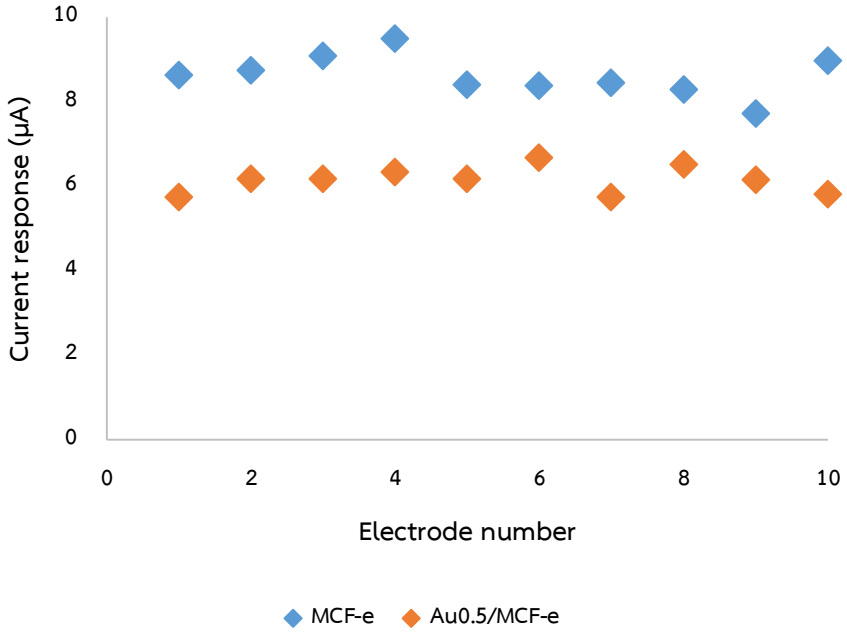

Figure 4.25 Current responses of MCF-e and Au0.5/MCF-e modified biosensors using amperometric technique at applied potential of +105 mV (vs Ag/AgCl) in PBS pH 9.0 with 40 mM of acetylthiocholine as the substrate at 25±2°C.

Chapter 5
Conclusion

5.1 Selection of suitable MCF nanocomposite for enzyme sensor

The experimental results obtained in the present work revealed significant roles of template removal methods on MCFs pore characters, silanol group residue enzyme loading, activity, and storage stability. MCF-a, MCF-c and MCF-e were of spherical structures with particle diameters of 2-3 μm.

5.2 The synthesis of Au/MCF nanocomposite by chemical reduction

The Au/MCF nanocomposites were successfully synthesized by chemical reduction. In this method, the gold ions were adsorbed on aminopropyl functionalized MCF. It was found that the functionalization agent, APTS, also could attach pore surface during the adsorption process. The synthesis conditions strongly affected the number and distribution of gold nanoparticles. Moreover, the adsorption time and gold precursor concentration influenced on the number of gold nanoparticles and size of gold nanoparticles as well. Nevertheless, size of gold nanoparticles could be strongly controlled by the adsorption time. With increasing adsorption time from up to 3 h, the main size of gold nanoparticles have changed as smaller size. Since the increase strongly affect the gold precursor concentration which was expected that the amount of gold nanoparticles should affect on enzyme immobilization as well as biosensor application. Therefore, the adsorption time for 3 h and gold precursor of 0.5 mM were chosen to test this condition on MCF support. In order to ensure considerable number of gold nanoparticles, gold precursor concentrations were tested by electrochemical response.

5.3 The immobilization of AChE and biosensor application on MCF and Au/MCF nanocomposite

MCF-e and AuNPs/MCF-e nanocomposites were used for enzyme immobilization, enzyme loadings were determined at 55.8 and 47.62% respevtively.

MCF-e/AChE and MCF/AuNPs/AChE were then applied as a receptor of biosensor for detection of chlorpyrifos. The obtained biosensors were denoted as SPCE/MCF-e/AChE/Chitosan and SPCE/MCF-e/AuNPs/AChE/Chitosan. The cyclic voltammogram of thiocholine released from the enzymatic hydrolysis showed the oxidation peak at +1.05 V. For MCF-e, the inhibitions of chlorpyrifos were in the linear ranges of 0.5 to 200 ppb (sensitivity 0.1028 nA/ppb) and 200 to 2000 ppb (sensitivity 0.0241 nA/ppb) with detection limit of 0.894 ppb. On the other hand, the AuNPs/MCF-e performed that the linear range of chlorpyrifos responses were from 0.5 to 200 ppb (sensitivity 0.1388 nA/ppb) and 200 to 2000 ppb (sensitivity 0.0185 nA/ppb) with detection limit of 0.701 ppb. The stability of biosensor stored of MCF-e and AuNPs/MCF-e at 4^{o}C in dry condition were good since it could retain 74.25 and 77.57 % respectively of initial current response after 30 storage days.

5.4 The suggestion for further research

5.4.1 The effect of the TOES on synthetic condition should be studied.

5.4.2 The effect of ATPS content and additives to pore characteristics of materials should be improved.

REFERENCES

[1] Subagyono, D.J., Liang, Z., Knowles, G.P., and Chaffee, A.L. Amine modified mesocellular siliceous foam (MCF) as a sorbent for CO 2. Chemical Engineering Research and Design 89(9) (2011): 1647-1657.

[2] Wu, S., et al. Controlled immobilization of acetylcholinesterase on improved hydrophobic gold nanoparticle/Prussian blue modified surface for ultra-trace organophosphate pesticide detection. Biosensors and Bioelectronics 27(1) (2011): 82-87.

[3] Johansson, E.M. Controlling the pore size and morphology of mesoporous silica. (2010).

[4] Schmidt-Winkel, P., Lukens, W.W., Zhao, D., Yang, P., Chmelka, B.F., and Stucky, G.D. Mesocellular siliceous foams with uniformly sized cells and windows. Journal of the American Chemical Society 121(1) (1999): 254-255.

[5] Schmidt-Winkel, P., et al. Microemulsion templating of siliceous mesostructured cellular foams with well-defined ultralarge mesopores. Chemistry of Materials 12(3) (2000): 686-696.

[6] Lu, G.Q., Zhao, X.S., and Wei, T.K. Nanoporous materials: science and engineering. Vol. 4: Imperial College Press, 2004.

[7] Kruk, M. and Jaroniec, M. Surface and structural properties of modified porous silicas. Surfactant science series 78 (1999): 443-472.

[8] Ashayer, R., Mannan, S.H., and Sajjadi, S. Synthesis and characterization of gold nanoshells using poly(diallyldimethyl ammonium chloride). Colloids and Surfaces A: Physicochemical and Engineering Aspects 329(3) (2008): 134-141.

[9] Bai, Y., Yang, H., Yang, W., Li, Y., and Sun, C. Gold nanoparticles-mesoporous silica composite used as an enzyme immobilization matrix for amperometric glucose biosensor construction. Sensors and Actuators B: Chemical 124(1) (2007): 179-186.

[10] Gutiérrez, L.-F., Hamoudi, S., and Belkacemi, K. Synthesis of Gold Catalysts Supported on Mesoporous Silica Materials: Recent Developments. Catalysts 1(1) (2011): 97-154.

[11] Saha, K., Agasti, S.S., Kim, C., Li, X., and Rotello, V.M. Gold nanoparticles in chemical and biological sensing. Chemical reviews 112(5) (2012): 2739-2779.

[12] Khatri, R.A., Chuang, S.S., Soong, Y., and Gray, M. Carbon dioxide capture by diamine-grafted SBA-15: A combined Fourier transform infrared and mass spectrometry study. Industrial & Engineering Chemistry Research 44(10) (2005): 3702-3708.

[13] Wang, L. and Yang, R.T. Increasing selective CO2 adsorption on amine-grafted SBA-15 by increasing silanol density. The Journal of Physical Chemistry C 115(43) (2011): 21264-21272.

[14] Sayari, A. and Hamoudi, S. Periodic mesoporous silica-based organic-inorganic nanocomposite materials. Chemistry of Materials 13(10) (2001): 3151-3168.

[15] Grudzien, R.M., Grabicka, B.E., and Jaroniec, M. Effective method for removal of polymeric template from SBA-16 silica combining extraction and temperature-controlled calcination. Journal of Materials Chemistry 16(9) (2006): 819-823.

[16] Hruanun, C., Kirtikara, K., and Tanticharoen, M. Use of Sucrose Biosensors for food Industry : Minimization of Interference. King Mongkuts Institute of Technology Thonburi Departmart of Biotechnology (1994).

[17] Pletcher, D. A First Course in Electrode Process. RSCPublishing (2009).

[18] Liu, J. and Mattiasson, B. Microbial BOD sensors for wastewater analysis. Water Research 36(15) (2002): 3786-3802.

[19] Tomizawa, M. and Casida, J.E. Neonicotinoid insecticide toxicology: mechanisms of selective action. Annu. Rev. Pharmacol. Toxicol. 45 (2005): 247-268.

[20] Department, P.C. Water Pollution Problems from Rice fields and Management. (2011): 20-21.

[21] Perry, A.S., Yamamoto, I., Ishaaya, I., and Perry, R.Y. Insecticides in agriculture and environment: retrospects and prospects. Springer Science & Business Media, 2013.

[22] Milkani, E., Lambert, C.R., and McGimpsey, W.G. Direct detection of acetylcholinesterase inhibitor binding with an enzyme-based surface plasmon resonance sensor. Anal Biochem 408(2) (2011): 212-9.

[23] Jha, N. and Ramaprabhu, S. Development of MWNT based disposable biosensor on glassy carbon electrode for the detection of organophosphorus nerve agents. Journal of nanoscience and nanotechnology 9(9) (2009): 5676-5680.

[24] Pundir, C.S. and Chauhan, N. Acetylcholinesterase inhibition-based biosensors for pesticide determination: a review. Anal Biochem 429(1) (2012): 19-31.

[25] Hildebrandt, A., Bragós, R., Lacorte, S., and Marty, J.L. Performance of a portable biosensor for the analysis of organophosphorus and carbamate insecticides in water and food. Sensors and Actuators B: Chemical 133(1) (2008): 195-201.

[26] Hermida, L., Abdullah, A.Z., and Mohamed, A.R. Synthesis and Characterization of Mesostructured Cellular Foam (MCF) Silica Loaded with Nickel Nanoparticles as a Novel Catalyst. Materials Sciences and Applications 04(01) (2013): 52-62.

[27] Degirmenci, V., Yilmaz, A., and Uner, D. Selective methane bromination over sulfated zirconia in SBA-15 catalysts. Catalysis Today 142(1) (2009): 30-33.

[28] Hoffmann, F., Cornelius, M., Morell, J., and Froba, M. Silica-based mesoporous organic-inorganic hybrid materials. Angew Chem Int Ed Engl 45(20) (2006): 3216-51.

[29] Moritz, M. and Geszke-Moritz, M. Mesoporous materials as multifunctional tools in biosciences: Principles and applications. Materials Science and Engineering: C 49 (2015): 114-151.

[30] Kim, J., Desch, R.J., Thiel, S.W., Guliants, V.V., and Pinto, N.G. Adsorption of biomolecules on mesostructured cellular foam silica: Effect of acid concentration and aging time in synthesis. Microporous and mesoporous materials 149(1) (2012): 60-68.

[31] Takahashi, H., Li, B., Sasaki, T., Miyazaki, C., Kajino, T., and Inagaki, S. Catalytic activity in organic solvents and stability of immobilized enzymes depend on the pore size and surface characteristics of mesoporous silica. Chemistry of Materials 12(11) (2000): 3301-3305.

[32] Luckarift, H.R., Greenwald, R., Bergin, M.H., Spain, J.C., and Johnson, G.R. Biosensor system for continuous monitoring of organophosphate aerosols. Biosensors and Bioelectronics 23(3) (2007): 400-406.

[33] Luckarift, H.R., Johnson, G.R., and Spain, J.C. Silica-immobilized enzyme reactors; application to cholinesterase-inhibition studies. Journal of Chromatography B 843(2) (2006): 310-316.

[34] Luckarift, H.R., Spain, J.C., Naik, R.R., and Stone, M.O. Enzyme immobilization in a biomimetic silica support. Nature biotechnology 22(2) (2004): 211-213.

[35] Lettow, J.S., et al. Hexagonal to mesocellular foam phase transition in polymer-templated mesoporous silicas. Langmuir 16(22) (2000): 8291-8295.

[36] Chi, Y.-S., Lin, H.-P., and Mou, C.-Y. CO oxidation over gold nanocatalyst confined in mesoporous silica. Applied Catalysis A: General 284(1-2) (2005): 199-206.

[37] Chouyyok, W. The Immobilization Of Horseradish Peroxidase On Ag/Mesoporous Silica Nanocomposite. Department of Chemical Engineering Chulalongkorn University (2008).

[38] Orita, T., Tomita, M., Saito, T., Nishida, N., and Kato, K. Immobilization of cholesterol esterase in mesoporous silica materials and its hydrolytic activity toward diethyl phthalate. Materials Science and Engineering: C 32(4) (2012): 718-724.

[39] Jullaphan, O., Witoon, T., and Chareonpanich, M. Production Of Mesoporous Silica Adsorbent From Natural Solid Wastes. KU Engineering journal 75 (2011): 103-119.

[40] Pandya, P.H., Jasra, R.V., Newalkar, B.L., and Bhatt, P.N. Studies on the activity and stability of immobilized α-amylase in ordered mesoporous silicas. Microporous and mesoporous materials 77(1) (2005): 67-77.

[41] Schulz-Ekloff, G., Rathouský, J., and Zukal, A. Controlling of morphology and characterization of pore structure of ordered mesoporous silicas. Microporous and mesoporous materials 27(2) (1999): 273-285.

[42] Belmabkhout, Y., Serna-Guerrero, R., and Sayari, A. Adsorption of from dry gases on MCM-41 silica at ambient temperature and high pressure. 1: Pure adsorption. Chemical Engineering Science 64(17) (2009): 3721-3728.

[43] Xu, J., Chen, T., Wang, X., Xue, B., and Li, Y.-X. Preparation of mesoporous graphitic carbon nitride using hexamethylenetetramine as a new precursor and catalytic application in the transesterification of β-keto esters. Catalysis Science & Technology 4(7) (2014): 2126-2133.

[44] Yan, X., Zhang, L., Zhang, Y., Yang, G., and Yan, Z. Amine-Modified SBA-15: Effect of Pore Structure on the Performance for CO2Capture. Industrial & Engineering Chemistry Research 50(6) (2011): 3220-3226.

[45] Surathin, N. Acetylcholinesterase Biosensors Based On Gold Nanoparticles/Mesocellular Foam Silica Nanocomposites For Detection Of Pesticides. Department of Chemical Engineering Chulalongkorn University (2012).

[46] Ngammark, P. Fabrication Of Silica-Chitosan Nanocomposite Based On Acetylcholinesterase Biosensor For Pesticide Detection. Department of Chemical Engineering Chulalongkorn University (2011).

[47] Han, Y., Lee, S.S., and Ying, J.Y. Spherical siliceous mesocellular foam particles for high-speed size exclusion chromatography. Chemistry of Materials 19(9) (2007): 2292-2298.

[48] Jamalluddin, N.A. and Abdullah, A.Z. Effect of 1,3,5-trimethylbenzene dosage on the characteristics and activity of Fe(III) loaded mesocellular foam catalyst in the degradation of acid red B dye in aqueous solution. Applied Catalysis A: General 483 (2014): 1-9.

[49] Oda, Y., Fukuyama, K., Nishikawa, K., Namba, S., Yoshitake, H., and Tatsumi, T. Mesocellular foam carbons: aggregates of hollow carbon spheres with open and closed wall structures. Chemistry of Materials 16(20) (2004): 3860-3866.

[50] Sen, T., Tiddy, G.J.T., Casci, J.L., and Anderson, M.W. Meso-cellular silica foams, macro-cellular silica foams and mesoporous solids: a study of emulsion-mediated synthesis. Microporous and mesoporous materials 78(2-3) (2005): 255-263.

[51] Li, Q., Wu, Z., Feng, D., Tu, B., and Zhao, D. Hydrothermal stability of mesostructured cellular silica foams. The Journal of Physical Chemistry C 114(11) (2010): 5012-5019.

[52] Mokaya, R. Hydrothermally-induced morphological transformation of mesoporous MCM-41 silica. Microporous and mesoporous materials 44 (2001): 119-127.

[53] Han, Y., Lee, S.S., and Ying, J.Y. Siliceous mesocellular foam for high-performance liquid chromatography: Effect of morphology and pore structure. Journal of Chromatography A 1217(26) (2010): 4337-4343.

[54] Yao, M., et al. The effect of post-processing conditions on aminosilane functionalizaiton of mesocellular silica foam for post-combustion CO 2 capture. Fuel 123 (2014): 66-72.

[55] Li, W., Bollini, P., Didas, S.A., Choi, S., Drese, J.H., and Jones, C.W. Structural changes of silica mesocellular foam supported amine-functionalized CO2 adsorbents upon exposure to steam. ACS Appl Mater Interfaces 2(11) (2010): 3363-72.

[56] Ping, E.W., Venkatasubbaiah, K., Fuller, T.F., and Jones, C.W. Oxidative Heck Coupling Using Pd(II) Supported on Organosilane-Functionalized Silica Mesocellular Foam. Topics in Catalysis 53(15-18) (2010): 1048-1054.

[57] Shakeri, M. and Kawakami, K. Enhancement of Rhizopus oryzae lipase activity immobilized on alkyl-functionalized spherical mesocellular foam: Influence of alkyl chain length. Microporous and mesoporous materials 118(1-3) (2009): 115-120.

[58] Clark, D.S. and Blanch, H.W. Biochemical engineering. CRC Press, 1997.

[59] Chibata, I. Immobilized Enzymes Research and Development. (1978).

[60] Goradia, D., Cooney, J., Hodnett, B.K., and Magner, E. The adsorption characteristics, activity and stability of trypsin onto mesoporous silicates. Journal of Molecular Catalysis B: Enzymatic 32(5-6) (2005): 231-239.

[61] Lei, J., et al. Immobilization of enzymes in mesoporous materials: controlling the entrance to nanospace. Microporous and mesoporous materials 73(3) (2004): 121-128.

[62] Yiu, H.H., Wright, P.A., and Botting, N.P. Enzyme immobilisation using siliceous mesoporous molecular sieves. Microporous and mesoporous materials 44 (2001): 763-768.

[63] Chong, A.S.M. and Zhao, X.S. Design of large-pore mesoporous materials for immobilization of penicillin G acylase biocatalyst. Catalysis Today 93-95 (2004): 293-299.

[64] Deere, J., Magner, E., Wall, J.G., and Hodnett, B.K. Mechanistic and structural features of protein adsorption onto mesoporous silicates. The Journal of Physical Chemistry B 106(29) (2002): 7340-7347.

[65] Gimon-Kinsel, M.E., Groothuis, K., and Balkus, K.J. Photoluminescent properties of MCM-41 molecular sieves. Microporous and mesoporous materials 20(1) (1998): 67-76.

[66] Han, Y.-J., Stucky, G.D., and Butler, A. Mesoporous silicate sequestration and release of proteins. Journal of the American Chemical Society 121(42) (1999): 9897-9898.

[67] Takahashi, H., Li, B., Sasaki, T., Miyazaki, C., Kajino, T., and Inagaki, S. Immobilized enzymes in ordered mesoporous silica materials and improvement of their stability and catalytic activity in an organic solvent. Microporous and mesoporous materials 44 (2001): 755-762.

[68] Han, Y.-J., Watson, J.T., Stucky, G.D., and Butler, A. Catalytic activity of mesoporous silicate-immobilized chloroperoxidase. Journal of Molecular Catalysis B: Enzymatic 17(1) (2002): 1-8.

[69] Rana, S., Bajaj, A., Mout, R., and Rotello, V.M. Monolayer coated gold nanoparticles for delivery applications. Adv Drug Deliv Rev 64(2) (2012): 200-16.

[70] Ahirwal, G.K. and Mitra, C.K. Direct electrochemistry of horseradish peroxidase-gold nanoparticles conjugate. Sensors (Basel) 9(2) (2009): 881-94.

[71] Thobhani, S., et al. Bioconjugation and characterisation of gold colloid-labelled proteins. J Immunol Methods 356(1-2) (2010): 60-9.

[72] Zheng, Z., Li, H., Liu, T., and Cao, R. Monodisperse noble metal nanoparticles stabilized in SBA-15: Synthesis, characterization and application in microwave-

assisted Suzuki–Miyaura coupling reaction. Journal of Catalysis 270(2) (2010): 268-274.

[73] Petersen, R., Larsen, T., Andersen, O.Z., and Kildeby, N.L. Immobilization of Cutinase on Nanoparticles. Faculty of physics and nanotechnology Aalborg University (2006).

[74] Chen, W., Cai, W., Zhang, L., Wang, G., and Zhang, L. Sonochemical Processes and Formation of Gold Nanoparticles within Pores of Mesoporous Silica. J Colloid Interface Sci 238(2) (2001): 291-295.

[75] Lü, G., Zhao, R., Qian, G., Qi, Y., Wang, X., and Suo, J. A highly efficient catalyst Au/MCM-41 for selective oxidation cyclohexane using oxygen. Catalysis letters 97(3-4) (2004): 115-118.

[76] Mokhonoana, M.P., Coville, N.J., and Datye, A.K. Small Au nanoparticles supported on MCM-41 containing a surfactant. Catalysis letters 135(1-2) (2010): 1-9.

[77] Ghosh, A., Patra, C.R., Mukherjee, P., Sastry, M., and Kumar, R. Preparation and stabilization of gold nanoparticles formed by in situ reduction of aqueous chloroaurate ions within surface-modified mesoporous silica. Microporous and mesoporous materials 58(3) (2003): 201-211.

[78] Gabaldon, J.P., Bore, M., and Datye, A.K. Mesoporous silica supports for improved thermal stability in supported Au catalysts. Topics in Catalysis 44(1-2) (2007): 253-262.

[79] Chen, L., Hu, J., and Richards, R. Intercalation of aggregation-free and well-dispersed gold nanoparticles into the walls of mesoporous silica as a robust "Green" Catalyst for n-alkane oxidation. Journal of the American Chemical Society 131(3) (2008): 914-915.

[80] Cutrufello, M., et al. Synthesis, characterization and catalytic activity of Au supported on functionalized SBA-15 for low temperature CO oxidation. Journal of materials science 44(24) (2009): 6644-6653.

[81] Zhu, K., Hu, J., and Richards, R. Aerobic oxidation of cyclohexane by gold nanoparticles immobilized upon mesoporous silica. Catalysis letters 100(3) (2005): 195-199.

[82] Li, Z., Kübel, C., Pârvulescu, V.I., and Richards, R. Size tunable gold nanorods evenly distributed in the channels of mesoporous silica. ACS nano 2(6) (2008): 1205-1212.

[83] Zhao, L., Zhu, G., Zhang, D., Chen, Y., and Qiu, S. A surface modification scheme for incorporation of nanocrystals in mesoporous silica matrix. Journal of Solid State Chemistry 178(10) (2005): 2980-2986.

[84] Rinaudo, M. Chitin and chitosan: Properties and applications. Progress in Polymer Science 31(7) (2006): 603-632.

[85] Kang, X., Wang, J., Wu, H., Aksay, I.A., Liu, J., and Lin, Y. Glucose oxidase–graphene–chitosan modified electrode for direct electrochemistry and glucose sensing. Biosensors and Bioelectronics 25(4) (2009): 901-905.

[86] Krajewska, B. Application of chitin- and chitosan-based materials for enzyme immobilizations: a review. Enzyme and Microbial Technology 35(2-3) (2004): 126-139.

[87] Sun, X. and Wang, X. Acetylcholinesterase biosensor based on Prussian blue-modified electrode for detecting organophosphorous pesticides. Biosens Bioelectron 25(12) (2010): 2611-4.

[88] Chi, Y.-S., Lin, H.-P., and Mou, C.-Y. CO oxidation over gold nanocatalyst confined in mesoporous silica. Applied Catalysis A: General 284(1) (2005): 199-206.

[89] Chiang, C.-W., Wang, A., Wan, B.-Z., and Mou, C.-Y. High catalytic activity for CO oxidation of gold nanoparticles confined in acidic support Al-SBA-15 at low temperatures. The Journal of Physical Chemistry B 109(38) (2005): 18042-18047.

[90] Knöfel, C., Lutecki, M., Martin, C., Mertens, M., Hornebecq, V., and Llewellyn, P.L. Green solvent extraction of a triblock copolymer from mesoporous silica: Application to the adsorption of carbon dioxide under static and dynamic conditions. Microporous and mesoporous materials 128(1-3) (2010): 26-33.

[91] Karsa, D.R. and Ashworth, D. Industrial biocides: selection and application. Vol. 270: Royal Society of Chemistry, 2002.

[92] AlOthman, Z.A. and Apblett, A.W. Synthesis and characterization of a hexagonal mesoporous silica with enhanced thermal and hydrothermal stabilities. Applied Surface Science 256(11) (2010): 3573-3580.

[93] Liu, Y.-M., et al. Structure and catalytic properties of vanadium oxide supported on mesocellulous silica foams (MCF) for the oxidative dehydrogenation of propane to propylene. Journal of Catalysis 239(1) (2006): 125-136.

[94] Hiyoshi, N., Yogo, K., and Yashima, T. Adsorption characteristics of carbon dioxide on organically functionalized SBA-15. Microporous and mesoporous materials 84(1) (2005): 357-365.

[95] Huang, H.Y., Yang, R.T., Chinn, D., and Munson, C.L. Amine-grafted MCM-48 and silica xerogel as superior sorbents for acidic gas removal from natural gas. Industrial & Engineering Chemistry Research 42(12) (2003): 2427-2433.

[96] Hayakawa, S. and Hench, L.L. AM1 study on infra-red spectra of silica clusters modified by fluorine. Journal of non-crystalline solids 262(1) (2000): 264-270.

[97] Wang, X., Chan, J.C., Tseng, Y.-H., and Cheng, S. Synthesis, characterization and catalytic activity of ordered SBA-15 materials containing high loading of diamine functional groups. Microporous and mesoporous materials 95(1) (2006): 57-65.

[98] White, L. and Tripp, C. Reaction of (3-aminopropyl) dimethylethoxysilane with amine catalysts on silica surfaces. J Colloid Interface Sci 232(2) (2000): 400-407.

[99] Kresge, C., Leonowicz, M., Roth, W., Vartuli, J., and Beck, J. Ordered mesoporous molecular sieves synthesized by a liquid-crystal template mechanism. nature 359(6397) (1992): 710-712.

[100] Beck, J., et al. A new family of mesoporous molecular sieves prepared with liquid crystal templates. Journal of the American Chemical Society 114(27) (1992): 10834-10843.

[101] Zhao, D., Yang, P., Melosh, N., Feng, J., Chmelka, B.F., and Stucky, G.D. Continuous mesoporous silica films with highly ordered large pore structures. Advanced Materials 10(16) (1998): 1380-1385.

[102] Chouyyok, W., Panpranot, J., Thanachayanant, C., and Prichanont, S. Effects of pH and pore characters of mesoporous silicas on horseradish peroxidase

immobilization. Journal of Molecular Catalysis B: Enzymatic 56(4) (2009): 246-252.

[103] Meynen, V., Cool, P., and Vansant, E. Verified syntheses of mesoporous materials. Microporous and mesoporous materials 125(3) (2009): 170-223.

[104] Sing, K.S. Reporting physisorption data for gas/solid systems with special reference to the determination of surface area and porosity (Recommendations 1984). Pure and applied chemistry 57(4) (1985): 603-619.

[105] Imperor-Clerc, M., Davidson, P., and Davidson, A. Existence of a microporous corona around the mesopores of silica-based SBA-15 materials templated by triblock copolymers. Journal of the American Chemical Society 122(48) (2000): 11925-11933.

[106] Van Der Voort, P., Benjelloun, M., and Vansant, E.F. Rationalization of the synthesis of SBA-16: controlling the micro-and mesoporosity. The Journal of Physical Chemistry B 106(35) (2002): 9027-9032.

[107] Guo, W., Li, X., and Zhao, X. Understanding the hydrothermal stability of large-pore periodic mesoporous organosilicas and pure silicas. Microporous and mesoporous materials 93(1) (2006): 285-293.

[108] Sussman, J.L., et al. Atomic structure of acetylcholinesterase from Torpedo californica: a prototypic acetylcholine-binding protein. Science 253(5022) (1991): 872-879.

[109] Harlick, P.J. and Sayari, A. Applications of pore-expanded mesoporous silica. 5. Triamine grafted material with exceptional CO2 dynamic and equilibrium adsorption performance. Industrial & Engineering Chemistry Research 46(2) (2007): 446-458.

[110] Serna-Guerrero, R., Belmabkhout, Y., and Sayari, A. Triamine-grafted pore-expanded mesoporous silica for CO2 capture: Effect of moisture and adsorbent regeneration strategies. Adsorption 16(6) (2010): 567-575.

[111] Kim, S., Ida, J., Guliants, V.V., and Lin, Y. Tailoring pore properties of MCM-48 silica for selective adsorption of CO2. The Journal of Physical Chemistry B 109(13) (2005): 6287-6293.

[112] Witoon, T., Tatan, N., Rattanavichian, P., and Chareonpanich, M. Preparation of silica xerogel with high silanol content from sodium silicate and its application as CO 2 adsorbent. Ceramics International 37(7) (2011): 2297-2303.

[113] Danon, A., Stair, P.C., and Weitz, E. FTIR study of CO2 adsorption on amine-grafted SBA-15: elucidation of adsorbed species. The Journal of Physical Chemistry C 115(23) (2011): 11540-11549.

[114] Norouzi, P., Pirali-Hamedani, M., Ganjali, M., and Faridbod, F. A novel acetylcholinesterase biosensor based on chitosan-gold nanoparticles film for determination of monocrotophos using FFT continuous cyclic voltammetry. Int J Electrochem Sci 5(10) (2010): 1434-1446.

[115] Lei, Z., Zhang, L., and Wei, X. One-step synthesis of silver nanoparticles by sonication or heating using amphiphilic block copolymer as templates. J Colloid Interface Sci 324(1) (2008): 216-219.

[116] Qiu, H., Xu, C., Huang, X., Ding, Y., Qu, Y., and Gao, P. Immobilization of laccase on nanoporous gold: comparative studies on the immobilization strategies and the particle size effects. The Journal of Physical Chemistry C 113(6) (2009): 2521-2525.

[117] Giljohann, D.A., Seferos, D.S., Patel, P.C., Millstone, J.E., Rosi, N.L., and Mirkin, C.A. Oligonucleotide loading determines cellular uptake of DNA-modified gold nanoparticles. Nano letters 7(12) (2007): 3818-3821.

[118] Zhang, Y., Zhang, Y., Wang, H., Yan, B., Shen, G., and Yu, R. An enzyme immobilization platform for biosensor designs of direct electrochemistry using flower-like ZnO crystals and nano-sized gold particles. Journal of Electroanalytical Chemistry 627(1) (2009): 9-14.

[119] Zamfir, L.-G., Rotariu, L., and Bala, C. A novel, sensitive, reusable and low potential acetylcholinesterase biosensor for chlorpyrifos based on 1-butyl-3-methylimidazolium tetrafluoroborate/multiwalled carbon nanotubes gel. Biosensors and Bioelectronics 26(8) (2011): 3692-3695.

[120] Ion, A.C., et al. Acetylcholinesterase voltammetric biosensors based on carbon nanostructure-chitosan composite material for organophosphate pesticides. Materials Science and Engineering: C 30(6) (2010): 817-821.

[121] Krasinski, A., et al. In situ selection of lead compounds by click chemistry: target-guided optimization of acetylcholinesterase inhibitors. Journal of the American Chemical Society 127(18) (2005): 6686-6692.

[122] Gan, N., Yang, X., Xie, D., Wu, Y., and Wen, W. A disposable organophosphorus pesticides enzyme biosensor based on magnetic composite nano-particles modified screen printed carbon electrode. Sensors (Basel) 10(1) (2010): 625-638.

[123] Du, D., Ye, X., Cai, J., Liu, J., and Zhang, A. Acetylcholinesterase biosensor design based on carbon nanotube-encapsulated polypyrrole and polyaniline copolymer for amperometric detection of organophosphates. Biosensors and Bioelectronics 25(11) (2010): 2503-2508.

[124] Caetano, J. and Machado, S.A. Determination of carbaryl in tomato “in natura” using an amperometric biosensor based on the inhibition of acetylcholinesterase activity. Sensors and Actuators B: Chemical 129(1) (2008): 40-46.

[125] Guerrieri, A., Monaci, L., Quinto, M., and Palmisano, F. A disposable amperometric biosensor for rapid screening of anticholinesterase activity in soil extracts. Analyst 127(1) (2002): 5-7.

[126] Dutta, K., Bhattacharyay, D., Mukherjee, A., Setford, S., Turner, A., and Sarkar, P. Detection of pesticide by polymeric enzyme electrodes. Ecotoxicology and Environmental Safety 69(3) (2008): 556-561.

[127] Zamora, P., Narváez, A., and Domínguez, E. Enzyme-modified nanoparticles using biomimetically synthesized silica. Bioelectrochemistry 76(1) (2009): 100-106.

APPENDIX

Log table of experiment

Table A.1 Amount of amine loading in support of MCF-c and MCF-e was calculate by comparing initial and final weight of support from TGA sample holder (pan).

Material	Sample weight in pan before analysis (mg)	Weight loss of APTS from TGA (%)	APTS weight per sample weight in pan (mg)	Amount of APTS (mmol)	Amount of APTS per 1 g MCF (mmol/g)
MCF-c/APTS	8.92	9.13	0.81	3.68×10^{-3}	0.41
MCF-e/APTS	8.09	15.24	1.23	5.57×10^{-3}	0.69

Note MW of APTS = 221.37 g/mol

Table A.2.1 Amount of immobilized enzyme on support structure and surface properties of MCFs and surface-modified MCFs in PBS pH 6 at 4°C for 2 h.

Material	Initial AChE concentration before immpbilization (mg/ml)	Non-immobilized AChE		Immobilized AChE	
		mg/ml	%	mg/ml	%
MCF-c	0.5	0.231	46.24	0.269	53.76
MCF-c/APTS	0.5	0.376	75.19	0.124	24.81
MCF-c/Au0.1mM	0.5	0.352	70.44	0.148	29.56
MCF-c/Au0.5mM	0.5	0.248	49.62	0.252	50.38
MCF-c/Au1.0mM	0.5	0.147	29.37	0.353	70.63
MCF-e	0.5	0.221	44.20	0.279	55.80
MCF-e/APTS	0.5	0.374	74.72	0.126	25.28
MCF-e/Au0.1mM	0.5	0.351	70.25	0.149	29.56
MCF-e/Au0.5mM	0.5	0.262	52.38	0.238	47.62
MCF-e/Au1.0mM	0.5	0.143	28.56	0.357	71.44

Determination of AChE loading

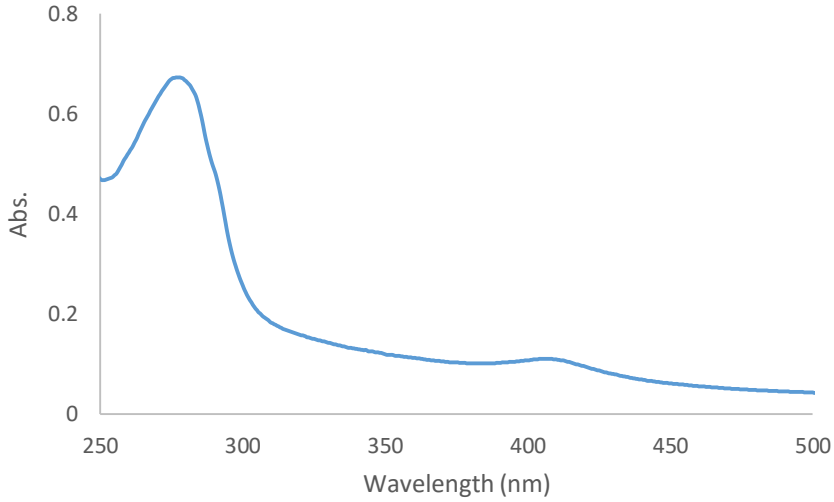

Figure A.2.1 Wave length peak of AChE at 277 nm.

Table A.2.2 Data of calibration curve for determination of AChE concentration at 277 nm.

AChE concentration (mg/ml)	Absorbance at 277 nm			
	Sample 1	Sample 1	Sample 1	Average
0.10	0.06	0.06	0.06	0.06
0.25	0.16	0.16	0.16	0.16
0.50	0.33	0.33	0.33	0.33
1.00	0.67	0.66	0.67	0.67

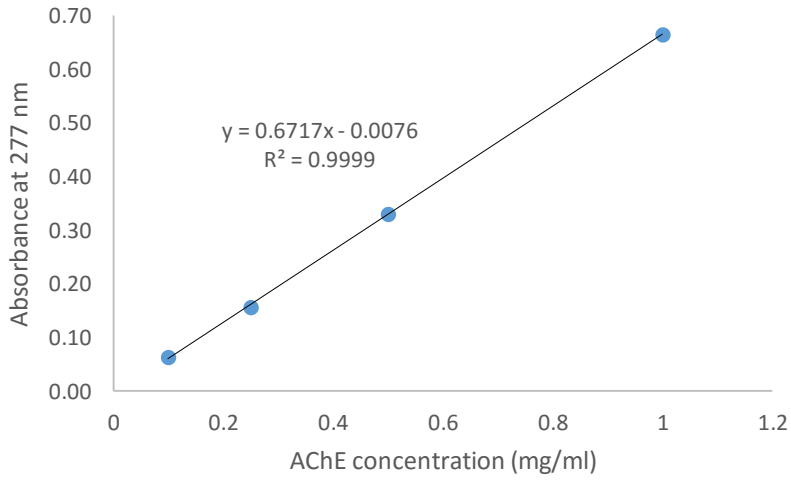

Figure A.2.2 Calibration curve of AChE by UV-vis method

Table A.2.3 Determination of non-immobilized from calibration curve by using UV spectrophotometer at 277 nm.

Material	Absorbance of non-immobilized AChE at 277 nm				Non-immobilized AChE concentration (mg/ml)
	Sample 1	Sample 2	Sample 3	Average	
MCF-c	0.150	0.149	0.145	0.148	0.231
MCF-c/APTS	0.246	0.245	0.245	0.245	0.376
MCF-c/Au0.1mM	0.221	0.232	0.234	0.229	0.352
MCF-c/Au0.5mM	0.156	0.158	0.163	0.159	0.248
MCF-c/Au1.0mM	0.097	0.095	0.081	0.091	0.147
MCF-e	0.139	0.141	0.143	0.141	0.221
MCF-e/APTS	0.245	0.235	0.250	0.243	0.374
MCF-e/Au0.1mM	0.220	0.230	0.235	0.228	0.351
MCF-e/Au0.5mM	0.170	0.170	0.165	0.168	0.262
MCF-e/Au1.0mM	0.090	0.090	0.085	0.088	0.143

Table A.3.1 Activity of AChE per an electrode (3 µl) was calculated by Ellman's method on support stricture and surface properties of MCF-e and surface-modified MCF-e(s).

Material	Activity from 0.5 mg/ml Initial AChE concentration before immobilization (%)	Activity of Non-immobilized AChE (%)	Activity of Immobilized AChE (%)
MCF-e	100	38.65	61.35
MCF-c/APTS	100	68.87	31.13
MCF-e/Au0.1mM	100	68.48	31.52
MCF-e/Au0.5mM	100	50.06	49.94
MCF-e/Au1.0mM	100	18.41	81.59

Determination of AChE activity

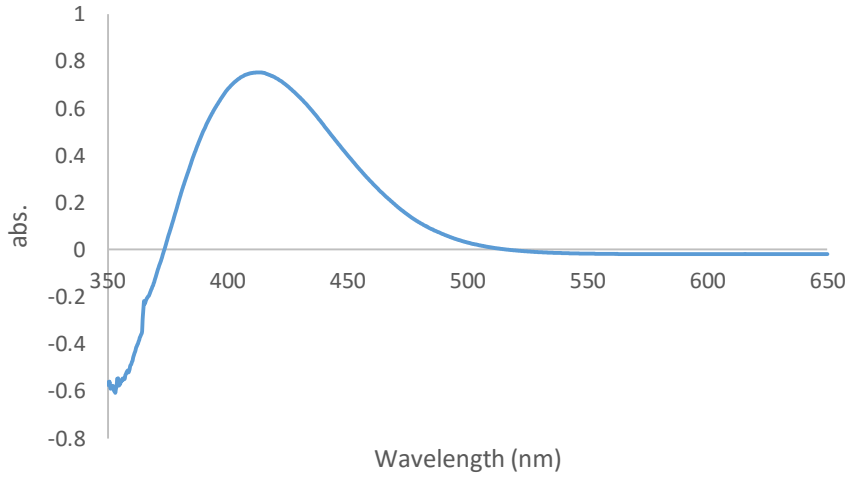

Figure A.3.1 Wave length peak of thiocholine chloride react with DTNB to produce the yellow acid at 410 nm.

Table A.3.2 Data of calibration curve for determination of activity per an electrode (3 µl) in each AChE concentration at 410 nm.

AChE concentration (mg/ml)		Absorbance at 277 nm			
mg/ml	AChE activity (%)	Sample 1	Sample 1	Sample 1	Average
0.0625	12.5	0.004	0.004	0.004	0.004
0.1250	25.0	0.061	0.062	0.063	0.062
0.2500	50.0	0.185	0.188	0.190	0.188
0.5000	100.0	0.446	0.425	0.457	0.452

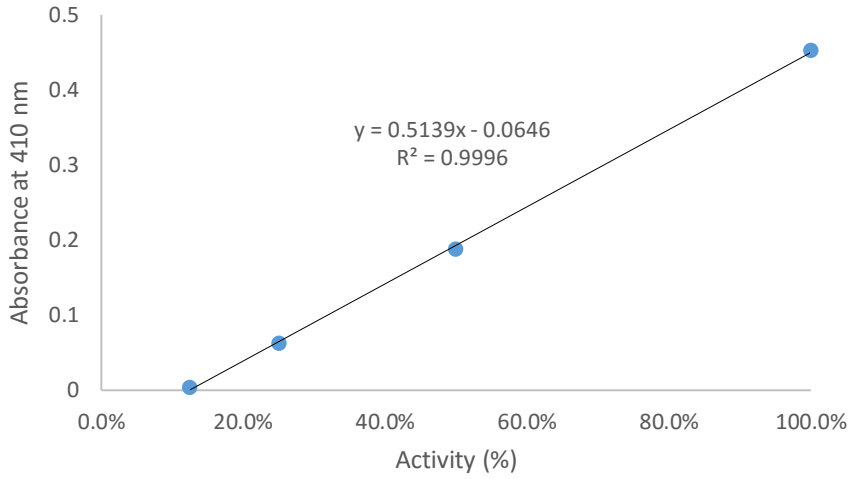

Figure A.3.2 Calibration curve of AChE activity by UV-vis method.

Table A.3.2 Activity determination of non-immobilized from calibration curve by using UV spectrophotometer at 410 nm.

Material	Absorbance of non-immobilized AChE at 410 nm				% AChE activity loss
	Sample 1	Sample 2	Sample 3	Average	
MCF-e	0.142	0.161	0.099	0.134	38.65
MCF-c/APTS	0.258	0.317	0.293	0.289	68.87
MCF-e/Au0.1mM	0.284	0.266	0.312	0.287	68.48
MCF-e/Au0.5mM	0.202	0.192	0.184	0.193	50.06
MCF-e/Au1.0mM	0.054	0.031	0.005	0.030	18.41

Table A.4 Current response in anodic peak of each electrode with variation concentration of ATCl including PBS pH 9.0.

Material	Anodic peak current (μA)		
	15 mM	40 mM	80 mM
MCF-c	5.88	11.66	12.88
MCF-e	19.30	26.51	26.42

Table A.5.1 The difference of current response of each modified MCF-e electrode after incubate with 2000 ng/ml Chlorpyrifos for different time period in detection system including PBS pH 9.0 and 40 mM ATCl.

Time (min)	Current response (μA) of modified MCF-e electrode										SD	RSD
	before	After	$\%I_1$	before	After	$\%I_2$	before	After	$\%I_3$	$\%I_{Avg}$		
10	9.35	5.52	43.00	8.94	4.91	45.03	9.40	5.39	42.59	43.54	1.31	0.030
15	9.11	4.28	52.99	8.93	4.42	50.45	8.99	4.48	50.17	51.20	1.55	0.030
20	8.74	2.88	66.77	9.01	3.25	63.93	8.62	3.00	65.23	65.31	1.42	0.022
30	9.10	3.09	65.98	8.78	2.84	67.66	8.68	2.77	68.10	67.24	1.12	0.017
40	8.75	3.13	64.08	9.02	3.37	62.59	8.92	3.11	65.14	63.94	1.28	0.020

Table A.5.2 The difference of current response of each modified MCF-e/Au0.5mM electrode after incubate with 2000 ng/ml Chlorpyrifos for different time period in detection system including PBS pH 9.0 and 40 mM ATCl.

Time (min)	Current response (μA) of modified MCF-e/Au0.5mM electrode										SD	RSD
	before	After	$\%I_1$	before	After	$\%I_2$	before	After	$\%I_3$	$\%I_{Avg}$		
10	6.03	3.65	39.48	6.03	3.71	38.54	5.75	3.33	42.06	40.03	1.82	0.045
15	5.79	3.32	42.54	5.75	3.11	45.85	5.94	3.29	44.52	44.30	1.67	0.038
20	5.86	2.92	50.22	5.81	2.67	54.01	5.98	2.81	53.00	52.41	1.97	0.037
30	6.17	2.01	67.41	5.75	1.90	66.86	5.81	1.90	67.22	67.16	0.28	0.004
40	6.06	2.12	64.97	6.04	2.02	66.51	5.75	2.01	65.07	65.52	0.86	0.013

Table A.6.1 Chlorpyrifos detection of SPCE/MCF-e/AChE/Chitosan biosensor in range of 0.5 to 2000 ng/ml containing PBS pH 9.0 and 40 mM ATCl.

Chlorpyrifos concentration (ng/ml)	Current response (μA)		$\%I_1$	Current response (μA)		$\%I_2$	Current response (μA)		$\%I_3$	$\%I_{Avg}$	SD	RSD
	before	After		before	After		before	After				
0.5	7.11	6.73	5.22	7.73	7.28	5.92	10.01	9.47	5.43	5.53	0.358	0.065
2	9.17	8.62	6.00	8.74	8.23	5.83	9.44	8.88	5.92	5.92	0.088	0.015
50	8.45	7.44	11.96	9.99	8.91	10.74	10.59	9.28	12.42	11.71	0.867	0.074
100	8.64	7.12	17.53	8.97	7.37	17.88	8.39	6.87	18.06	17.82	0.267	0.015
200	9.15	6.88	24.87	8.63	6.32	26.81	7.50	5.55	25.92	25.87	0.968	0.037
700	9.28	6.13	33.95	9.56	6.21	34.97	8.30	5.33	35.73	34.89	0.892	0.026
1200	9.58	4.58	52.15	10.28	5.09	50.51	9.50	4.81	49.38	50.68	1.393	0.027
2000	9.08	3.00	66.93	8.41	2.63	68.72	9.19	2.90	68.41	68.02	0.957	0.014

Table A.6.2 Chlorpyrifos detection of SPCE/MCF-e/AuNPs/AChE/Chitosan biosensor in range of 0.5 to 2000 ng/ml containing PBS pH 9.0 and 40 mM ATCl.

Chlorpyrifos concentration (ng/ml)	Current response (μA)		$\%I_1$	Current response (μA)		$\%I_2$	Current response (μA)		$\%I_3$	$\%I_{Avg}$	SD	RSD
	before	After		before	After		before	After				
0.5	5.47	5.36	2.03	6.86	6.76	1.53	6.33	6.25	1.19	1.58	0.422	0.266
2	6.18	6.05	2.20	4.98	4.88	1.90	6.15	5.98	2.70	2.27	0.402	0.178
50	5.44	4.92	9.56	5.57	5.03	9.83	7.56	6.80	10.12	9.84	0.280	0.028
100	7.17	6.13	14.49	5.75	4.96	13.85	5.37	4.66	13.36	13.90	0.566	0.041
200	6.18	4.29	30.59	4.86	3.42	29.54	5.70	3.98	30.13	30.09	0.527	0.017
700	6.94	3.94	43.27	6.51	3.82	41.36	4.98	2.78	44.23	42.95	1.460	0.034
1200	6.67	3.35	49.76	6.94	3.46	50.12	5.52	2.82	48.91	49.60	0.620	0.013
2000	5.48	1.97	64.12	5.06	1.73	65.87	5.08	1.88	63.03	64.34	1.432	0.022

Table A.6.3 Current response of each electrode with inhibition of PBS pH 9.0 for determining detection limit.

Modified Electrode	Current response (μA)		$\%I_1$	Current response (μA)		$\%I_2$	Current response (μA)		$\%I_3$	Current response (μA)		$\%I_4$	Current response (μA)		$\%I_5$	SD	RSD
	B	A		B	A		B	A		B			B	A			
MCF-e	9.54	9.52	0.15	1.00	9.99	0.19	9.58	9.57	0.15	9.54	9.52	0.22	9.28	9.26	0.16	0.031	0.18
MCF-e/Au	5.81	5.79	0.20	6.94	6.93	0.16	6.17	6.16	0.14	6.18	6.17	0.11	5.52	5.51	0.15	0.032	0.21

Note B = before inhibition, A = after inhibition, and MCF-e/Au containing Au precursor of 0.5 mM

Table A.7.1 % current response of SPCE/AChE/Chitosan biosensor with difference retention time at 4°C and 34°C.

Storage time (day)	Current response (μA)								Residual current response (%)	
	Electrode storage at 4°C				Electrode storage at 34°C					
	1	2	3	Average	1	2	3	Average	4°C	34°C
0	5.33	4.41	4.58	4.78	5.36	5.44	4.43	5.08	100.00	100.00
10	3.78	3.75	3.43	3.65	3.90	2.31	2.71	2.98	76.49	58.60
20	2.99	2.96	2.63	2.86	1.63	1.92	1.88	1.83	59.88	36.01
30	1.93	2.40	2.39	2.24	0.98	1.07	1.20	1.09	46.94	21.42
60	1.29	1.13	1.07	1.17	0.60	0.59	0.61	0.60	24.41	11.79

Table A.7.2 % current response of SPCE/MCF-e/AChE/Chitosan biosensor with difference retention time at 4°C and 34°C.

Storage time (day)	Current response (μA)								Residual current reponse (%)	
	Electrode storage at 4°C				Electrode storage at 34°C					
	1	2	3	Average	1	2	3	Average	4°C	34°C
0	8.19	7.10	9.20	8.17	8.09	9.13	8.17	8.46	100.00	100.00
10	6.49	8.04	7.35	7.29	7.21	5.89	6.90	6.67	89.31	78.76
20	6.83	6.24	6.89	6.65	4.50	4.76	5.98	5.08	81.47	60.02
30	6.07	5.99	6.13	6.06	3.57	3.91	4.67	4.05	74.26	47.84
60	2.64	2.04	3.23	2.64	0.51	1.05	0.75	0.77	32.33	9.08

Table A.7.3 % current response of SPCE/MCF-e/AuNPs/AChE/Chitosan biosensor with difference retention time at 4°C and 34°C.

Storage time (day)	Current response (μA)								Residual current reponse (%)	
	Electrode storage at 4°C				Electrode storage at 34°C					
	1	2	3	Average	1	2	3	Average	4°C	34°C
0	6.60	5.97	7.03	6.54	6.85	6.57	7.00	6.81	100.00	100.00
10	6.02	5.93	6.24	6.06	5.51	4.80	5.29	5.20	92.77	76.35
20	5.54	5.46	5.96	5.65	4.74	4.05	4.67	4.49	86.50	65.87
30	4.96	4.91	5.34	5.07	3.32	4.59	3.57	3.83	77.57	56.19
60	2.16	1.99	2.57	2.24	0.89	0.90	1.02	0.94	34.26	13.77

Table A.8 Current response in 10 replicates of electrode production by amperometry technique applied potential +1.05 V containing PBS pH 9.0 and 40 mM ATCl at 25°C.

Modified electrode	Current response (μA) of modified electrode	
	MCF-e	MCF-e/Au0.5mM
1	8.64	5.75
2	8.74	6.18
3	9.08	6.18
4	9.50	6.33
5	8.41	6.17
6	8.39	6.67
7	8.45	5.75
8	8.30	6.51
9	7.73	6.15
10	8.97	5.81
Average	8.62	6.15
SD	0.488	0.312
RSD	0.057	0.051

VITA

Mr. Nithi Thananukool was born on May 2nd, 1989 in Nakhonratchasima, Thailand. He received the Bachelor's Degree of Engineering from the Department of Chemical Engineering, Khon Kaen University 2013. After graduation, he entered study for a Master's Degree with a major in Chemical Engineering at the Department of Chemical Engineering, Faculty of Engineering, Chulalongkorn University and completed the program in 2016.